VILNIUS UNIVERSITY
STATE RESEARCH INSTITUTE
CENTER FOR PHYSICAL SCIENCES AND TECHNOLOGY

VADIMAS DUDOITIS

SOURCE APPORTIONMENT OF FINE AND CARBONACEOUS AEROSOL PARTICLES IN URBAN AND BACKGROUND ENVIRONMENTS

Doctoral dissertation
Physical sciences, Physics (02P)

Vilnius, 2015

Dissertation was prepared at the State Research Institute Center for Physical Sciences and Technology, Vilnius, Lithuania during the period from 2010 to 2015.

Scientific supervisor:

dr. Vidmantas Ulevičius (State Research Institute Center for Physical Sciences and Technology, physical sciences, physics – 02P)

CONTENTS

LIST OF ABBREVIATIONS

ACSM	aerosol chemical speciation monitor
AGL	above ground level
AMS	aerosol mass spectrometer
APS	aerodynamic particle sizer
ASL	above sea level
BC	black carbon
CPC	condensation particle counter
CWT	concentration weighted trajectory
D_A	aerodynamic diameter
D_P	particle diameter
D_M	mobility diameter
GHG	greenhouse gases
HYSPLIT-4	Hybrid single particle Lagrangian integrated trajectory
IRMS	isotope ratio mass spectrometry
LRT	long-range transport
LV-OOA	low-volatility oxygenated organic aerosol
ME	multi-linear engine
MOUDI	micro-orifice uniform deposition impactor
NPF	new particle formation
NR-$PM_{1.0}$	non-refractory particulate matter with cut-size D_{50} = 1.0 μm
OA	organic aerosol
OOA	oxygenated organic aerosol
PCA	principal component analysis
PM	particulate matter
PM_x	particulate matter with cut-size diameter D_{50} at x = 10, 2.5 or 1.0 μm.
PNC	particle number concentration
PNSD	particle number size distribution
PSCF	potential source contribution function
RF	radiative forcing

RH	relative humidity
SA	source apportionment
SD	standard deviation
SMPS	scanning mobility particle sizer
SOA	secondary organic aerosol
SV-OOA	semi-volatile oxygenated organic aerosol
TC	total carbon
TOF	time of flight
$\delta^{13}C_{TC}$	carbon stable isotope ratio (^{13}C:^{12}C).
WD	wind direction
WS	wind speed

1 INTRODUCTION

Fine and ultrafine particles has drawn an attention due to their impact on climate change and health effects. The major anthropogenic sources affecting aerosol particle number concentration (PNC) in urban environment are vehicle exhaust emissions, biomass burning and photo-chemical nucleation (Pey *et al.*, 2008; Perez *et al.*, 2010; Sirinivas *et al.*, 2010). However, estimation of ultrafine particle sources is a great challenge as their contribution vary from one location to another, new particle formation (NPF) is governed by different process and weather conditions plays important role (Foy and Schauer, 2015).

Carbonaceous aerosols has demanded more attention in recent years as it affects the atmosphere by scattering and absorbing solar irradiation, participates in the cloud formation processes and reacts with other aerosol and gas constituents (Chung et al, 2012; Burkart *et al.*, 2011). The main anthropogenic sources of carbonaceous aerosol are biomass burning and fossil fuel combustion. The presence of black carbon (BC) particles on snow, sea ice and glaciers causes a decrease in the surface albedo and accelerates the melt of ice and snow (Hadley and Kirchstetter, 2012). The anthropogenic forcing of the climate systems will be better assessed, if the sources and spatial distributions of aerosol constituents will be better evaluated. Despite the widespread need for source apportionment (SA) data, there is little information available on receptor modelling results from different European countries (Viana *et al.*, 2008).

In this work receptor modelling of PNC and BC mass concentration was applied. Better estimation of BC spatial distribution and its origin in the South-Eastern Baltic Sea region was achieved. These results are useful in producing more precise climate global warming predictions. The combined aerosol particle sizing technique and carbon stable isotope ratio ($\delta^{13}C_{TC}$) analysis proved to be suitable for estimating fossil fuel combustion and non-fossil emission sources.

The purpose of the research

The purpose of this research was to identify and quantify the processes end sources of fine and carbonaceous aerosol particles in urban and marine background environments. The main tasks of this research were formed, as follows:

1. To perform a long-term measurements and data analysis of aerosol particle number concentration and black carbon in urban and marine background environments and to investigate the main processes, governing their spatial and temporal variation.
2. To investigate carbonaceous aerosol particles and their sources in South-Eastern Baltic Sea region during the vegetation burning.
3. To combine aerosol particle sizing techniques with the carbon stable isotope ratio ($\delta^{13}C_{TC}$) analysis for apportionment of fossil fuel combustion and non-fossil fuel emission sources.

The novelty of the thesis

1. Aerosol particle sources in the urban environment were estimated applying quantitative receptor-oriented modelling methods.
2. It was determined that complex measurements combining $\delta^{13}C_{TC}$ analysis and aerosol particle sizing techniques are appropriate for fossil fuel combustion and non-fossil fuel emission source evaluation.

The practical value of the thesis

1. Better evaluation of black carbon spatial distribution in the atmosphere was achieved by applying receptor modelling of atmospheric pollution sources. It helps to produce more precise climate global warming predictions.

2. The receptor modelling of atmospheric pollutants in the South-Eastern Baltic Sea region provides useful source apportionment data for assessing air quality policies both in the region and in Europe.

Statements to be defended

1. The long-range transport of air mass increases particle number concentration in urban environment up to 2.2 times in autumn, 1.6 times in the winter and 2.3 times in spring.
2. The long-range transport of air masses is the main contributor to the increase of black carbon mass concentration up to 1.5 times in autumn, 4.5 times in the winter and 1.8 times in the spring season in the South Eastern Baltic Sea region.
3. During vegetation burning event background mass concentration of organic aerosol increased up to 50% in the Eastern Baltic Sea region.
4. The fossil fuel combustion is the major source contributor in the fine particles mode size range ($D_A = 0.23$ μm; $SD = 0.02$ μm), while non-fossil fuel emission source has the major contribution in the coarse particle mode size range ($D_A = 7.05$ μm; $SD = 3.56$ μm), either accounting from 60% to 100%.

Approbation

Results of the research, which are presented in the thesis, were published in 6 scientific journals with Impact Factor from Thomson Reuters Web of Knowledge database and in 11 presentations at international and national scientific conferences.

Scientific publications related to the topic of the thesis:

1. S. Byčenkienė, V. Ulevičius, **V. Dudoitis** and J. Pauraitė, Identification and characterization of black carbon aerosol sources in the East Baltic region, Adv. Meteorol. Vol. 2013, Article ID 380614 (2013).
2. V. Ulevičius, S. Byčenkienė, K. Plauškaitė and **V. Dudoitis**, Variation of particle number concentration and size distributions at the urban environment in Vilnius (Lithuania), Nucleation and atmospheric aerosols: 19th International Conference, AIP Publishing LLC. Vol. 1527, 527–530 (2013).
3. S. Byčenkienė, K. Plauškaitė, **V. Dudoitis** and V. Ulevičius, Urban background levels of particle number concentration and sources in Vilnius, Lithuania, Atmos. Res. 143, 279–292 (2014).
4. S. Byčenkienė, **V. Dudoitis** and V. Ulevičius, The use of trajectory cluster analysis to evaluate the long-range transport of black carbon aerosol in the South-Eastern Baltic region, Adv. Meteorol. Vol. 2014, Art. ID 137694 (2014).
5. A. Mašalaitė, A. Garbaras, **V. Dudoitis**, V. Ulevičius, D. Čeburnis and V. Remeikis, Elucidating carbonaceous aerosol sources by the stable carbon $\delta^{13}C_{TC}$ ratio in size segregated particles, Atmos. Res. 158, 1–12 (2015).
6. **V. Dudoitis**, S. Byčenkienė, K. Plauškaitė, G. Mordas and V. Ulevičius, Relationships between atmospheric carbonaceous particles and air masses in a background marine atmosphere, Acta Geophys., accepted (2015).

Conference presentations related to the thesis:

1. J. Šakalys, D. Valiulis, **V. Dudoitis**, K. Kvietkus and V. Ulevičius, Aerosol particle chemical component density variation in urban environment, 40th Lithuanian National Physics Conference, 2013.06.10–12, Vilnius, Lithuania.
2. **V. Dudoitis**, V. Ulevičius, K. Plauškaitė-Šukienė and G. Mordas, The comparison of the light scattering coefficient measured in urban and coastal environments, European Aerosol Conference (EAC 2013), 2013.09.01–06, Prague, Czech.
3. S. Byčenkienė, V. Ulevičius, **V. Dudoitis** and J. Andriejauskienė, Identification and characterization of black carbon aerosol sources in Lithuania, European Aerosol Conference (EAC 2013), 2013.09.01–06, Prague, Czech.
4. V. Ulevičius, A. S. H. Prévôt, K. Plauškaitė-Šukienė, S. Byčenkienė, G. Mordas, **V. Dudoitis**, V. Remeikis, A. Garbaras, K. Kvietkus, I. Garbarienė, J. Dommen, J. G. Slowik, C. Bozzetti and U. Baltensperger, Project AEROLIT (Aerosol in Lithuania): Investigation of primary-secondary and regional local contributions to particulate matter in the South-Eastern Baltic region, European Aerosol Conference (EAC 2013), 2013.09.01–06, Prague, Czech.
5. S. Byčenkienė, J. Pauraitė, **V. Dudoitis** and V. Ulevičius, Sources of wintertime black carbon aerosols in an atmosphere in Vilnius, Open Readings 2014, 2014.03.19–21, Vilnius, Lithuania.
6. S. Byčenkienė, J. Pauraitė, **V. Dudoitis** and V. Ulevičius, Sources of wintertime black carbon aerosols in an atmosphere in Vilnius, International Aerosol Conference (IAC 2014), 2014.08.28–09.02, Busan, South Korea.
7. V. Ulevičius, A. S. H. Prévôt, S. Byčenkienė, K. Plauškaitė, G. Mordas, C. Bozzetti, **V. Dudoitis**, V. Remeikis, A. Garbaras, J. Dommen,

J. G. Slowik, J. Blees and F. Canonaco, Source apportionment of the carbonaceous aerosol in the South-Eastern Baltic region, International Aerosol Conference (IAC 2014), 2014.08.28–09.02, Busan, South Korea.

8. **V. Dudoitis**, S. Byčenkienė, K. Plauškaitė, N. Prokopčiuk, G. Mordas and V. Ulevičius, Receptor models application in long-range transport of carbonaceous aerosol particles in coastal environment, Open Readings 2015, 2015.03.24–27, Vilnius, Lithuania.
9. **V. Dudoitis**, V. Ulevičius, S. Byčenkienė, K. Plauškaitė, G. Mordas, C. Bozzetti, R. Froehlich and A. S. H. Prévôt, Long-range transport of carbonaceous aerosol at coastal site in the South-Eastern Baltic region, European Aerosol Conference (EAC 2015), 2015.09.06–11, Milan, Italy.
10. V. Ulevičius, S. Byčenkienė, C. Bozzetti, A. Vlachou, K. Plauškaitė, G. Mordas, **V. Dudoitis**, G. Abbaszade, J. Blees, R. Fröhlich, K. R. Dällenbach, F. Canonaco, J. G. Slowik, J. Dommen, R. Zimmermann, J. Schnelle-Kreis, G. A. Salazar, K. Agrios, S. Szidat, I. El Haddad and A. S. H. Prévôt (2015). Fossil and non-fossil source contributions to atmospheric carbonaceous aerosols during grassland fires. European Aerosol Conference (EAC 2015), 2015.09.06–11, Milan, Italy.
11. C. Bozzetti, M. Xiao, V. Ulevičius, I. El Haddad, K. R. Dällenbach, **V. Dudoitis**, G. Mordas, J. G. Slowik, U. Baltensperger, and A. S. H. Prévôt (2015). Argon Offline-AMS source apportionment of organic aerosol over a yearly cycle for 3 different stations in Lithuania. European Aerosol Conference (EAC 2015), 2015.09.06–11, Milan, Italy.

Author's contribution

Author organised measurement campaigns, participated in field research experiments, processed and evaluated data, presented scientific results. Author's contribution included:

1. Participating in field measurements, organising long-term and short-term measurement campaigns at Preila Environmental pollution research station and Vilnius site.
2. Calibration of the scientific equipment. Participation in equipment intercomparison workshops.
3. Data processing and analysis of aerosol measurement data, and interpretation of obtained results.
4. Publishing the research results in scientific journals and presenting them at the conferences.

2 LITERATURE REVIEW

2.1 Atmospheric aerosol particles: origin, composition, transformation, climate and health effects

2.1.1 Definition of physical properties

An aerosol is generally defined as a colloid of fine solid particles or liquid droplets, suspended in gaseous environment (Baron and Willeke, 2001). Aerosol particles can be emitted into the atmosphere by natural (e.g. plants, ocean, desert, volcanoes, etc.) and anthropogenic (e.g. traffic, industrial and domestic combustion processes, etc.) sources. In this reason their physical properties and chemical composition vary with their origin and processing. Based on the different formation processes aerosol particles, which are originated from natural and anthropogenic sources, that consequently determine their chemical composition, size and shape characteristics. Aerosol particles can be directly emitted (primary) into the air or they can form in the atmosphere by gas-to-particle conversion such as nucleation, condensation, heterogeneous and multiphase chemical reactions (secondary) (Hallquist *et al.*, 2009). Atmospheric aerosol particles can be classified into separate modes according to their size, i.e. particle diameter (D_p): nanoparticles ($D_p < 50$ nm), ultrafine ($D_p < 100$ nm), fine ($D_p < 1.0$ µm) and coarse particles (1.0 µm $< D_p < 100$ µm). The ultrafine particles can be further divided into nucleation (< 30 nm) and Aitken mode particles (30 nm $< D_p <$ 100 nm). In the troposphere aerosol particle number and mass concentrations typically vary in the range of about 10^2–10^5 cm^{-3} and 1–100 µg·m^{-3}, respectively (Mooibroek *et al.*, 2011). Typically, aerosol particle number concentration (PNC) peak is observed in the nucleation and/or Aitken modes. Nucleation mode aerosol particles are mainly formed via homogeneous nucleation involving gas-to-particle conversion, while Aitken and accumulation mode particles are formed through coagulation of nucleation mode particles and condensational growth (Kulmala *et al.*, 2004). Ultrafine particles can also be directly emitted into the

atmosphere by combustion sources (e.g. fossil fuel, biomass burning, coal combustion, vehicle exhausts) (Ning *et al.*, 2013), but can also be produced by secondary formation processes involving sulphur and nitrogen oxides to form ammonium nitrate and sulphate in the particle phase and oxidation processes involving organic gaseous precursors. Whereas coarse mode particles are typically formed by mechanical processes and include resuspended material due to the action of the wind over the soil, sea spray, volcanic and other natural emissions (Fig. 1).

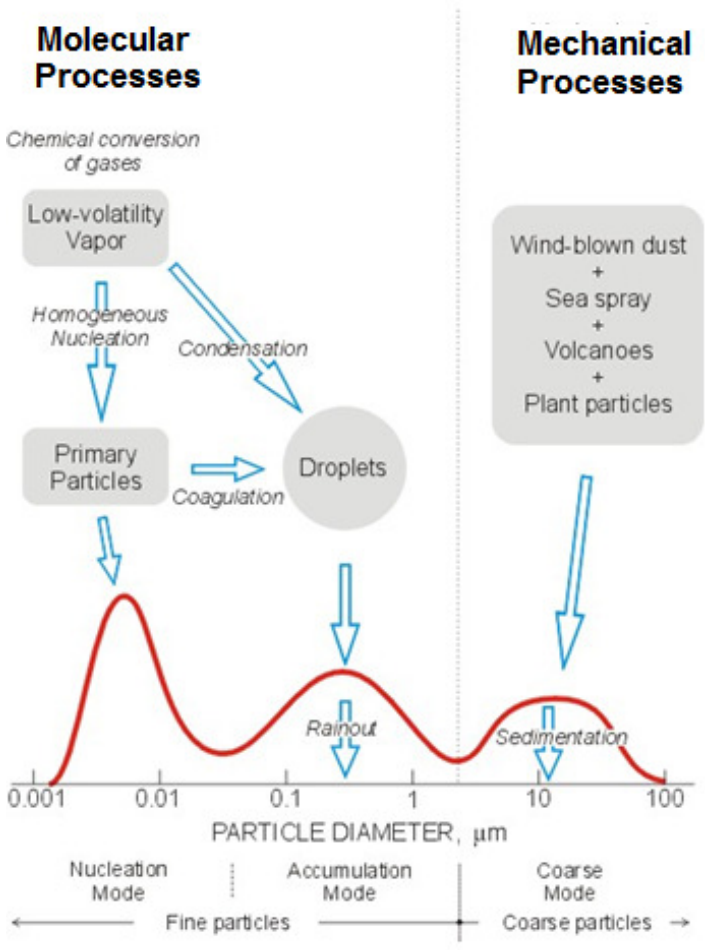

Fig. 1. Scheme of typical atmospheric aerosol size distributions, sources, formation mechanisms and removal processes for different modes (source[1]: *www.ems.psu.edu*)

Aerosol particles smaller than a few micrometers in diameter in dry air masses can have average lifetimes from several days up to a few weeks in the

lower troposphere (Zhang, 2001, Hoppel, 2002). However wet weather conditions can greatly reduce the amount of atmospheric aerosol, particularly water-soluble material.

In general, the predominant aerosol particle species are classified as sulphate, nitrate, ammonium, sea salt, mineral dust, organic compounds, and black or elemental carbon, each of which typically contributes about 10–30% of the overall mass load. However the relative abundance of different aerosol constituents can vary by an order of magnitude or more at different locations, times, meteorological conditions and particle size fractions (Perez *et al.*, 2010; Reche *et al.*, 2011).

2.1.2 Effects of aerosol particles on climate and health

In their most recent report, the Intergovernmental Panel on Climate Change (Stocker *et al.*, 2013) concluded that the quantification of aerosol radiative forcing is more complex than the quantification of radiative forcing by greenhouse gases (GHG) because aerosol mass and PNC are highly variable in space and time. This variability is largely due to the much shorter atmospheric lifetime of aerosol particles in comparison with the major GHG. It is well established that after entering into Earth's atmosphere the optical path of solar radiation is physically transformed by absorption, attenuation, scattering or reflectivity. Besides, clouds act as an optical filter, selectively transmitting short wavelength and reflecting long wavelength light. Solar radiation is absorbed on the planet surface and is re-emitted in a form of infrared light, which is partly trapped in the lower atmosphere and partly transmitted into the space. In such way the Earth is conserving its energy and keeps the planet warm (Barkstrom *et al.*, 1989; Allan, 2004; Forster and Taylor, 2006). In climate terminology, this process is called RF. It shows the capacity of forcing agents (i.e. clouds, gases, aerosol, landscape) to affect the Earth's energy balance of incoming and outgoing radiation (Forster *et al.*, 2007). The positive RF means that the energy balance is increased and the surface temperature is

rising, on the contrary, negative RF means cooling of the planet (Fig. 2). The GHG are forcing the climate to warm up, in 2013 combined RF for methane and CO_2 gases was 2.38 $W \cdot m^{-2}$ (Butler and Montzka, 2015; Meinshausen *et al.*, 2011). With small exceptions, aerosol particles act as negative climate forcing agents in several ways. First of all, aerosol particles participate in cloud formation, the presence of sulphate aerosol in the cloud increases the number of cloud condensation nuclei (Boucher and Lohmann, 1995; Lohmann *et al.*, 2010).

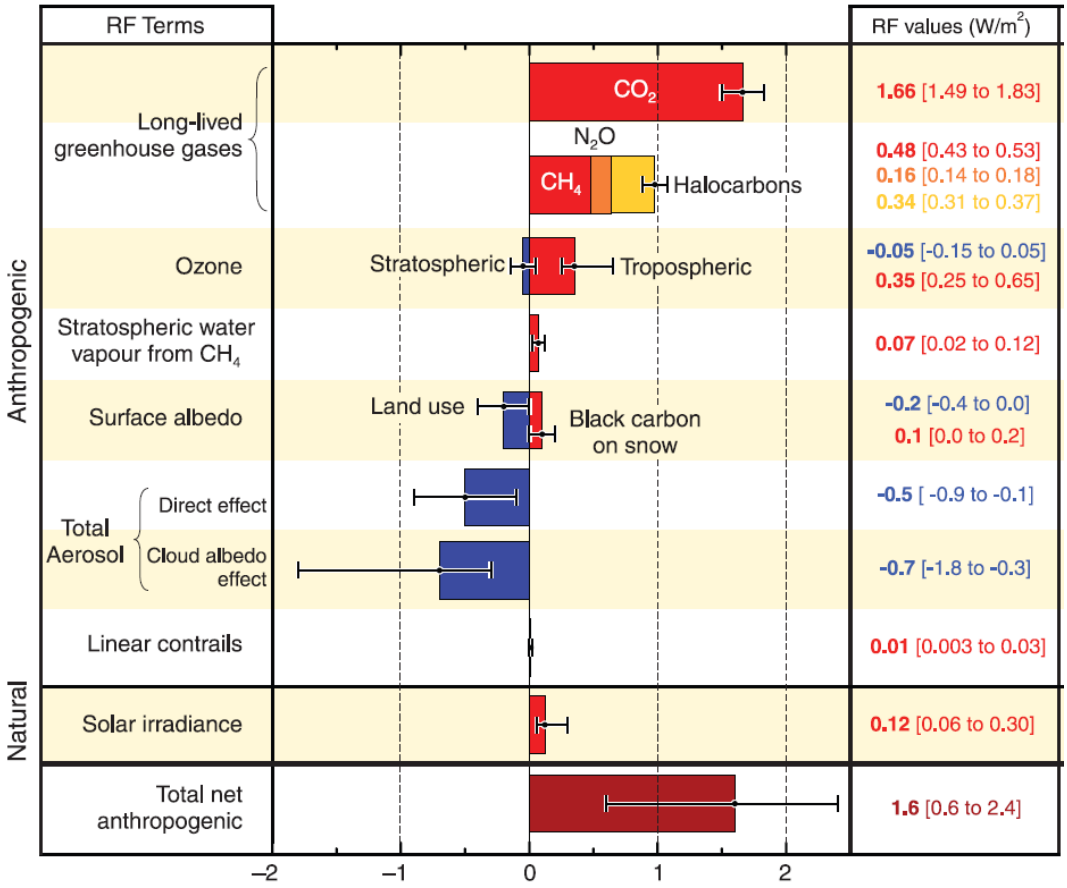

Fig. 2. Bar chart for anthropogenic radiative forcing for the period of 1750–2011 (source[2]: *www.climatechange2013.org*)

Cloud optical properties are changed, and the reflectivity of short wavelength light is increased. It was estimated that the cloud albedo RF was –0.90 $W \cdot m^{-2}$ (Forster and Taylor, 2006). Aerosol particles are scattering light by themselves, this effect depends on the size of particle diameter. Due to the

scattering, organic aerosol (OA), nitrates and sulphates act as the cooling agents of the atmosphere. The anthropogenic forcing by aerosol particles has one of the largest uncertainties in current climate simulations (Carslaw *et al.*, 2013; Lohmann and Ferrachat, 2010).

Historically, volcanoes, sand storms and forest fires were the main natural causes of negative RF, however this balance has been corrected by the anthropogenic activity. Fossil fuel combustion and biomass burning significantly contribute to carbonaceous aerosol emission in the atmosphere. These particles are transformed into the secondary organic aerosol (SOA) by accumulating volatile organic compounds (VOCs) in the atmosphere (Kroll and Seinfeld, 2008). BC is other form of carbon, which is originated from incomplete combustion processes. Unlike organic carbon, it absorbs light very well, thus it increases forcing of Earth's radiative budget (Stocker *et al.*, 2013). Soot mixed with snow and ice reduces its surface albedo and accelerates the melt processes (Hadley and Kirchstetter, 2012). The anthropogenic forcing of the climate systems will be better assessed, if the sources and spatial distributions of aerosol constituents are better evaluated.

Natural aerosol particles are probably 4 to 5 times larger than anthropogenic ones on a global scale, but regional variations in man-made pollution may change this ratio significantly in certain areas, particularly in the industrialised Northern Hemisphere (Seinfeld and Pandis, 2012).

The adverse impacts of aerosol particles on the human health (Brook *et al.*, 2010) have stimulated the scientific community to research urban air quality. The European Union (EU) and other international organisations, has established tough targets for air quality in order to minimise adverse health effects. Although only mass concentration of atmospheric particulates is the subject to regulation, the debates continue about which aerosol particle size fraction is more harmful to our health. This is important from a public health point of view because ultrafine particles may be more toxic per unit mass than the larger size fractions of aerosol (Sioutas *et al.*, 2005; Pope *et al.*, 2002). The relation between mass and number concentration is inverse. For instance, $PM_{2.5}$

well correlates with accumulation mode particles (> 100 nm), but do not correlate with ultrafine particles (< 100 nm), which account to most of the PNC (Rodríguez *et al.*, 2007).

The EU set two limit values for PM_{10} concentrations: annual average – 40 $\mu g \cdot m^{-3}$, 24-h limit value – 50 $\mu g \cdot m^{-3}$ not to be exceeded more than 35 times a calendar year (2008/EC/50). However, the implementation of the EU air-quality directives and introduction of more stringent vehicle emission standards were deferred since some countries were unable to meet the pre-existing limit value. Consequently, the reduction of aerosol mass concentration has increased the concentration of ultrafine particles in Western countries (Morawska *et al.*, 2002).

The attention of air quality legislators is drawn to identification of aerosol particle sources and their spatial distribution in various environments. Therefore, the urban areas are of particular interest due to the fact that both intensive aerosol particle emission sources and denser human population are located there. Understanding the origins, transformations, and fate of atmospheric aerosol is critical to determining the extent to which these particles affect climate and human health.

2.1.3 Carbonaceous aerosol particles

Carbonaceous aerosol (OA and BC) has received more attention in recent years for its impact on visibility degradation (BC is a major component affecting light absorption), influence on RF, climate and human health (Mauderly and Chow, 2008; Stocker *et al.*, 2013). The main sources of carbonaceous aerosol particles are biomass and fossil fuel burning, and the atmospheric oxidation of gas-phase biogenic emissions and anthropogenic VOCs (Bond *et al.*, 2013; Stocker *et al.*, 2013). Both, OA and BC have different optical and chemical properties and, thus produce different impact on atmospheric composition and climate. BC is characterized by its strong absorption of visible light and by its resistance to chemical transformation

(Petzold *et al.*, 2013). BC is a common product of carbonaceous matter incomplete combustion: wood burning in oxygen-deficient atmosphere (Schwartz and Lewis, 2012), change in chemical structure due to heating (Chow *et al.*, 2004). BC can be transported far away from remote emission sources since its atmospheric lifetime is in the order of several days up to a few weeks (Koch *et al.*, 2009). The sources and processes governing carbonaceous aerosol composition and concentration are highly complex, therefore, the identification of controlling factors is challenging.

The submicron inorganic fraction is mainly composed of sulphates, nitrates, and ammonium, the formation chemistry of which is relatively well understood (Seinfeld and Pandis, 2012). In contrast, OA is composed of thousands of species, many of them unidentified (Goldstein and Galbally, 2007) and with poorly characterized formation pathways. Despite its importance on global (e.g. climate) and local (e.g. pollution toxicity) scales (Kanakidou *et al.*, 2005), carbonaceous aerosol has only in the past decade become a subject of great scientific concern and topic of methodical investigation.

Characterisation of the organic content of aerosol particles has been in the focus of research by aerosol mass spectrometers (AMSs) and aerosol chemical speciation monitors (ACSMs) (e.g. Canagaratna *et al.*, 2007; Wexler and Johnston, 2008, Huang *et al.*, 2014, Bougiatioti *et al.*, 2014). Widespread field deployments of AMS and ACSM instruments, especially in the Northern Hemisphere, have demonstrated that 20–50% of $PM_{2.5}$ and up to 70% of $PM_{1.0}$ consist of carbonaceous aerosol particles (Zhang *et al.*, 2007). Factor analyses of the mass spectra (m/z) have been used to classify the organic components into hydrocarbon-like, which largely represents fresh fossil fuel combustion–related emissions; biomass, which stems largely from open burning; and various degrees of oxidised organic, which characterise relatively fresh to more completely aged SOA. It is known that aged SOA around the world has similar organic oxidation levels. High-resolution ACSM measurements are able to determine the average oxidation state of SOA as a function of aging in field

measurements. Carbonaceous aerosol particles are defined either by their physical properties or by the measurement method that is used (Poschl, 2003; Watson *et al.*, 2005). Such variety of methods brings common misconception when results obtained by different measurement equipment must be comparable (Petzold *et al.*, 2013). In global modelling studies data sets should be independent of the chosen measurement method, thus defining carbonaceous aerosol properties on all levels are equally important.

Identification of natural and anthropogenic aerosol particles in the atmosphere is equally important in source apportionment (SA) studies. Carbonaceous aerosol particles carry on the isotopic signature of their precursors (i.e. biogenic and fossil fuel hydrocarbons). Thus, the $\delta^{13}C_{TC}$ values are a useful tracer to distinguish the origin of carbonaceous particle sources, as different sources generally exhibit rather unique $\delta^{13}C_{TC}$ values (Ke *et al.*, 2007). Despite numerous ambient air studies reporting stable carbon isotope values (Narukawa *et al.*, 2008 and Widory *et al.*, 2004), it is still difficult to apportion between fossil and non-fossil combustion sources based only on $\delta^{13}C_{TC}$ values (Dusek *et al.*, 2013). Main aerosol research groups are working on various methods for fossil and non-fossil source estimation. Determination of carbon isotope (^{14}C) in carbonaceous aerosol particle samples is the most reliable one for estimating fossil fuel combustion and non-fossil emission sources (Lewis *et al.*, 2004; Szidat, 2006). However, this robust analysis is expensive and requires large amount of carbon in the sample (> 10 μg per measurement). The novelty of a combined ^{13}C analysis and an aerosol sizing technique is that it is suitable for fossil and non-fossil source estimation and requires less amount of carbon in the sample (> 0.5 μg per measurement) than in case of ^{14}C. Thus, the new approach based on $\delta^{13}C_{TC}$ values of size segregated aerosol particles and physical aerosol diameter sizing technique was used for distinguishing carbonaceous sources of fossil and non-fossil fuel combustion.

2.2 Source apportionment with receptor models

Contrary to the dispersion models, the receptor models use the measured pollutant concentrations at receptor sites to quantify source contributions. They don't describe the complicated dispersion process but use algorithm to compute the contributions from different sources (Watson *et al.*, 2002). Therefore this kind of models can be used for SA. In atmospheric studies, an approach of SA is used in order to estimate pollution sources geographically at the given receptor location (Fig. 3). The application of receptor models requires quantitative data on air pollutant concentrations, and good knowledge about atmospheric processes (Fig. 4). The main advantage of this method is its simplicity, ability to combine various atmospheric aerosol and meteorological data and no need to apply sophisticated mathematical models. Application example of this method is correlation of meteorological parameters: wind speed and direction (*WD* and *WS*), air temperature (*T*), precipitation and relative humidity (*RH*) with levels of measured particulate matter (PM; Henry *et al.*, 2002). Correlations also can be identified among pollutants themselves, for instance, PM values versus gaseous emissions. Another example, PM levels in urban environment, on the roadsides or in the canyon streets are subtracted from the measured regional background, in order to evaluate contribution of local source (Lenschow *et al.*, 2001).

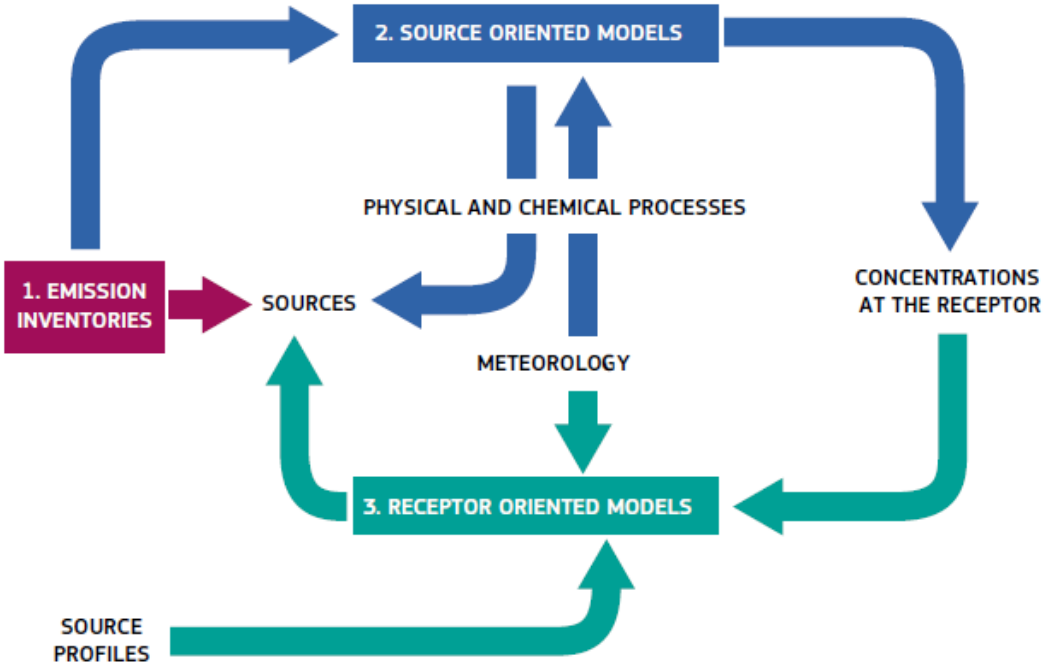

Fig. 3. Schematic representation of source apportionment by various techniques (Belis *et al.*, 2014)

Evaluation of pollution levels following time pattern, for example, diurnal cycles, working days vs. weekends, rush hours versus ordinary hours is a good approach of applying this method (Ruuskanen *et al.*, 2001, Gomišček *et al.*, 2004). Receptor modelling is a method to apportion the measured concentration of air pollutants at receptor site to their emission sources by solving a mass balance equation using multivariate analysis (Hopke 2003; Pekey *et al.*, 2004; Viana *et al.*, 2008). Several different computational approaches have been used for solving inverse pollutant transport. Air mass back trajectory analysis is frequently used to point out the direction and sources of air pollution at a receptor site (Paschalidou *et al.*, 2015). Trajectory clustering techniques, which assign trajectories into representative spatial groups, are a popular method to combine the flow climatology and pollutant transport pathways with particle or gas measurements at a sampling station.

Atmospheric aerosol contains a complex mixture of particles both of natural and anthropogenic origin, which originate from a variety of sources and are defined either as primary or secondary aerosol (Seinfeld and Pandis, 2012).

In recent years a number of research studies have focused not only on understanding the formation processes, chemical composition but also on SA of atmospheric aerosol particles (Harrison *et al.*, 1996, Lanz *et al.*, 2007). For the interpretation of source areas, the concentration weighted trajectory (CWT) and potential source contribution function (PSCF) analysis was used in several research studies (Hoh and Hites, 2004; Salvador and Chan, 2004).

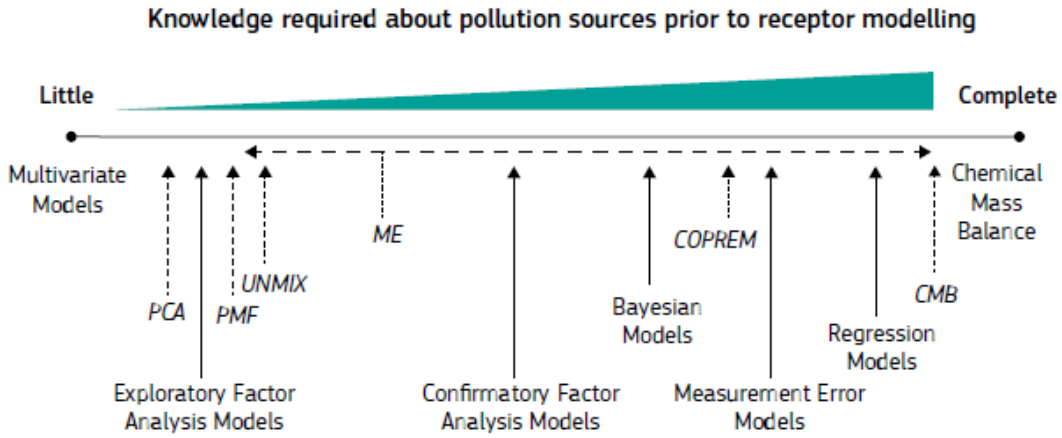

Fig. 4. Knowledge of air pollution sources required for different receptor models (Viana *et al.*, 2008)

Most of SA studies cannot provide information about geographical location of sources or the effect of polluted regions downwind of receptor site. SA results are frequently supplemented by procedures to identify the direction of air masses associated with high pollution levels or where compounds of interest come from (Rizzo and Scheff, 2007; Gildemeister *et al.*, 2007; Du and Rodenburg, 2007). For small scales this can be done by wind rose analysis, on the other hand, the long-range transport (LRT) may be better evaluated using air mass backward trajectories model (Draxler and Rolph, 2014). Air mass back trajectory analysis is frequently used to point out the direction and sources of air pollution at a receptor site (San José *et al.*, 2005). Back trajectories trace the path of a polluted air parcel backward in time and have long been used to track the history and pathway of air parcels arriving at a specific location since they were first developed in the 1940s (Petterssen, 1940). Computational advances in the 1960s allowed isentropic analysis and

trajectory calculations to be performed graphically on computers (Danielsen and Bleck, 1967). Trajectory clustering techniques, which assign trajectories into representative spatial groups, are a popular method to combine the flow climatology and pollutant transport pathways with particle or gas measurements at a sampling station (Sirois and Bottenheim, 1995; Dorling *et al.*, 1992).

2.3 Sources of combustion related to aerosol particles in urban environment

Atmospheric dynamic processes change the physical and chemical characteristics of combustion generated aerosol particles after they are emitted into the atmosphere. Previous studies have suggested that the major influence on contributions to the PNC is caused by the included vehicle exhaust emissions during the traffic peak hours and photochemical nucleation events (Ketzel *et al.*, 2004, Cyrys *et al.*, 2008, Pey *et al.*, 2008), the residential heating during winter periods (Hussein *et al.*, 2004) and new particle formation (NPF) by photochemical reactions (Perez *et al.*, 2010). Typically, the formation process occurs over large areas (Plauškaitė *et al.*, 2010). Therefore, it may significantly contribute to changing the regional climate (Spracklen *et al.*, 2008). In recent years, these events have been studied extensively in background (O'Dowd *et al.*, 2002; Rodríguez *et al.*, 2005) and also urban (or polluted) areas (Tuch *et al.*, 2006; Kulmala *et al.*, 2005). It was found that the anthropogenic emission sources such as manufactories, biofuel burning (Karvosenoja *et al.*, 2008; Kumar *et al.*, 2010), the aircraft activity (Hu *et al.*, 2009), the natural sources (Holmes, 2007), the biomass burning (Simmonds *et al.*, 2005; Wardoyo, 2007) and the LRT (Beverland *et al.*, 2000) were important contributors to the PNC mostly in the size range below 300 nm. The aerosol particles from the residential combustion can sometimes grow in size in the urban environment mainly due to condensation of gases (Park *et al.*, 2008). The exhaust emissions from the gasoline and diesel-fuel vehicles

remain the dominant source in polluted urban environments (Harrison *et al.*, 2011; Srinivas *et al.*, 2011).

The size range for the road traffic emissions is consistent with the particle number size distributions (PNSDs) for the gasoline direct injection and the diesel engines with the majority of particles in the size diameter interval of 20–60 nm and 20–130 nm, respectively (Maricq *et al.*, 1998, Morawska *et al.*, 1998; Morawska *et al.*, 2008). These can alone contribute up to about 90% of the total PNCs (Perez *et al.*, 2010) reaching magnitudes of 10^4–10^5 cm^{-3} during the nucleation events (Cheung *et al.*, 2011). In the case of the South-Eastern Baltic Sea region, NPF has been studied by Plauškaitė *et al.* (2010) in a relatively clean marine background environment. These studies revealed NPF taking place more frequently in conjunction with high levels of solar radiation. In spite of its importance, no long-term continuous measurement campaigns studying the PNC dynamics have been carried out at urban sites in Lithuania so far. As NPF was found to be a regional phenomenon it was expected that NPF would also occur in the polluted urban areas.

2.4 Sources of carbonaceous aerosol in background environment

Open biomass burning and residential heating provides a substantial contribution to carbonaceous aerosol particles in the atmosphere (Radzi Bin Abas *et al.*, 2004; Zhang *et al.*, 2008; Saarnio *et al.*, 2010). Fine particles directly emitted from biomass burning sources are described as primary OA. The SOA is formed in the atmosphere as the plume ages through photochemical processes driven by sunlight (Capes *et al.*, 2008). The North and Eastern European countries are considered to play a significant role for the microphysical, chemical and optical aerosol properties in the Baltic Sea region (Zawadzka *et al.*, 2013; Mann *et al.*, 2014). The LRT of atmospheric aerosol particles is a transboundary problem that can have significant impacts on aerosol particle levels in the background European areas (Abdalmogith and

Harrison, 2005, Moroni *et al.*, 2015), when air masses arrive during suitable meteorological conditions from regions with high emissions.

The main type of biomass burning in South-Eastern Baltic sea region in early spring is vegetation burning. Long-term measurements of carbonaceous aerosol particles performed in this area (Ovadnevaite *et al.*, 2006, Ulevicius *et al.*, 2010, Byčenkienė *et al.*, 2011) reported a yearly occurrence of high biomass burning OA levels during March–April related to regional transport from the Kaliningrad region, Ukraine and South-Western part of Russia surrounding the Black Sea, but information on the nature and chemical composition of the biomass burning aerosol in Lithuania is still limited The LRT of emissions from forest and agricultural fires to Europe was recognized previously and pollutants from fires in Canada (Müller *et al.*, 2005) and the USA have been observed. The emission sources of fine particles during LRT events have been studied in Northern Europe as well. As the mass concentrations of fine particles are commonly lower in Northern Europe countries compared with Central Europe LRT can have a notable impact on the concentration levels (Anttila *et al.*, 2008). It was shown that emissions from wildfires from the Ukraine and European part of Russia increases the aerosol particle mass concentrations in these countries frequently during spring and summer (Ovadnevaite *et al.*, 2007; Saarikoski *et al.*, 2007).

2.5 Conclusions

Radiative climate forcing is rapidly increased by anthropogenic activity and the release of trace gases into the atmosphere. However, with small exceptions, aerosol particles act as negative climate forcing agents, and thus can help to increase the surface albedo. In order to better understand the processes in the atmosphere, aerosol particle physical and chemical properties should be investigated. Particle number concentration and size distribution are good methods for evaluating processes submicron particles undergo in various environments.

Carbonaceous aerosol particles are good indicators for biomass burning activity, thus in recent years, SA have come to the forefront of air pollution research. The knowledge of aerosol particle origin and contribution to pollution level can help better understand the sources of local air pollution at a given location.

3 INSTRUMENTATION AND RESEARCH METHODS

3.1 Instrumentation

3.1.1 Condensation particle counter

Airborne particle counters are usually used to assess examine number concentration in various environments and assess the main particle pollution sources and formation processes. Several elaborate particle counting techniques are widely used in measuring aerosol particles below 1 µm in size. Standard optical particle counters struggle to measure particles smaller than 300 nm, thus the range for < 300 nm particle detection is extended by using condensation particle counter (CPC). One of the basic physical aerosol parameter, PNC was measured using CPC. The working principle of particle detection of such counters is based on the intensity of scattered light (Mordas *et al.*, 2008). In CPCs, aerosol particles are grown by a condensation to a micron sizes, thus allowing easy detection with simple optics (Fig. 5). CPC is operated on three basic principles: super-saturation of the working fluid, aerosol particle droplet growth due to the condensation of super-saturated vapour and scattered light detection by photo detector from aerosol particles. First of all, prior detection particles are grown in the heated butanol (or other working fluid) chamber. The environment is fully saturated. The injected aerosol particles become the tiny grains for further growth by working fluid condensation on the surface. In this case, there are several limitations for such measurement.

Most of the counters are counting particles directly by the amount of light each of them scatters. Increased particle concentration will dramatically increase scattered light coincidence at the detector. Thus, light scattering pattern for different PNC segments should be described.

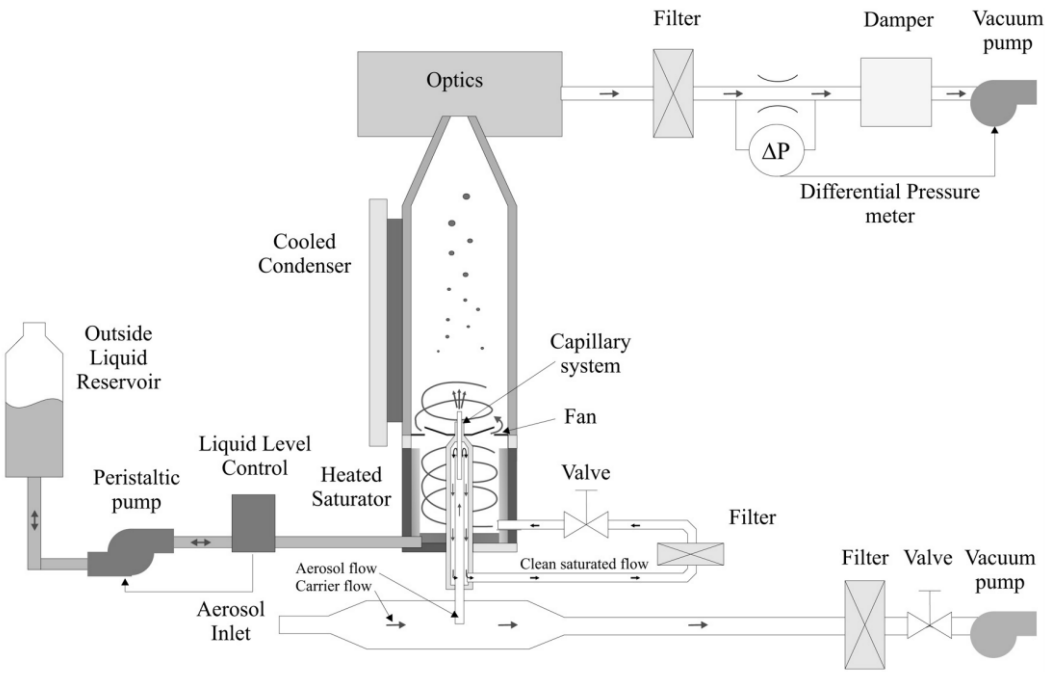

Fig. 5. Principal scheme of CPC (model UF-02proto). The main instrument components are depicted: working fluid container, saturator, condenser and particle detection section consisting of laser and optics (Mordas *et al.*, 2008).

The critical super-saturation for homogeneous nucleation is typically around 300%. The smallest size at which condensation will occur at a particular super-saturation is referred to as the Kelvin diameter. This size dependence is because vapour molecules are able to escape more easily from a curved than flat surface thus increasing saturation vapour pressure with decreasing radius of curvature. In CPCs, super-saturation is controlled to be in the range of 100–200%. However, critical super-saturation must be avoided so that droplets will not form in particle-free air. Working parameters of CPC (model UF-02proto) are described, as follows: working fluid – butanol; aerosol sample flow – 1 $L \cdot min^{-1}$.; condenser temperature is 10°C; saturator temperature is 43°C; cut-size diameter – 4.3 nm; the maximum detection limit of aerosol particle concentration is $1.5 \cdot 10^5$ cm^{-3}; estimated error varies in the range from 5% to 10%.

The PNC was measured each 1 min and averaged for 1-h data sets. The average, median, *SD*, percentiles (5^{th}, 25^{th}, 75^{th}, 95^{th}), minimal and maximal PNC values were calculated.

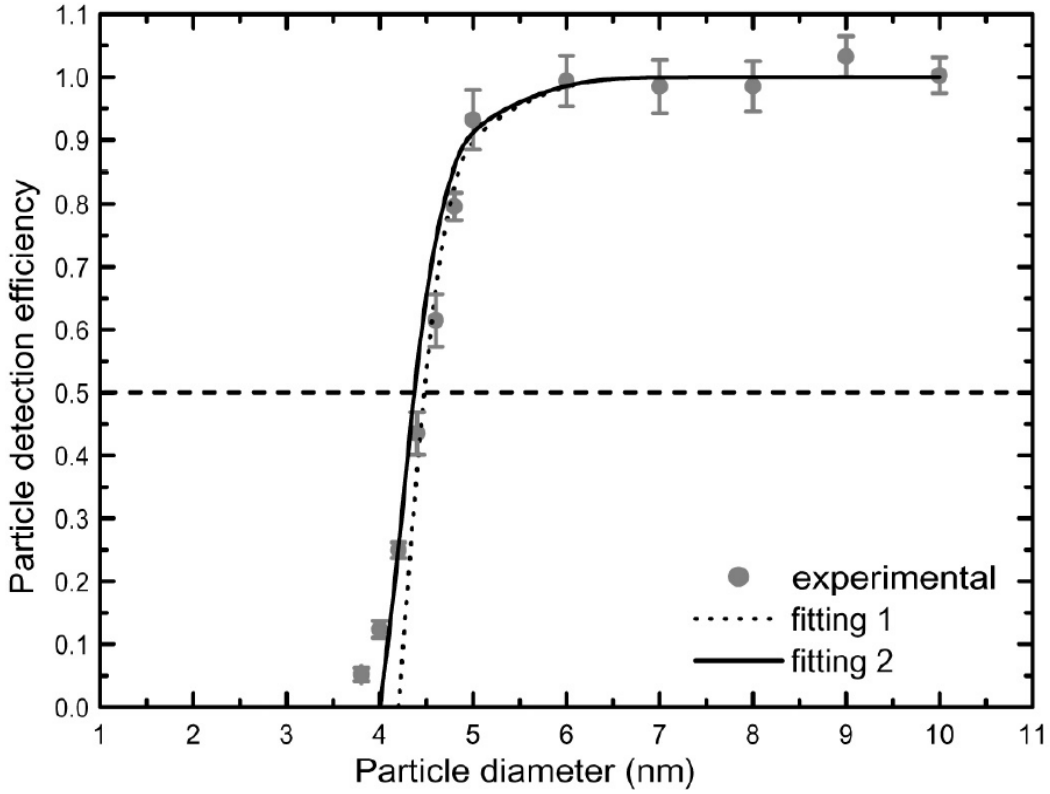

Fig. 6. Particle detection efficiency of a UF-02proto as a function of the particle size for silver particles. Two (Mordas *et al.*, 2008).

CPCs are mainly used to provide PNC measurements. Any information on the original size of particles is lost because of condensational growth. Other instruments, such like differential mobility particle sizer or scanning mobility particle sizer (SMPS), combined with CPC, can be used for aerosol particle size distribution measurements. Additionally several CPCs with different lower cut-sizes can be used to provide fast response of ultrafine particle detection, but with a rough estimation (Kulmala *et al.*, 2007).

3.1.2 Aerodynamic particle sizer

The aerodynamic particle sizer (APS, TSI model 3321) uses the time of flight (TOF) technique in order to measure the aerosol particle size distribution (Fig. 7). Particles are illuminated with two laser beams of light separated in space from 90 to 100 μm. The beams are vertically and horizontally polarized. The TOF technique for aerodynamic sizing of particles involves acceleration of aerosol particles in a response to the accelerated flow of the aerosol sample through a nozzle (APS Model 3321 instruction manual, 2004).

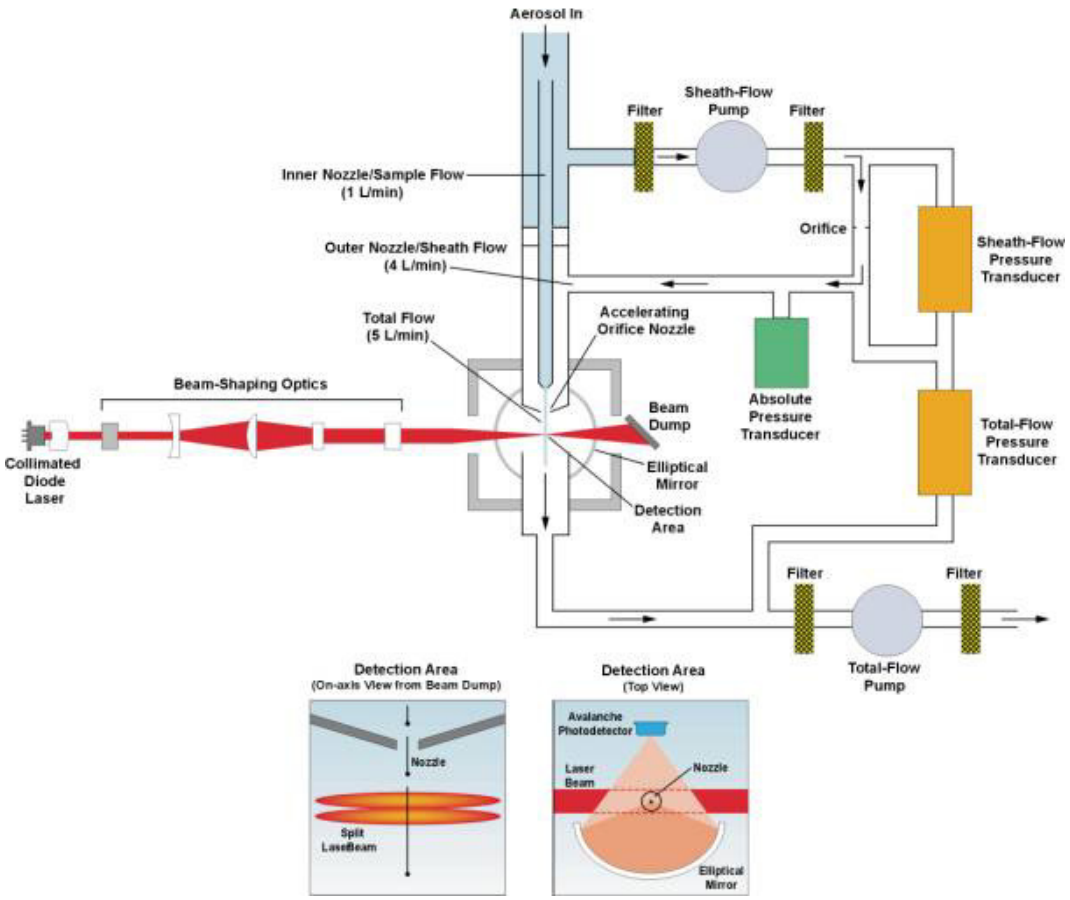

Fig. 7. Principal scheme of aerodynamic particle sizer (APS, TSI model 3321, instruction manual, 2004)

The detected signal of particle movement between two laser beams yield two crests peak response. Hereafter, this response is analysed and classified into 4 categories, i.e. events. The 1st event occurs when the signal of small particle cannot stay above the threshold, and only one crest is detected. This

event corresponds to the particle concentration in the size channel < 0.523 µm, and TOF is not calculated. The 2nd event stands for valid TOF measurements – two crests above the threshold are detected. The aerosol particle concentration and its size are calculated. The 3rd type of event represents more than two crests detection, thus it is not included in the results. Finally, the 4th type of event is outside the maximum detection time limit – 4.096 µs. This occurs due to large re-circulating particles.

The lower detection limit of the particle size is defined by the wavelength, optical properties of the source and the detector, and the physics of light itself. On the other end, the large aerosol particle detection is influenced by sampling and particle losses on the walls. It is suggested that the counting efficiency in APS channels is increasing by going from small to large particle size bins (30% at 0.5 µm; 90% at 1.0 µm) (Peters and Leith, 2003). The manufacturer of APS (TSI model 3321) states that detecting of concentrations of up to 1000 cm^{-3} at 0.5 µm and 10 µm, will result in the coincidence of < 5% and < 10%, respectively. The APS samples aerosol at 1.0 ± 0.1 $L \cdot min^{-1}$, while the sheath flow – 4.0 ± 0.1 $L \cdot min^{-1}$. Detected aerosol particle aerodynamic diameter (D_A) is in the range from 0.5 to 20.0 µm.

3.1.3 Scanning mobility particle sizer

The SMPS classifies aerosol particles according to their mobility in the electric field (Sioutas, 1999). There are three main components in SMPS structure: the neutraliser, the differential mobility analyser (DMA) and the CPC. During measurements, aerosol particles pass through an inertial impactor, which removes large particles outside the measurement range, thus the multiple charging errors in data inversion are reduced. In the neutraliser charged aerosol particles reach Fuch's equilibrium (Fuchs, 1963; Kim *et al.*, 2005). Then the particles enter the DMA. At this point particles are being separated according to their electrical mobility. Negative direct power supply (0–10 kV) was applied to the rod in the middle of the cylinder (Dubey and

Dhaniyala, 2008). Ramping or stepping the voltage yields an electrical particle mobility distribution, which is inverted into a PNSD (Wiedensohler *et al.*, 2012). Particles with the same sign charge as rod are repelled towards and deposited on the outer wall, those with a neutral charge exit with excess sheath flow. Only those particles with distinct electrical mobility size (combination of correct charge and particle movement velocity) were bent into the exit slit, where PNC is counted by CPC. The principal scheme of the SMPS is presented in Fig. 8. The typical flow parameters for SMPS IfT model: aerosol flow was 1.0 ± 0.2 L·min^{-1}, sheath flow – 5.0 ± 0.1 L·min^{-1}. The detection efficiency and the losses in the transport lines and inside the DMA are evaluated from laminar flow tube diffusion loss equations. The measurement duration was 5 min and the aerosol PNSD was measured in 71 bins. The measurement size range was from 9 to 840 nm.

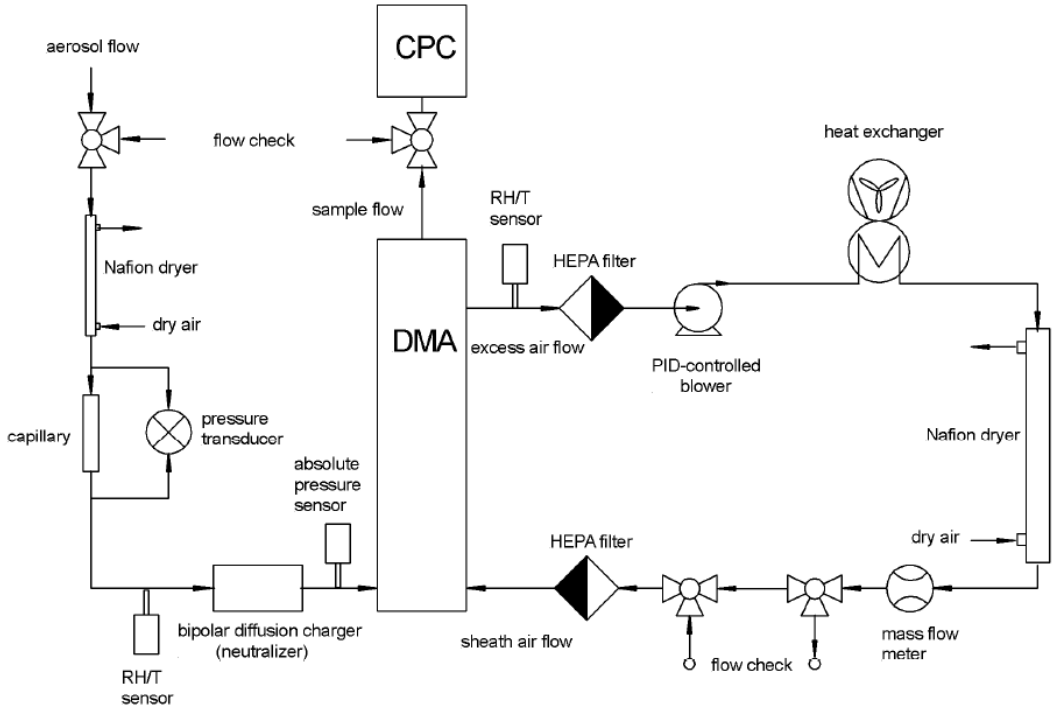

Fig. 8. Principal scheme of scanning mobility particle sizer (SMPS, model IFT, Wiedensohler *et al.*, 2012).

The multi-lognormal distribution function was considered as the best approach to parameterise PNSD (Seinfeld and Pandis, 2008). A common lognormal mode is presented in Eq. (1):

$$\frac{\mathrm{dN}}{\mathrm{d}\log \mathrm{dD_p}} = \frac{\mathrm{N_{TOT}}}{\sqrt{2\pi}\log\sigma_\mathrm{g}} \exp\left(-\frac{\left(\log \mathrm{D_p} - \log \mathrm{D_g}\right)^2}{2\left(\log\sigma_\mathrm{g}\right)^2}\right), \quad (1)$$

N_{TOT} – total particle number concentration (also can be replaced by surface, volume or mass concentration), D_g is the geometric mean diameter, σ_g – the geometric standard deviation, D_P is the particle diameter. The right side of the equation is a multi-lognormal distribution function and the left side is measured PNSD.

In lognormal size distributions, D_g of normal distribution is replaced by the count median diameter (CMD). The lognormal particle size distribution is symmetrical. Then distribution is symmetrical, the mean and the median are equal. Therefore, for a lognormal size distribution Eq. (2):

$$D_\mathrm{g} = CMD = (D_1^{n_1} \cdot D_2^{n_2} \cdot D_3^{n_3} \ldots D_N^{n_N})^{1/N}, \quad (2)$$

where D_i – a midpoint particle size, n_i – number of particles in group *i* having a midpoint size D_i and $N = \sum n_\mathrm{i}$. The geometric standard deviation describes how the values are spread in the distribution, it is always > 1.0, It was calculated using Eq. (3):

$$\sigma_\mathrm{g} = 10^{\sqrt{\frac{\sum_{D_{\mathrm{i,min}}}^{D_{\mathrm{i,max}}} (\log D_\mathrm{i})^2 \cdot \frac{\mathrm{d}N}{\mathrm{d}\log D_\mathrm{p}} \cdot \mathrm{d}\log D_\mathrm{p}}{N_{\mathrm{mode}}} - (\log D_\mathrm{g})^2}}, \quad (3)$$

where $D_{\mathrm{i,min}}$ and $D_{\mathrm{i,max}}$ are the upper and lower limits of the particle size distribution mode, N_{mode} is the total particle number concentration of the mode. In a lognormal distribution, 95% of particle diameters fall within a size range of $D_\mathrm{g} \pm 2 \cdot \sigma_\mathrm{g}$. The lower limit of this distribution is $D_\mathrm{g} \cdot \sigma_\mathrm{g}^{-2}$ and the upper limit – $D_\mathrm{g} \cdot \sigma_\mathrm{g}^{2}$. Aerosol particle size distribution with lower σ_g values are considered to be monodisperse and wider distributions, i.e. $\sigma_\mathrm{g} > 1.25$ – polydisperse.

3.1.4 Aethalometer

The Aethalometer (Magee Sci., model AE31) was deployed to measure aerosol particle light-absorption properties in the marine background environment of the South-Eastern Baltic Sea region. This instrument provides real-time data and can be operated continuously for a long time without interference. The general principles of its operation are the optical absorption of carbonaceous aerosol particles on the quartz filter. The measurements are conducted sequentially at the seven wavelengths (λ 370, 450, 520, 590, 660, 880 and 950 nm). The values obtained at the wavelength of 880 nm are considered to be the standard value for BC concentration measurement (Kirchstetter and Novakov, 2007). The optical attenuation method is well described in Eq. (1):

$$\mathrm{BC} = \frac{\sigma_{ABS}}{\alpha_{ABS}} = \frac{1}{\alpha_{ABS}} \frac{\mathrm{A}}{Q} \frac{\Delta ATN}{\Delta t}, \quad (1)$$

where σ_{ABS} is absorption coefficient in nm^{-1}, α_{ABS} is mass absorption efficiency in $\mathrm{m}^2 \cdot \mathrm{g}^{-1}$, A is an area spot (cm^2), Q is a flow rate in $\mathrm{L} \cdot \mathrm{min}^{-1}$ and ΔATN is a change of light attenuation during the period of time Δt.

The aethalometer converts light attenuation to the BC mass using a fixed specific attenuation cross-section α_{ABS} of 16.6 $\mathrm{m}^2 \cdot \mathrm{g}^{-1}$ of BC and the spot size 0.5 cm^2, other settings depend on the chosen operation settings (Hansen and Schnell, 2005). The Aethalometer output was calculated to mass concentration in notation of $\mu\mathrm{g} \cdot \mathrm{m}^{-3}$ through an internal conversion use assuming the mass absorption efficiency. In order to compensate filter loading effects and filter shadowing effects and error correction an empirical algorithms (Weingartner *et al.*, 2003, Virkkula *et al.*, 2007) were used.

3.1.5 Aerosol chemical speciation monitor

An aerosol chemical speciation monitor (ACSM; An Aerodyne Research Inc.) was deployed at marine background environment site in Preila for the purposes of measuring continuous non-refractory (NR) chemical components: organic components, nitrate, ammonium, sulphate and chloride (Table 1).

Table 1. Main ion fragments used to identify inorganic and organic aerosol species in ACSM mass spectra (Canagaratna *et al.*, 2007)

Group	Molecule/ Species	Ion fragments	Mass fragments
Water	H_2O	H_2O^+ , OH^+, O^+	**18**, 17, 16
Ammonium	NH_3	NH_3^+, NH_2^+, NH^+	17, **16**, 15
Nitrate	NO_3	HNO_3^+, **NO_2^+, NO^+**	63, **46, 30**
Sulphate	H_2SO_4	$H_2SO_4^+$, HSO_3^+, SO_3^+, **SO_2^+, SO^+**	98, 81, 80, **64, 48**
Organic (OOA)	$C_NH_MO_Y$	H_2O^+, CO^+, **CO_2^+**, **$H_3C_2O^+$**, HCO_2^+, $C_NH_M^+$	18, 28, **44**, **43**, 45, ..
Organic (HOA)	C_NH_M	$C_NH_M^+$	27, 29, **41, 43, 55, 57,** 69, 71

A impactor PM_{10} was supplied in front of the sampling inlet to remove coarse particles with a cut-off size at 10 μm. The residence time in the sampling tube is 5 s. The resulting aerosol flow passed through a Nafion drier (PermaPure LLC, model MD-110-48S-4) and 2.5 m long stainless steel sampling tube with 6 mm outer diameter before reaching the ACSM inlet.

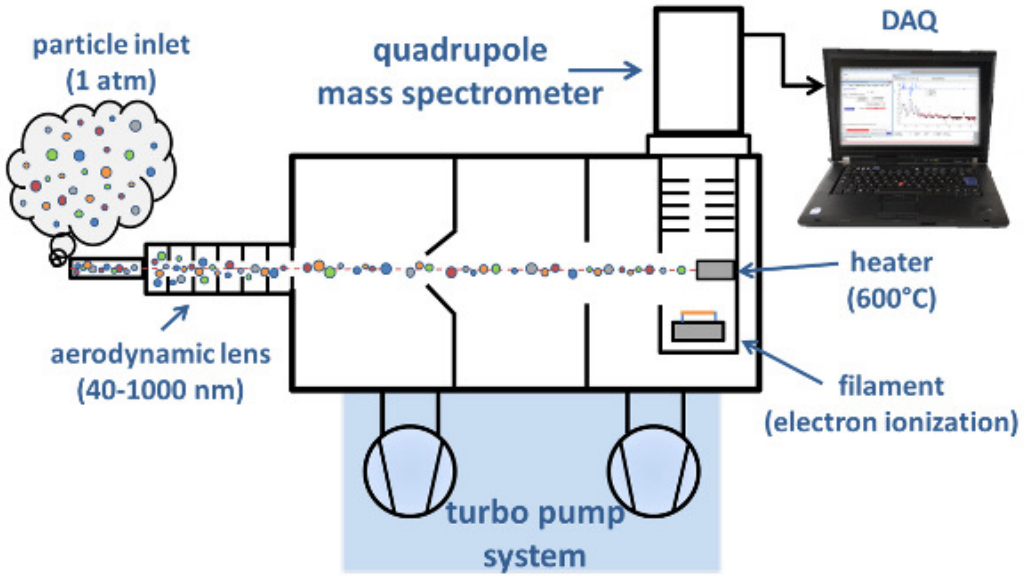

Fig. 9. Principal representation of aerosol chemical speciation monitor (ACSM, Aerodyne Research, Inc., source[3]: *beta.dwd.de*)

Aerosol particles with D_A varying from 40 to 1000 nm were sampled at a flow rate of 1 L min^{-1} into ACSM through a 100 µm critical orifice mounted at the inlet of an aerodynamic lens (Fig. 9). The particles are then directed onto a resistively heated surface where NR-$PM_{1.0}$ components are flash vaporised on impaction with the vaporiser typically operated at 600°C and ionized by 70 eV electron impact. During this study, the ACSM was operated at a time resolution of 30 min for typical aerosol component loadings in notation of µg·m^{-3} with mass spectrometer scan rate of 500 ms·amu^{-1} and mass to charge ratio (m/z) varying from 10 to 150. The detailed description of ACSM has been given in (Ng *et al.*, 2011a). The m/z calibration of the analyser was determined based on measured air (N_2-28, O_2-32, Ar-40) and water vapour (H_2O-18, 17) in the spectra, which is always present. Chemically resolved aerosol composition and aerosol mass spectra (< 200 amu) were used to extract the chemically speciated aerosol component loadings. The time series of mass spectra were processed using multivariate factor analysis method to extract chemically distinct groups. NH_4NO_3 is used as the calibration aerosol because it is well focused by the

aerodynamic lens (all particles reach the vaporiser) and it vaporises with 100% efficiency (CE = 1).

3.1.6 The carbon stable isotope ratio analysis

The carbon stable isotope ratio analysis (Boutton, 1991) was performed with the elemental analyser (Flash EA 1112) coupled with the isotope ratio mass spectrometer (IRMS, Thermo Finnigan Delta Plus Advantage model) (Fig. 10). The aluminium foil samples were cut into equal pieces and were packed into tin capsules (Garbaras *et al.*, 2008).

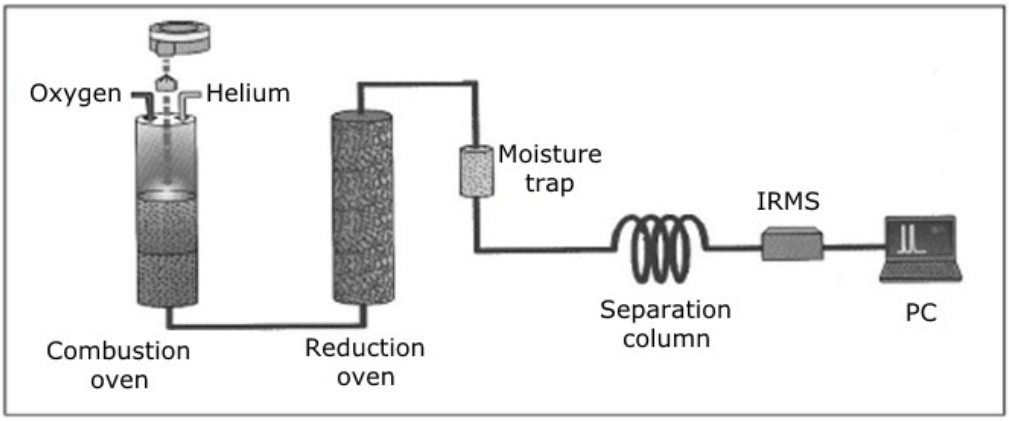

Fig. 10. Principal scheme of isotope ratio mass spectrometry (Garbaras *et al.*, 2008)

The packed samples were combusted instantaneously in the furnace filled with oxygen gases at the temperature of 1020°C. All gases are transferred into the reduction column, which was maintained at 650°C. The water vapour of the sample is removed by using the magnesium perchlorate trap. Then the gas mixture is separated in the column PoraPlot Q (at the temperature of 50°C). Separated gas was delivered to the mass spectrometer ionisation cell through the gas distribution device ConFlow III. The helium flow is maintained at 80 mL·min^{-1}. The value of ionized CO_2 is measured with IRMS using operational software and results were reported as $\delta^{13}C_{TC}$ in notation of per mill (‰) units in Eq. (2):

$$\delta^{13}C_{TC} = \left(\frac{\left(\frac{^{13}C}{^{12}C}\right)_{sample}}{\left(\frac{^{13}C}{^{12}C}\right)_{standard}} - 1 \right) * 1000‰, \quad (2)$$

^{13}C:^{12}C isotopic ratio of carbon in the sample was compared to the reference standard Pee Dee Belemnite, which has one of the largest ^{13}C:^{12}C ratio in the world – $1.124 \cdot 10^{-2}$ (Brand, 1996). The total carbon (TC) concentration in the sample was estimated from the calibration curve of a combusted sample of well known carbon material.

Additional measurement data was obtained from the Environmental Protection Agency (EPA, source[4]: *stoteles.gamta.lt*) stations in Vilnius (Savanorių and Lazdynai) and in Klaipeda city centre. Data contained mass concentration of PM_{10}, trace gases (NO, NO_x, NO_2, SO_2, CO, O_3) and meteorological parameters (air temperature (*T*), *RH*, wind speed (*WS*), wind direction (*WD*) and atmospheric pressure (*p*)). PM_{10} measurements were conducted with the particulate dust monitor (Environnement S. A. model MP101M), which is based on β-attenuation. Continuous NO_x measurements were conducted with NO_2 analyser (Environnement S. A. model AC31M) based on chemiluminescence method. SO_2 measurements were based on UV fluorescence method (Environnement S. A. model AF21M), CO measurements were based on infrared gas filter correlation (Environnement S. A. model CO11) and ozone measurements were based on UV absorption (Environnement S. A. model O341M).

3.2 Research methods

3.2.1 Receptor models

The PSCF and CWT methods belong to a group of hybrid receptor models (Cheng *et al.*, 2013; Han *et al.*, 2007), because both concentration of pollutants (i.e. BC mass concentration, PNC, $PM_{2.5}$) and air mass backward trajectories are used for SA. They are used for determining the areas which contribute the most to the pollution levels at the receptor site.

The PSCF technique for source identification is a conditional probability that air mass in upwind areas passing through the grid cell $i \times j$ will have had the same or higher than criterion value concentration upon arrival at the trajectory endpoint (Ashbaugh *et al.*, 1985; Pekney *et al.*, 2006; Hopke, 2003). In particular, PSCF and CWT methods can be expressed by Eq. (3):

$$C_{i,j} = \frac{\sum_{T=1}^{L} f(C_T)\tau_{i,j,T}}{\sum_{T=1}^{L} \tau_{i,j,T}}, \quad (3)$$

where *i* and *j* are the indices of the trajectory segments; *L* is the total number of the trajectories; $f(C_T)$ is a conditional function of mean concentration C_T at the receptor site, measured on arrival of trajectory *T*; $\tau_{i,j,T}$ is the number of trajectory *T* segment endpoints in a grid cell $i \times j$ divided by the total number of endpoints for trajectory *T*. The meaning of $C_{i,j}$ can be interpreted as the intensity of sources in the grid cell $i \times j$.

In PSCF method, $f(C_T)$ is the step function that equals 0, when the concentration C_T is below a certain value, and is equal to 1 when the concentration values are above or equal to the criterion value (Kabashnikov *et al.*, 2011). A small number of trajectory segment endpoints result in high $C_{i,j}$ values with significant uncertainties. In order to avoid such discrepancy for grid cell with low number of trajectory endpoints, an empirical weight function $W(\tau_{i,j,T})$ (Zeng and Hopke, 1988; Ara Begum *et al.*, 2005) is considered:

$$W(\tau_{i,j,T}) = \begin{cases} 1.0; & \tau_{i,j,T} \leq 10 \\ 0.7; & 6 \leq \tau_{i,j,T} \leq 9 \\ 0.4; & 3 \leq \tau_{i,j,T} \leq 5 \\ 0.2; & \tau_{i,j,T} \leq 2 \end{cases}, \quad (4)$$

The meaning of $W(\tau_{i,j,T}) = 1$ is that only one trajectory has passed over the grid cell $i \times j$. By this method, air masses from potential source locations, which are crossing the receptor site, are evaluated. This analysis excludes evaluation of emission inventory of a pollutant (Lucey *et al.*, 2001). Another limitation of this model is that grid cell $i \times j$ can obtain $C_{i,j}$ value only when concentration value measured at the receptor site is equal to or higher than the

criterion value. Thus, it is useful method for identifying strong emission sources and problematic for moderate ones (Wang *et al.*, 2006).

In order to calculate the CWT values, the whole geographic region covered by the backward trajectories is divided into a gridded $i \times j$ array. The geographical domain covers an area of interest, based on the maximum distance travelled by the trajectories during the observation period, with receptor site in the centre of domain. Each grid cell is assigned with a weighted concentration $C_{i,j}$ by averaging sample concentrations at the receptor site and associating it with backward trajectories as defined in Eq. (3). In case of CWT method $f(C_T) = C_T$ (Hsu *et al.*, 2003). The whole calculations are repeated for all trajectories.

3.2.2 Air mass trajectory cluster and sector analysis

K-mean trajectory clustering method was performed for analysing the association between aerosol particle physical parameters (i.e. aerosol component loadings, BC and PNC) and their attribution to the air mass origin (Beddows *et al.*, 2009; Dall'Osto *et al.*, 2011). The geographical coordinates were converted to Cartesian coordinate system (*x*, *y*) using the azimuthal equidistant projection with the central point set to geographical position of the receptor site as in Eqs. (5) and (6). The homogeneity within clusters was achieved by minimizing the angle distances between the corresponding coordinates of the individual trajectories (Sirois *et al.*, 1995):

$$d_{12} = \frac{1}{n}\sum_{i=1}^{n} cos^{-1}\left(0.5\frac{A_i+B_i-C_i}{\sqrt{A_iB_i}}\right), \quad (5)$$

where

$$A_i = (X_1(i) - X_0)^2 + (Y_1(i) - Y_0)^2, \quad (6a)$$

$$B_i = (X_2(i) - X_0)^2 + (Y_2(i) - Y_0)^2, \quad (6b)$$

$$C_i = (X_2(i) - X_1)^2 + (Y_2(i) - Y_1)^2. \quad (6c)$$

The variables X_0 and Y_0 define the position of the receptor site, $X_1(i)$, $Y_1(i)$ and $X_2(i)$, $Y_2(i)$ coordinates of i segment for trajectories 1 and 2. In order to reduce

the number of errors in the model, the trajectories of similar history, which have the similar path of advection and velocity of air flow, were grouped into similar clusters.

Trajectory sector analysis is a statistical approach used for computation of mean concentrations from various clusters to evaluate the effect of air masses arriving from geographical sector on pollutant concentration at the receptor site. In this thesis, the trajectory cluster directions were defined by 6 sectors of 60° each, starting with the 1st sector from 20° to 80°. Eqs. (7) and (8) were used to calculate the mean concentration (C_j) from sector j:

$$C_j = \frac{\sum_{i=1}^{N} C_i f_{i,j}}{N_j}, \quad (7)$$

$$N_j = \sum_{i=1}^{N} f_{i,j}, \quad (8)$$

The relative contribution ($\%C_j$) from sector j was calculated in Eq. (9):

$$\%C_j = \frac{C_j N_j}{\sum_{j=1}^{6} C_j N_j \times 100}, \quad (9)$$

where N is the total number of trajectories, C_i – the concentration of pollutant in i trajectory, $f_{i,j}$ – the time passed through the sector j for the i trajectory, and N_j – the total time during which trajectories passed through sector j (Zhu *et al.*, 2011).

3.2.3 Principal component analysis

Measurements of the ambient aerosol particles provide better understanding of atmospheric processes. Nowadays different aerosol particle physical properties are measured simultaneously by such network sites as GAWSIS, AERONET (Holben *et al.*, 1998) and ACTRIS (Asmi *et al.*, 2012). Gathering and combining aerosol measurement data accumulates large data sets, which must be processed in order to be suitable for atmospheric and climate modelling. Different aerosol properties are frequently inter-comparable, for instance, aerosol particle size and shape vs. total aerosol light scattering (Pollack and Cuzzy, 1980; Chamaillard *et al.*, 2006), accumulation

mode refractory soot volume vs. total aerosol light absorption (Clarke *et al.*, 2004).

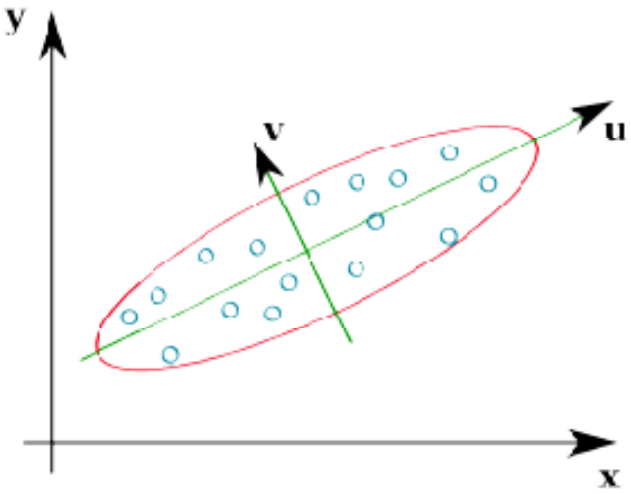

Fig. 11. Principal component analysis: transformation of Cartesian coordinate system

One of the way of simplifying variable aerosol parameters in the data sets is by applying principal component analysis (PCA, Everitt and Howell, 2005; Jeon *et al.*, 2001). In PCA model, it is convenient to express variable parameters in terms of its principal components (PC) rather than relying on Cartesian coordinate system (Fig. 11).

In order data to be suitable for analysis, data sets mathematically undergo linear orthogonal transformation, so that a component with the largest variance becomes a new coordinate axis, it is called primary principal component (PC_1). The second principal component (PC_2) is perpendicular to the primary axis, thus such operation will fulfil the condition that transformed data set variables must be linearly uncorrelated. This relation is depicted in Eq. (10), as follows:

$$PC_i = \sum_{j=1}^{J-1} b_{i,j} \cdot v_j, \quad (10)$$

$b_{i,j}$ is a factor loading, which indicate how strongly a specific original variable v_j contributes to the principal component PC_i. Each data set may have the same number of principle components as variables or less, but for analysis only

those with the largest variance are important. Variance of the data set points is expressed by using pairs of two parameters: an eigenvector is a direction of the PC_i and eigenvalue is the variance of this direction. The PCs with an eigenvalue greater than or equal to 1, are in general considered as being of statistical significance (Kaiser criterion), other components with eigenvalue less than 1 may be neglected.

3.2.4 Determination of aerosol particle mass

For evaluation of aerosol particle mass concentration SMPS-APS measurement data was processed, based on the algorithms, relating aerosol particle size diameters and particle volume size distribution (Sioutas *et al.*, 1999; Peters *et al.*, 2006; Shen *et al.*, 2002). As two sizing equipment use different principles of operation, in case of SMPS mobility diameter (D_M) and in case of APS aerodynamic diameter (D_A) are converted into physical equivalent diameter. In Eq. (11), the physical equivalent diameter relates to D_A (Hinds, 2012):

$$D_{VE} = D_A \sqrt{\left(\chi \frac{\rho_0}{\rho_P} \frac{C_S(D_A)}{C_S(D_{VE})}\right)}, \quad (11)$$

where χ is dynamic particle shape (for spherical particles: $\chi = 1$), ρ_0 – a reference density in g·cm^{-3}, ρ_P – particle density in g·cm^{-3}, $C_S(D_A)$ and $C_S(D_{VE})$ – Cunningham slip correction factors for aerodynamic and physical equivalent diameters. In Eq. (12) the physical equivalent diameter relates to D_M (DeCarlo *et al.*, 2004):

$$D_{VE} = D_M \left(\frac{C_S(D_{VE})}{\chi\, C_S(D_M)}\right), \quad (12)$$

where $C_S(D_M)$ is Cunningham slip correction factor for D_M. Combining Eqs. (2) and (3), the D_M relation to D_A is estimated in Eq. (13):

$$D_M = D_A \sqrt{\frac{\rho_0}{\rho_P}} \left(\frac{\chi}{C_S(D_{VE})}\right)^{3/2} C_S(D_M) \sqrt{C_S(D_A)}., \quad (13)$$

Simplified version of Eq. (13) is derived by taking into account several

assumptions: particles are spherical, therefore $\chi = 1$ and $D_M = D_{VE}$. This newly settled conditions are depicted in Eq. (14):

$$D_M = D_A \sqrt{\frac{1}{\rho_p}}, \quad (14)$$

where particle density ρ_P is chosen according to aerosol particle chemistry, its size and environmental conditions (Šakalys *et al.*, 2015).

In this thesis, while combining particle size distributions, derived from APS-SMPS measurements, no correction factor was applied for SMPS concentrations, due to the lack of overlapping size range from both of the equipments (Khlystov *et al.*, 2004). The aerosol particle density was $\rho_P = 1.3$ g·cm^{-1}. PNSD for each size interval were converted to volume and to mass concentrations using the following Eq. (15):

$$M_{TOT} = \frac{\pi}{6} \rho_P N \left(\frac{D_A}{\sqrt{\rho_p}} \right)^3, \quad (15)$$

3.2.5 Organic aerosol triangular plot

Simplified method of characterizing the aging of OA in the atmosphere from ACSM has been identified. OA is classified mainly by hydrocarbon-like and oxygenated OA (HOA and OOA, respectively) (Volkamer *et al.*, 2006). The mass spectrum of OOA highly resembles aged and oxidised OA and correlates with SO_4^{2-}, thus it can be estimated as a good indicator for SOA (Zhang et al, 2005). It could be deconvolved into semi-volatile OOA (SV-OOA) and low-volatility OOA (LV-OOA). The m/z 43 ions are identified mostly acid-derived species – mostly $C_2H_3O^+$, and m/z 44 ions are as non-acid oxygenates – mostly CO_2^+ (Russell *et al.*, 2011). Two most dominant components of OOA spectra are plotted against each other: f_{44} (ratio of m/z 43 to total signal) vs. f_{43} (Ng *et al.*, 2011b).

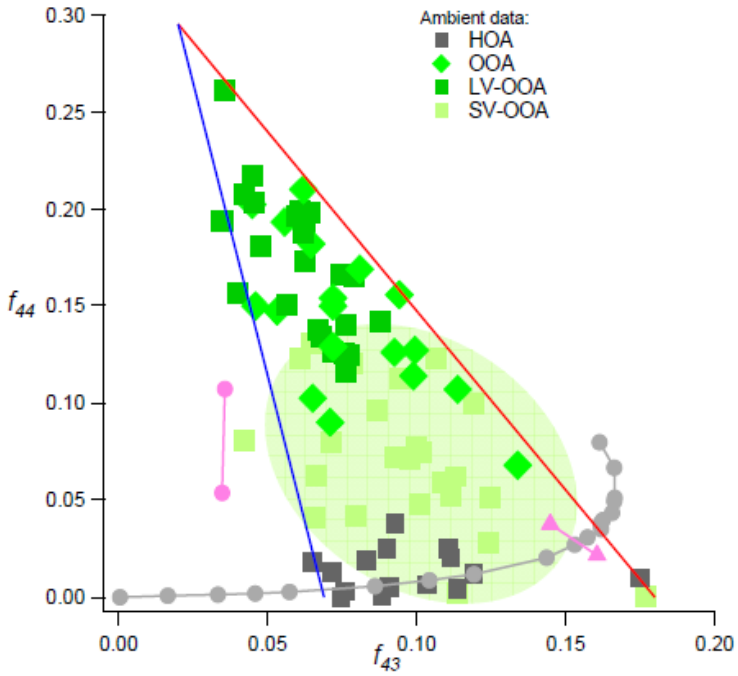

Fig. 12. Triangle plot (f44 vs. f43) for all the OOA components obtained from AMS measurements (Ng *et al.*, 2011b)

All OA components fall within a triangular space, which is limited by two lines ($y = -0.602 \cdot x + 0.415$ and $y = -1.844 \cdot x + 0.332$) (Fig. 12). These lines intersect at (0.020; 0.295). The HOA components have $f_{44} < 0.05$; SV-OOA and LV-OOA components concentrate in the lower and upper halves of the triangle, respectively.

3.2.6 Bayesian isotope mixing model

Stable carbon isotope analysis is an extensively used tool for determining cycles and fluxes of elemental carbon in various systems: ecological, marine environment, geology and atmospheric research. One type of application is mass balance equations and the distinct isotopic signatures of various sources to determine their relative contributions to the mixed signature in an end product. (Phillips and Gregg, 2003; Parnell and Phillips, 2012) Such approach proved to be useful for estimating the contribution of various food sources to a consumer's diet (Semmens *et al.*, 2009). In this study, Bayesian carbon stable isotope mixing method was extended to air filter analysis. A case of single

isotope with two mixing sources (Phillips and Gregg, 2001) was applied for estimating contribution of fossil fuel combustion and non-fossil fuel source as in Eq. (16):

$$\delta^{13}C_0 \cdot k_0 = \delta^{13}C_1 \cdot k_1 + \delta^{13}C_2 \cdot k_2, \quad (16)$$

where $\delta^{13}C_0$ is the measured value of the sample, k_0 is the measured amount of CO_2 measuring TC in relative units, $\delta^{13}C_1 = -28.0‰$ is the isotope ratio of fossil fuel combustion, $\delta^{13}C_2$ varied between $-24.0‰$ and $-26.0‰$. k_1 and k_2 are the relative contributions of the two sources when k_1 is contribution of the fossil fuel source and $k_2 = k_0 - k_1$ is the contribution of the non-fossil fuel source. k_1 was obtained as a model value.

3.2.7 Measurement locations

Vilnius is the capital of Lithuania and is situated in the South-Eastern region by the Neris river. The measurement site is located in the outskirts of the city (54°38' N, 25°18' E) at Center for Physical Sciences and Technology.

Fig. 13. Urban background measurement station in Vilnius city

There are highway roads Vilnius–Klaipėda (A1) in W direction and Vilnius–Druskininkai (A4) in SW direction close to the station (Fig. 13). Traffic data for roads shows that the annual daily traffic intensity in 2012 for A1 was 18,096 vehicle·day^{-1} (17% of all vehicles were heavy-duty) and A4 was 20,245 vehicle·day^{-1} (10% of all vehicles were heavy-duty) (source[5]: *www.lakd.lt*). The elevation of the site is 165 m above sea level (ASL) and the

sampling line is 11 m above ground level (AGL). This measurement site is classified as an urban background location, where the urban area is strictly defined as the sector between 0° and 90° directions.

The Preila Environmental pollution research station (55°55' N, 21°04' E) is located on the coast of the Baltic Sea, on the Curonian Spit (Fig. 14). The site is located 2 km from Preila village in the South (S) direction, 11 km from Nida in the South West (SW) direction. There are no major sources of anthropogenic pollution at the site. Nearest industrial cities and ports are Klaipėda (40 km in the N direction) and Kaliningrad (90 km in the SW direction).

Fig. 14. Marine background measurement site at Preila Environmental pollution research station

There is a regional road Smiltynė–Nida (167) passing by 0.3 km from the station. Traffic data for road 167 shows that the annual daily traffic intensity in 2013 was 619 vehicle·day^{-1} (4% of all vehicles were heavy-duty) (source[5]: *www.lakd.lt*). The elevation of the site is 5 m ASL and the sampling line is 4 m AGL. The Preila station is located in marine background environment.

3.3 Conclusions

It was shown that by applying various receptor modelling techniques, aerosol particle sources, contribution and spatial distribution can be evaluated. This is important if we want to reach a better understanding of anthropogenic

RF of the climate systems. In this work aerosol particle physical properties were explored with the measurements conducted by SMPS, aethalometer, CPC and an innovative approach of combining aerosol measurement techniques and stable carbon isotope mass spectrometry was investigated. ACSM data expanded aerosol exploration into the field of chemistry and provided more information about aerosol formation and sources during vegetation burning events.

4 RESULTS

4.1 Source apportionment of fine particle number concentration in urban environment

The aim of this study was to investigate the source areas and processes affecting urban aerosol PNC. The measurements were conducted at Vilnius urban background site from June 1st, 2010 to September 30th, 2011, excluding period from October to December 2010. The applied receptor models: PSCF, CWT and air mass trajectory clustering were implemented to characterise the seasonal variations of aerosol PNC. In addition, aerosol particle size distribution (PNSD), the PCA, PM_{10}, meteorological data and trace gases were used to characterise the processes aerosol particles undergo in urban environment.

4.1.1 Seasonal variability of particle number concentration in urban environment

The aerosol PNC levels measured in Vilnius displayed a large variability mainly related to daily and seasonal activities (Fig. 15). There were two distinct trends for seasonal PNC values: winter–spring peak rising in April, 2011 ($1.90 \cdot 10^4$ cm^{-3}; *SD* $1.50 \cdot 10^4$ cm^{-3}) and the decline during the summer season with the lowest PNC values between July and August, 2011 ($3.8 \cdot 10^3$ cm^{-3}; *SD* $3.00 \cdot 10^3$ cm^{-3}). The monthly average concentrations in autumn varied from $3.4 \cdot 10^3$ cm^{-3} (*SD* $3.0 \cdot 10^3$ cm^{-3}) in October to $1.20 \cdot 10^4$ cm (*SD* $8.0 \cdot 10^3$ cm^{-3}) in September.

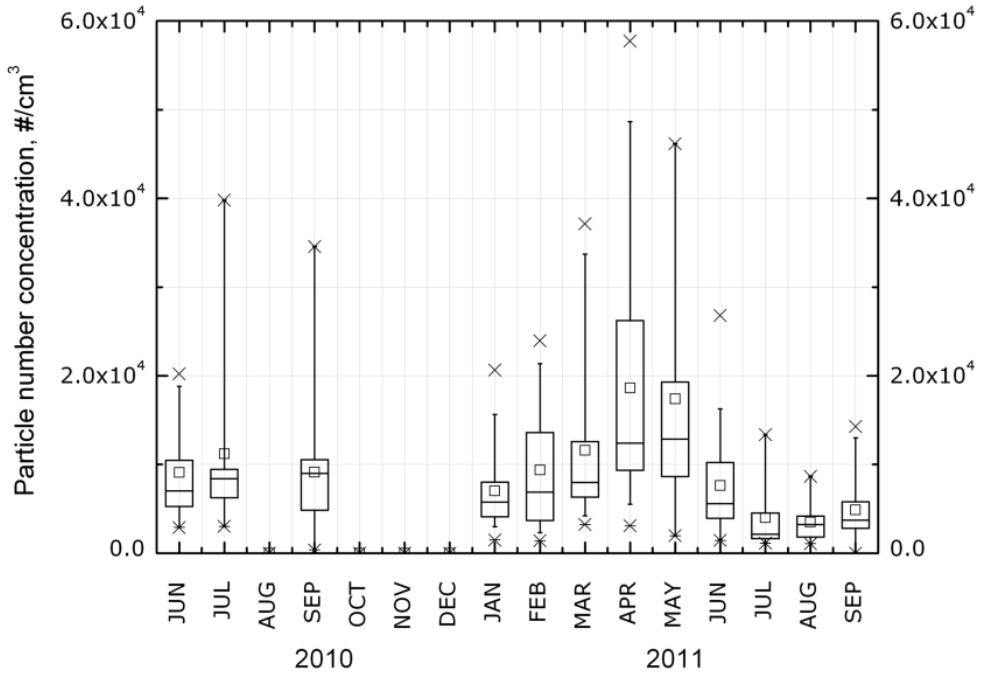

Fig. 15. Monthly variations of PNC at Vilnius, June 2010–September 2011. Boxplot: horizontal lines represent median, boxes – 25th and 75th percentiles, whiskers – 5th and 95th percentiles, floating squares – mean and cross marks – min and max values

Table 2. Particle number concentration values in urban stations

Site location	**Description**	**Study period**	**Reported values, cm^{-3}**	**Reference**
Augsburg (DE)	urban	April 2001–June 2003, September–December 2003	$1.02 \cdot 10^{4}$ A	Aalto *et al.*, 2005
Brisbane (AU)	urban	1996–1997	$0.8 \cdot 10^{4}$–$1.54 \cdot 10^{4}$ A	Thomas & Morawska, 2002
Budapest (HU)	urban	November 2008–November 2009	$1.18 \cdot 10^{4}$ A	Salma *et al.*, 2011
Gwangju (KR)	urban	2006–2007	$7.4 \cdot 10^{3}$ W	Park *et al.*, 2008
Helsinki (FI)	urban (marine)	May 1997–March 2001	$1.67 \cdot 10^{4}$ A	Hussein *et al.*, 2004
Stockholm (SE)	urban	April 2001–December 2003	$1.03 \cdot 10^{4}$ A	Aalto *et al.*, 2005
Vilnius (LT)	urban	June 2010–September 2011 *	$1.00 \cdot 10^{4}$ A	This study

[A]– PNC mean values reported annually

[W]– PNC mean values reported in winter

** – October–December 2010 were excluded from analysis

The PNC values, observed in Vilnius, were well in agreement with those reported in other urban stations (Table 2). Aerosol concentrations depend on several factors, i.e. traffic intensity, seasonal variation and weather conditions. During the cold season, when the air temperature dropped below zero, the higher aerosol PNCs were usually observed. This can be explained by the accumulation of aerosol particles in lower altitude due to increased emissions and weaker atmospheric convection (Gao *et al.*, 2007). As seen in the studies (Meyer, 2012; Karvosenoja *et al.*, 2008), the use of fossil fuel and wood burning for domestic heating could yield a major increase in aerosol particles. During the spring, atmospheric pollution from vegetation burning events in South-Eastern Baltic Sea region is one of the main contributor to the PNC increase in Vilnius urban environment.

4.1.2 Diurnal variation of aerosol particle number concentration

From monthly diurnal PNC cycles during 2010 study period (Fig 16) it was observed that there were two cycles of PNC increase: at the rush hours and during the evening. Black line represents average monthly PNC values, lower and upper grey lines – 16^{th} and 84^{th} percentiles, respectively. Such percentiles were chosen because they represented data range of mean PNC $\pm 1 \cdot \sigma$ for normal probability distribution.

Most of the time during the summer PNC values were higher than estimated background PNC level ($5.0 \cdot 10^3$ cm^{-3}), except for the noon hours in July and August. The morning peak reached its maximum at 7:00 (GMT + 2) and PNC was $9.9 \cdot 10^3$ cm^{-3}. It can be related with the increased traffic emissions during the rush hours, as there are major roads near the measurement site. Evening PNC growth during the summer usually started from 19:00 (GMT + 2) and reached its maximum at 22:00 (GMT + 2). The PNC values

were in the range from $7.2 \cdot 10^3$ to $1.15 \cdot 10^4$ cm^{-3}. The evening cycle variation can be explained with the change of height in the boundary layer. In September PNC values were the highest from the observed data of the year 2010. Maximum PNC values ($1.84 \cdot 10^4$ cm^{-3}) was observed in the morning 07:00 (GMT + 2). This can be explained by a rapid increase of vehicles traffic in the streets of Vilnius as many people return from the holidays and education year at schools and universities starts. In October PNC values are lower than in summer due to the instrument failure and not enough data was gathered for correct month representation.

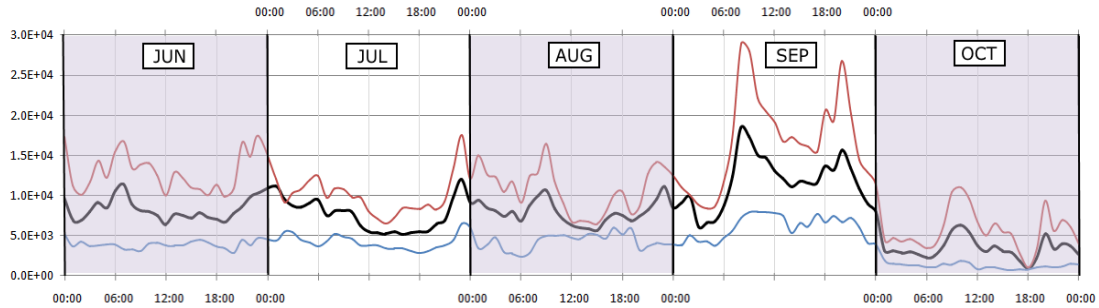

Fig. 16. Diurnal cycles of PNC (1-h mean) depicted at Vilnius measurement site for each month during 2010 study period

Similar weekday pattern was observed in other urban stations in Stockholm and Helsinki (Aalto *et al.*, 2005, Hussein *et al.*, 2004)), however particle number measurements at background station in Preila (Lithuania) didn't reveal diurnal cycle trend. This suggests that the increase of aerosol particles can be associated with local pollution sources within the urban area.

4.1.3 Principal component analysis of atmospheric pollutants

In order to identify the main sources contributing to the increase of fine particles in urban environment, the PCA was conducted. PM_{10}, trace gases and meteorological data was obtained from the EPA stations (Savanorių and Lazdynai) and PNC measurements were made at urban background station in Vilnius. The PCA results are presented in the Table 3, and the analysis is

limited to the first three principal components, as the majority of data variance (74%) was explained by these components.

Table 3. Principal component matrix. PM_{10}, trace gas and meteorological data was obtained from the EPA stations (Savanorių and Lazdynai) and PNC from the urban background measurement station in Vilnius. Significant factor loadings (with absolute values > 0.6) are in bold.

Components	**PC_1**	**PC_2**	**PC_3**
PM_{10}	0.74	0.15	–0.02
SO_2	0.19	**0.73**	–0.29
NO	0.59	0.23	**0.60**
NO_2	**0.90**	0.11	–0.34
NO_x	**0.94**	0.19	0.01
O_3	**–0.90**	0.16	0.18
RH	0.20	**–0.77**	–0.27
p	–0.51	0.39	–0.41
WS	**–0.77**	–0.12	0.42
CO	**0.62**	–0.56	0.02
PNC	0.55	0.16	0.59
Variance explained	45%	17%	12%

PNC, PM_{10}, NO_x and NO_2 had the most significant (absolute values > 0.6) factor loadings for the primary component (PC_1), which explained 45% of data variance. PC_1 indicated the influence of fossil fuel combustion from traffic emissions. PNC had a negative correlation with meteorological parameters (*WS* and *p*). The mixing and dilution of pollutants in the atmosphere is increased with higher boundary layer (higher *p* values) and stronger wind (higher *WS* values). The chemical balance of NO_x and ozone explained negative factor loading of ozone (–0.90). The PC_2 explained 17% of the variance in data. SO_2 (0.73) and carbon monoxide (–0.56) gases had significant factor loadings. The PC_2 was attributed with specific domestic

heating sources: coal burning and fossil fuel combustion, because they strongly emitted SO_2 gases (Streets and Waldhoff, 2000; Marković *et al.*, 2008). The PC_3 had a high factor loadings of nitrogen monoxide (0.60) gases and PNC (0.59), explaining 12% of variance in data. Strong nitrogen monoxide and negative (or weak) PM_{10}, nitrogen dioxide and sulphur dioxide factor loadings indicated emission source from vehicle engines for PC_3. PNC correlation with nitrogen monoxide suggested that fresh vehicle exhaust gases became a source for NPF. In PC_1 and PC_2 the correlation of PNC with PM_{10} indicated that the increase of pollution level in urban environment had affected PNC values.

4.1.4 Receptor modelling of aerosol particle sources in urban environment

PSCF model, CWT method and air mass trajectory cluster analysis were run with the seasonal data for winter, spring, summer and autumn in order to identify the main atmospheric circulation pathways influencing PNC (Figs. 17 and 18). There are four dominant paths of air masses reaching Lithuania: from the W, NW, SW and SE. The long and fast moving trajectories were disaggregated into groups originating from more distant W and NW regions. Members of this cluster have extremely long transport patterns; some of them cross over North Sea, Northern Europe or the Nordic countries. Trajectories belonging to S–SW typically follow a flow pattern over the Poland and Germany. Generally such trajectories have short transport patterns, indicative of slow-moving air masses.

In spring no clusters exceed the season mean of $1.63 \cdot 10^4$ cm^{-3}, but 1st cluster (26% of trajectories) was recognized as polluted one, which indicates that the air masses associated with this cluster lead to higher PNC values ($1.27 \cdot 10^4$ cm^{-3}; *SD* $1.0 \cdot 10^3$ cm^{-3}) in Vilnius (Fig. 17). About 21% of trajectories were assigned to the 3rd cluster with the lowest concentration of $5.5 \cdot 10^3$ cm^{-3} (*SD* $1.22 \cdot 10^4$ cm^{-3}), thus this cluster had less effect on PNC values in Vilnius. The 2nd cluster 2 (17% of trajectories) represents the most

important transport pathway with the highest PNC ($1.55 \cdot 10^4$ cm^{-3}; *SD* $8.6 \cdot 10^3$ cm^{-3}) among the six clusters in winter (Fig. 18).

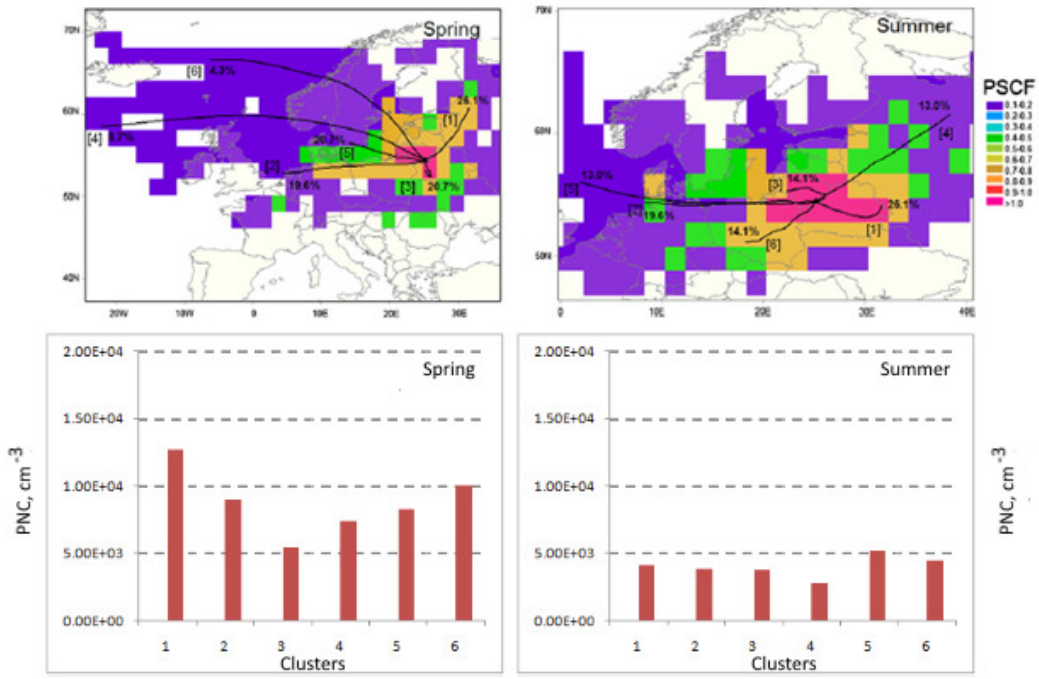

Fig. 17. Backward air mass trajectories (duration 72-h) and PNC (1-h mean) are grouped into 6 clusters during the warm season (spring and summer). Potential source maps depict PNC (1-h mean) seasonal variation. Air mass backward trajectories were computed for 72-h over urban background site in Vilnius at 100 m AGL.

The second important transport pathway in winter season was associated with cluster 6 (7% of trajectories), which had the second high PNC ($1.23 \cdot 10^4$ cm^{-3}; *SD* $1.09 \cdot 10^4$ cm^{-3}). The number of trajectories assigned to the 3rd cluster was high (36% of trajectories), therefore, the pathway represented by this cluster was considered important for lowest PNC ($9.9 \cdot 10^3$ cm^{-3}; *SD* $7.6 \cdot 10^3$ cm^{-3}). In autumn, the pathway represented by 4th cluster was most polluted ($1.12 \cdot 10^4$ cm^{-3}; *SD* $6.3 \cdot 10^3$ cm^{-3}), while those of the 5th ($4.1 \cdot 10^3$ cm^{-3}; *SD* $7.7 \cdot 10^3$ cm^{-3}) and 6th clusters ($4.0 \cdot 10^3$ cm^{-3}; *SD* $2.5 \cdot 10^3$ cm^{-3}) were relatively clean.

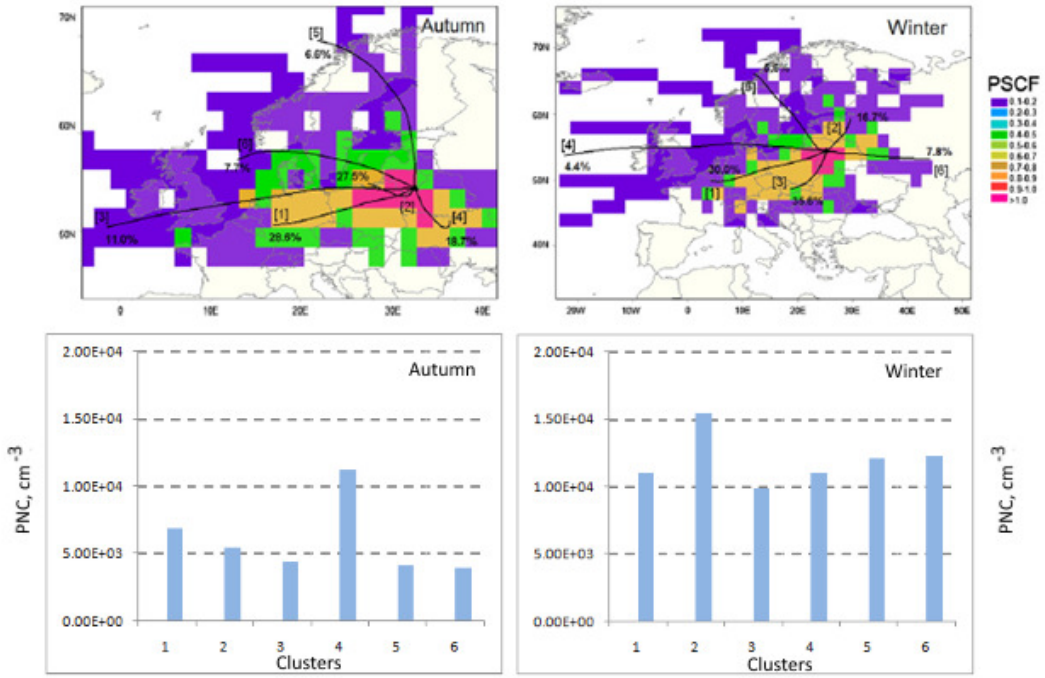

Fig. 18. Backward air mass trajectories (duration 72-h) and PNC (1-h mean) are grouped into 6 clusters during the cold season (autumn and winter). Potential source maps depict PNC (1-h mean) seasonal variation. Air mass backward trajectories were computed for 72-h over urban background site in Vilnius at 100 m AGL.

The CWT values revealed that PNC observed in Vilnius is not heavily affected by the LRT of air masses during summer as CWT values are less variable (Fig. 19). There are some trails approaching from the N (autumn) and NW (winter), indicating that regional transport from Northern Europe was not always negligible. Eastern parts of Belarus and Ukraine were the regions with high CWT values ($1.2 \cdot 10^4$ cm^{-3}) in autumn. The pollution accumulated in the southern countries' air masses presents a contribution, or rather a baseline, to which local emissions (which are possibly dominant) are added.

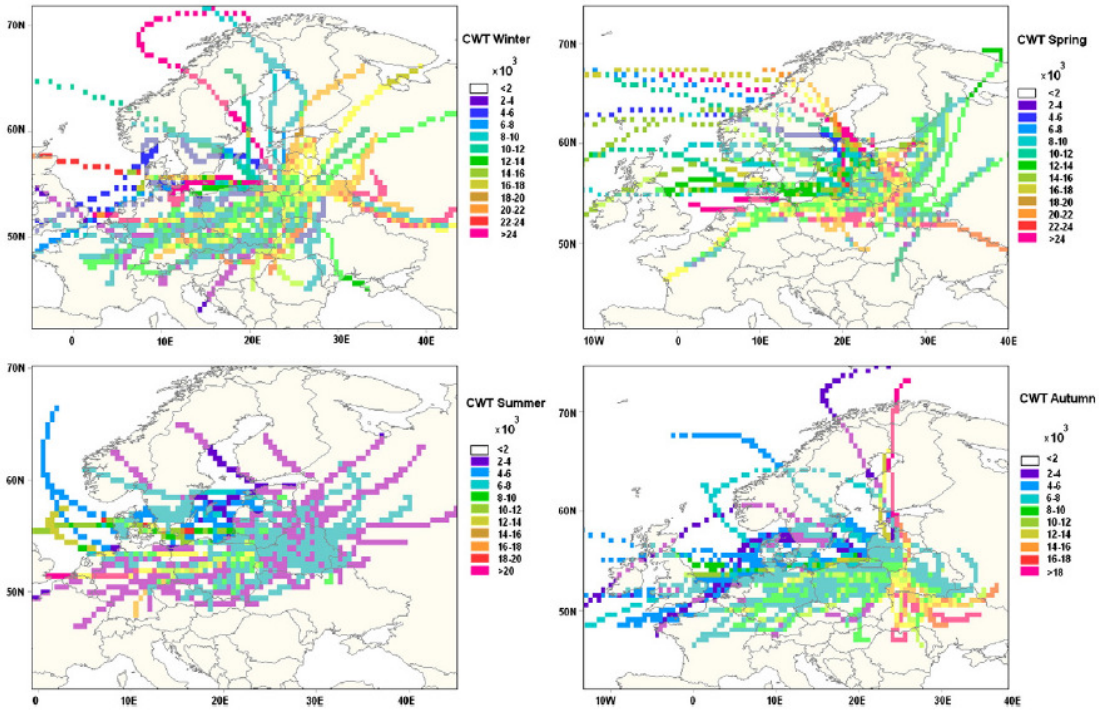

Fig. 19. Concentration weighted trajectory maps representing seasonal variation of PNC (1-h mean). Air mass backward trajectories were computed for 72-h over Vilnius measurement site at 100 m AGL.

4.1.5 Analysis of new particle formation events in urban background environment

In order to investigate the NPF events in urban background environment, the PNSD data for September was characterised by calculated PNC values in the nucleation ($N_{10–20}$), Aitken (N_{20-90}) and the accumulation ($N_{100–300}$) particle size ranges (Fig. 20). Three type of events in urban environment were identified on September 7th – the traffic/NPF, on September 18th – the NPF and on September 22nd – the traffic/residential heating (Fig. 21). Diurnal cycles of these events are presented in (Fig. 20). Typically, the maximum of the diurnal PNC variation may be attributed to transport emissions (Kittelson *et al.*, 2000) where under favourable conditions nucleation can occur, for example, in road tunnels and in open road areas (Kittelson and Watts, 2000).

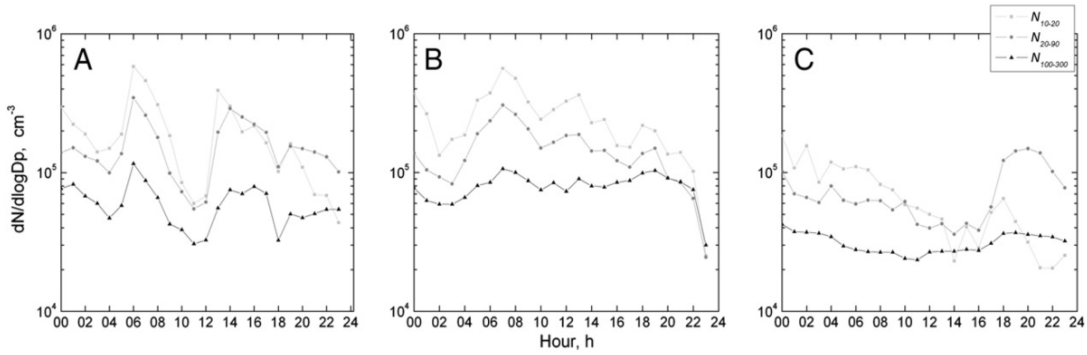

Fig. 20. Daily variability of PNC (cm^{-3}) in size ranges of 10–20 nm, 20–90 nm and 100–300 nm in Vilnius during the traffic/NPF (A), the traffic/residential heating (B) and the NPF (C) events

On the day of the traffic/NPF event a clear diurnal pattern of concentration increase during the rush hours (06:00–08:00 and 14:00–17:00, GMT + 2) were observed (Fig. 20 A). PNC increase in the second part of the day was also influenced by the NPF event starting from 13:00 (GMT + 2). $N_{20–90}$ overcame $N_{10–20}$ concentration from 19:00 (GMT + 2) indicating further aerosol particle growth after NPF event. The traffic/domestic heating episode showed that $N_{100–300}$ concentration was the main contributor to the elevated PNC level during the whole day and the morning increase of PNC during the rush hours was attributed to the traffic emissions (Fig. 20 B). The NPF episode, which was observed on September 18th, 2011, occurred in the evening. It is seen that $N_{20–90}$ concentration increases sharply starting from 17:00 (GMT + 2) indicating aerosol particle growth (Fig. 20 C).

Urban aerosol particles are influenced by several sources, which originate both locally and globally. Aerosol particle events can be characterised by PNSD time series and distribution parameters. These events are in details presented in Fig. 21 and PNSD parameters are listed in table 4. Common events in urban environment are, as follows: the traffic/NPF (Fig. 21 a, b), the NPF (Fig. 21 c, d), the traffic/residential heating (Fig. 21 e, f) events. The previously reported measurements at the traffic dominated sites determined

that the maximum PNC occurred for diameters around 20 nm (Wehner *et al.*, 2009).

Table 4. The parameters of PNSD in Vilnius during the traffic/NPF (A), the traffic/residential heating (B) and the NPF (C) events

Curves	A			B			C		
	1 (13h)	**2 (19h)**	**3 (22h)**	**1 (18h)**	**2 (20h)**	**3 (22h)**	**1 (10h)**	**2 (17h)**	**3 (23h)**
N_{TOT}(I)	$4.5 \cdot 10^5$	$1.1 \cdot 10^5$	$7.8 \cdot 10^4$	$1.5 \cdot 10^5$	$1.7 \cdot 10^5$	$1.1 \cdot 10^5$	$5.2 \cdot 10^5$	$1.9 \cdot 10^5$	$8.7 \cdot 10^4$
N_{TOT}(II)	$2.4 \cdot 10^5$	$3.2 \cdot 10^5$	$2.1 \cdot 10^5$	$5.5 \cdot 10^4$	$4.0 \cdot 10^4$	$3.4 \cdot 10^4$	$2.1 \cdot 10^5$	$0.8 \cdot 10^5$	$4.3 \cdot 10^4$
D_g(I)	15	10	9	33	42	48	8	13	6
D_g(II)	62	38	63	124	147	149	80	102	137
σ_g(I)	1.55	1.40	1.46	1.59	1.52	1.57	2.10	1.76	4.22
σ_g(II)	2.10	2.67	2.16	1.62	1.47	1.44	2.10	2.10	2.10

Vehicles directly emit a significant number of particles in the size range between 40 and 100 nm (Harris and Maricq, 2001). The results of analysis investigated with respect to the diurnal pattern of aerosol particle number concentration of each mode were considered.

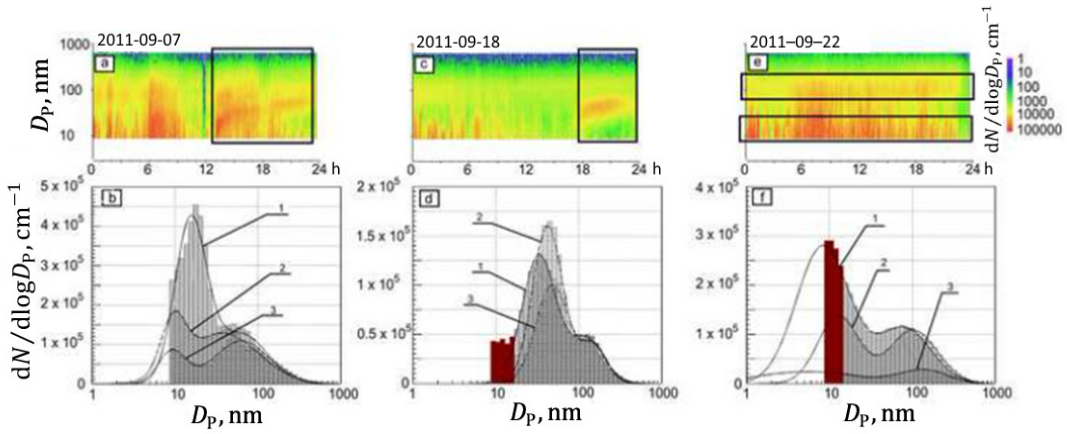

Fig. 21. Daily variability of aerosol PNSD at urban background station in Vilnius during the traffic/NPF (a, b), the NPF (c, d), the traffic/residential heating (e, f) events. Aerosol particle size distributions were depicted on the 7th 1 – 13:00, 2 – 19:00, 3 – 22:00 (b), on the 18th 1 – 18:00, 2 – 20:00, 3 – 22:00 (d) and on the 22nd of September, 2011 1 – 10:00, 2 – 17:00, 3 – 23:00. Time zone is GMT + 2.

As it is seen in Fig. 20, the particle size distribution on September 7th, 2011 showed the nucleation mode particles with the diameter of about 9–20 nm. It can be seen that a peak number concentration was observed during the early morning and afternoon of September 7th, while the PNC was relatively stable on September 22nd. The concentration of the nucleation mode was much higher than Aitken and accumulation modes, indicating the significant contribution of traffic pollution to the number concentration for both events.

4.1.6 Conclusions

1. The long-range transport of air masses increased the background level values of particle number concentration in Vilnius city. In autumn the air masses arriving from W and SE increased by 40% and 120% of the estimated background level ($5.0 \cdot 10^3$ cm^{-3}), respectively. In winter the air masses arriving from SW and NW resulted in 20% and 55% increase of the estimated background level ($1.0 \cdot 10^4$ cm^{-3}), respectively. In spring the air masses arriving from SW and NW increased the estimated background level ($5.0 \cdot 10^3$ cm^{-3}) by 65% and 130%, respectively.
2. The principal component analysis indicated correlation pattern of $N_{20\text{-}300}$ with NO (0.54) and NO_2 (0.90) gases. It confirmed that the variations in the particle number concentration diurnal patterns were mainly due to the traffic and biomass burning sources.
3. Potential source contribution function and concentration weighted trajectory methods, and air mass trajectory clustering demonstrated that additional possible source areas contributing to the elevated particle number concentration in Vilnius were Central Europe industrial areas.

4.2 Source apportionment of black carbon in the South-Eastern Baltic Sea region

The main sources of BC in the air masses, arriving at the background measurement station in Preila, were investigated by applying statistical methods and receptor models. The analysis is based on BC mass concentration data, obtained with aethalometer (Magee Sci., model AE31) at 880 nm, from January 1st to December 10th 2013, air mass backward trajectories were computed using Hybrid single particle Lagrangian integrated trajectory (HYSPLIT-4) model, global meteorological data-sets were obtained from NCEP-NCAR Reanalysis archive databases. Air masses were grouped into 6 clusters for each season. The PSCF and CWT methods helped us to estimate the major contributors of BC in the South-Eastern Baltic Sea region.

4.2.1 Black carbon concentration variations in marine background environment

BC optical measurements of carbonaceous aerosol particles have been shown to be well correlated with elemental carbon (EC) measurements (Lavanchy *et al.*, 1999). Moreover, BC is an indicator for anthropogenic activity, local and regional aerosol emission source identification. An analysis of spatial and temporal trends of BC in Preila is presented in the Fig. 22. The background BC mass concentration for 2013 was 0.71 $\mu g \cdot m^{-3}$ (*SD* 0.50 $\mu g \cdot m^{-3}$). It is comparable to 0.75 $\mu g \cdot m^{-3}$ for the period of 2008–2009 (Ulevičius *et al.*, 2010). The diurnal patterns of BC concentration for cold and warm seasons were different (Fig. 22). During the warm season the highest concentration levels were reached at 8:00–9:00 (GMT + 2), 15:00–17:00 (GMT + 2), and 20:00–22:00 (GMT + 2). The increase of the concentration in the morning and in the afternoon is likely due to vehicular primary emissions, and the evening peak is attributed to the boundary layer conditions. The hourly averages of the day in warm season were in the range from 0.38 $\mu g \cdot m^{-3}$ to 0.44 $\mu g \cdot m^{-3}$ and for cold season – from 0.56 $\mu g \cdot m^{-3}$ to 0.71 $\mu g \cdot m^{-3}$,

respectively. Due to anthropogenic activity, maximum concentration in the summer reached 1.15 $\mu g \cdot m^{-3}$ (*SD* 0.54 $\mu g \cdot m^{-3}$), though it has the lowest seasonal average – 0.50 $\mu g \cdot m^{-3}$(*SD* 0.36 $\mu g \cdot m^{-3}$).

Table 5. Black carbon concentration annual (or seasonal) values at rural stations

Site location	Description	Sampling time	Reported values, $\mu g \cdot m^{-3}$	Reference
Jungfraujoch (CH)	high-alpine (background)	July 1995–June 1997	0.21 [A]	Lavanchy *et al.*, 1999
K-puszta (HU)	rural (background)	July –August 1996	0.42 [S]	Molnár *et al.*, 1999
Mace Head (IE)	marine (background)	February 1990–April 1991	0.04 [A]	Jennings *et al.*, 1993
Hyytiäla (FI)	rural (background)	December 2004–December 2008	0.25–0.37 [A]	Hyvärinen *et al.*, 2011
Puijo (FI)	rural (background)	August 2006–December 2008	0.23 [A]	Hyvärinen *et al.*, 2011
Utö (FI)	marine (background)	November 2007–December 2008	0.23 –0.27 [A]	Hyvärinen *et al.*, 2011
Virolahti (FI)	rural (background)	September 2006–December 2008	0.39 –0.46 [A]	Hyvärinen *et al.*, 2011
Preila (LT)	**marine (background)**	**January–December 2013**	**0.71** [A]	**This study**

[A] – Mean values of black carbon concentration reported annually.

[S] – Mean values of black carbon concentration reported in summer.

The average BC concentration for the winter period was 1.10 $\mu g \cdot m^{-3}$ (*SD* 0.78 $\mu g \cdot m^{-3}$). The increase of BC concentrations in winter can be explained by increase of domestic heating both in the region and in Europe overall. During the cold season the highest BC concentration levels were reached in the evening and at night, the lowest concentrations were during the day. The seasonal variation of BC concentrations reveal that the monthly average values have maximum in January (1.42 $\mu g \cdot m^{-3}$) and gradually decline to minimum in August (0.44 $\mu g \cdot m^{-3}$) and then increases thereafter.

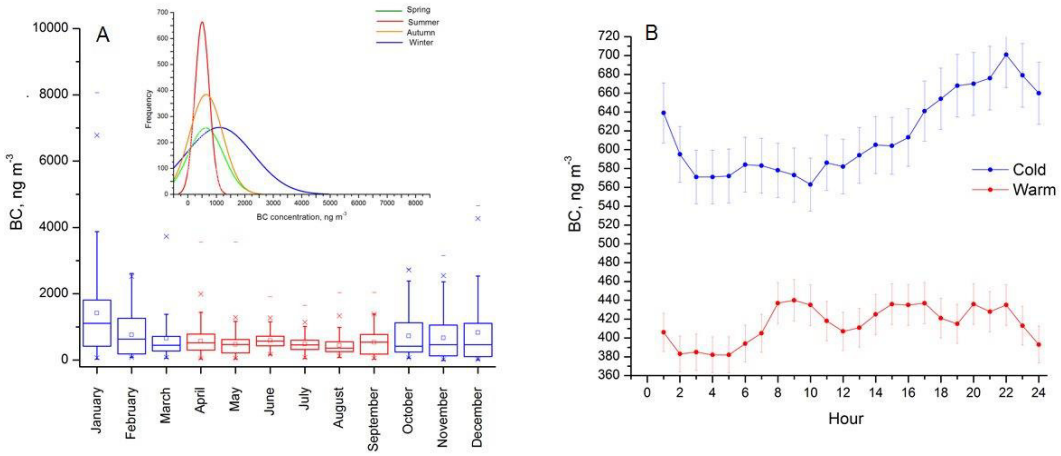

Fig. 22. A) Monthly variation of BC mass concentration in Preila during the study period. Box plots: horizontal lines represent median, boxes – 25th and 75th percentiles, whiskers – 5th and 95th percentiles, floating squares – mean. B) The diurnal cycles of BC (1-h mean) mass concentration during warm (April 1st–September 30th) and cold (January 1st–March 31st and October 1st–December 10th) seasons in Preila

4.2.2 Cluster analysis of air mass trajectories and black carbon

In order to identify the pathways of the LRT of air masses over Preila, receptor models (PSCF, CWT and cluster analysis of air mass back trajectories) were run with the data from all 4 seasons (Fig. 23). It was estimated that selection of 6 clusters fits best for the seasonal representation of air masses in marine background environment. It is seen that there are four dominant paths of air masses reaching Lithuania: from the W, NW, SW, and SE. The fast moving air masses were always observed from more distant W and NW regions. Air masses of this cluster have extremely long transport patterns; some of them cross over Northern Europe. Air masses arriving from S and SW typically flow over Poland, Kaliningrad (Russia) and Belarus. Generally, these trajectories have short transport patterns, indicating slow moving air masses. The high BC concentration event in this group are likely to be enriched by regional and local pollution sources.

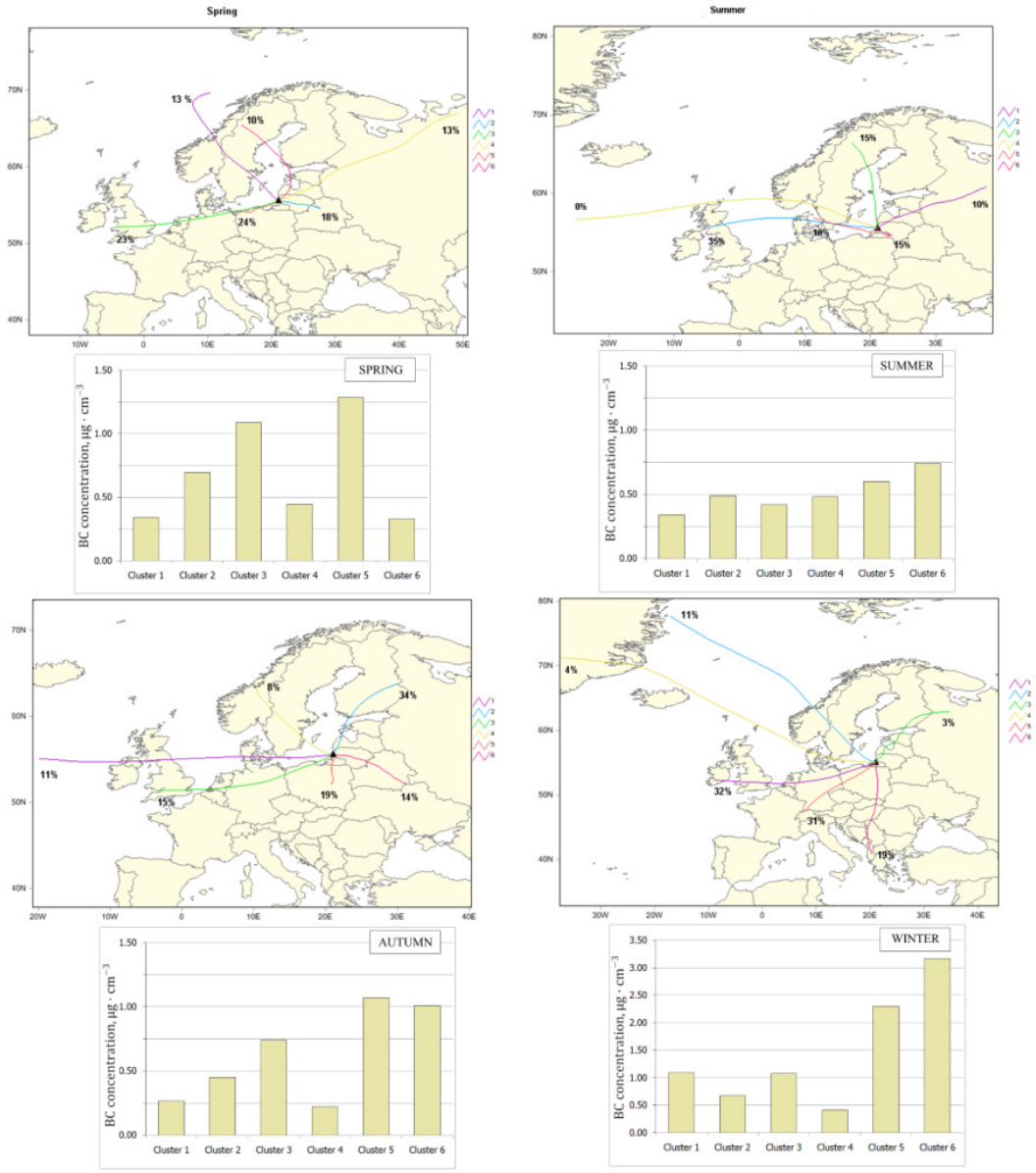

Fig. 23. Seasonal representation (spring, summer, autumn and winter) of air mass backward trajectories over Preila site grouped into six clusters. BC mass concentration represented in each trajectory clusters is depicted for each season

The highest concentrations for each season were found, as follows: in winter – 6th cluster 3.10 µg·m^{-3} (*SD* 1.20 µg·m^{-3}), in spring – 3rd cluster 1.28 µg·m^{-3} (*SD* 1.02 µg·m^{-3}), in summer – 6th cluster 0.72 µg·m^{-3} (*SD* 0.50 µg·m^{-3}) and in autumn –5th cluster 1.07 µg·m^{-3} (*SD* 0.70 µg·m^{-3}). During the spring continental air masses of 5th cluster were likely influenced by the wildfires in the region. Except for anthropogenic emissions of fossil fuel

combustion, biomass burning, including wildfire events, is an important contributor to the BC mass concentration in the South-Eastern Baltic Sea region.

The lowest BC mass concentration for each season were found, as follows: in winter – 4th cluster 0.45 μg·m^{-3} (*SD* 0.20 μg·m^{-3}), in spring – 6th cluster 0.33 μg·m^{-3} (*SD* 0.12 μg·m^{-3}), in summer – 1st cluster 0.35 μg·m^{-3} (*SD* 0.10 μg·m^{-3}) and in autumn – 4th cluster 0.22 μg·m^{-3} (*SD* 0.11 μg·m^{-3}). Generally, these clean air masses originate in the Northern parts of Europe or in the Atlantic ocean at average altitudes of around 3000 m and then sink down while moving above the sea. As these groups of air masses, typically, cross over the Baltic Sea and contain low level of BC concentrations within themselves.

The distribution of weighted trajectory concentrations (CWT) gives the information on the relative contribution of source regions potentially affecting BC concentration at Preila station. CWT is a function of BC concentration that was reported every 24-h and the residence time of a trajectory arriving at Preila location in each grid cell. The potential source maps for BC concentration and air masses arriving at 100 m AGL altitude at Preila during the study period for each season are given in Figs. 24 and 25. It is shown that the movement of air masses follows a seasonal pattern. During all seasons the air masses arriving from the Northern Europe were associated with the lowest BC concentration values. The short trajectories, originated from the SW and SE, carried the highest BC concentrations. In fact, the short trajectories represent air masses with low wind speed, thus resulting in poor mixing ratio. In this case, the sources in Central Europe were the largest contributors to the air quality in Preila in 2013.

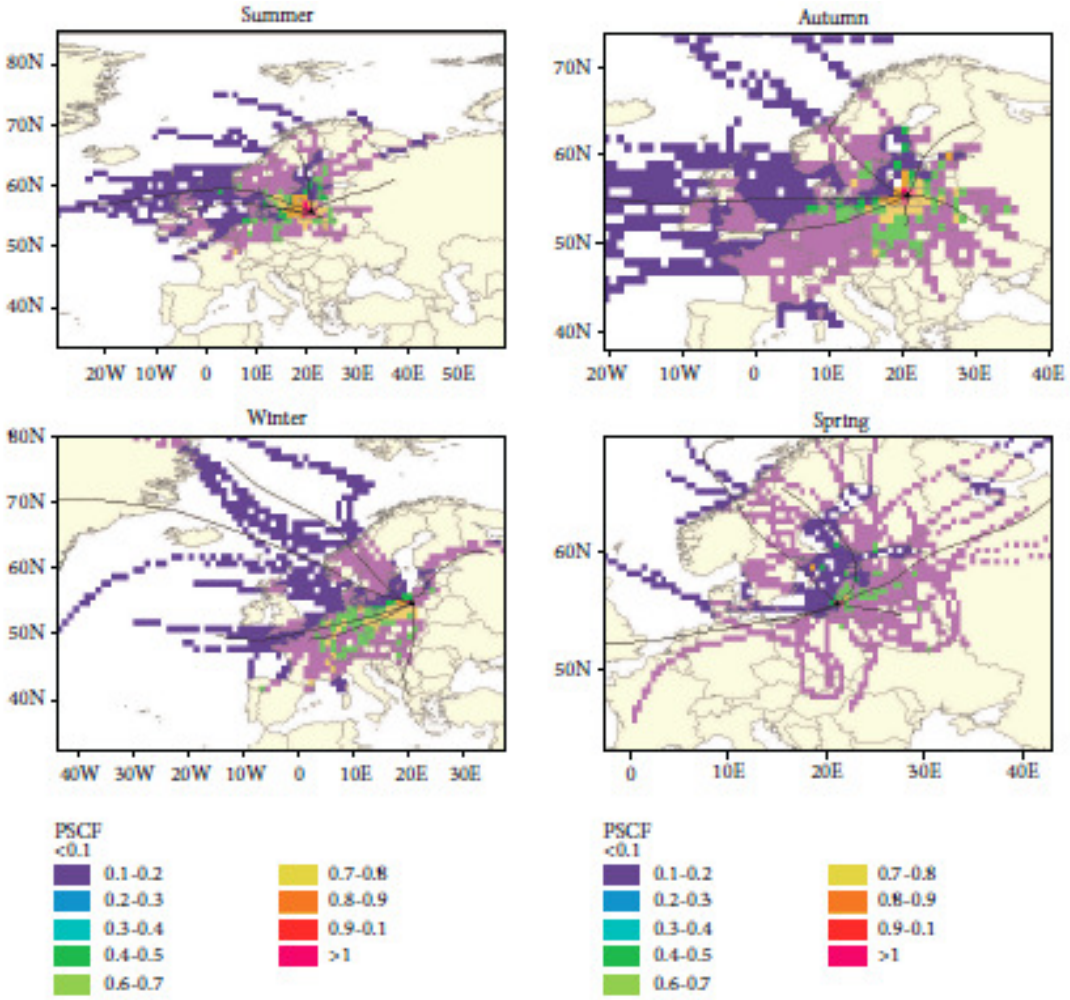

Fig. 24. Seasonal variations of the potential source maps for BC mass concentration (24-h mean). Air mass backward trajectories were computed for 72-h over Preila station at 100 m AGL

The highest average contribution to the observed BC concentrations during the winter season was from the air masses originated from Poland and Czech Republic. The most distinct air mass pattern in winter occurs from the West-Eastern Belarus and Poland also contributes significantly to BC concentrations at Preila station.

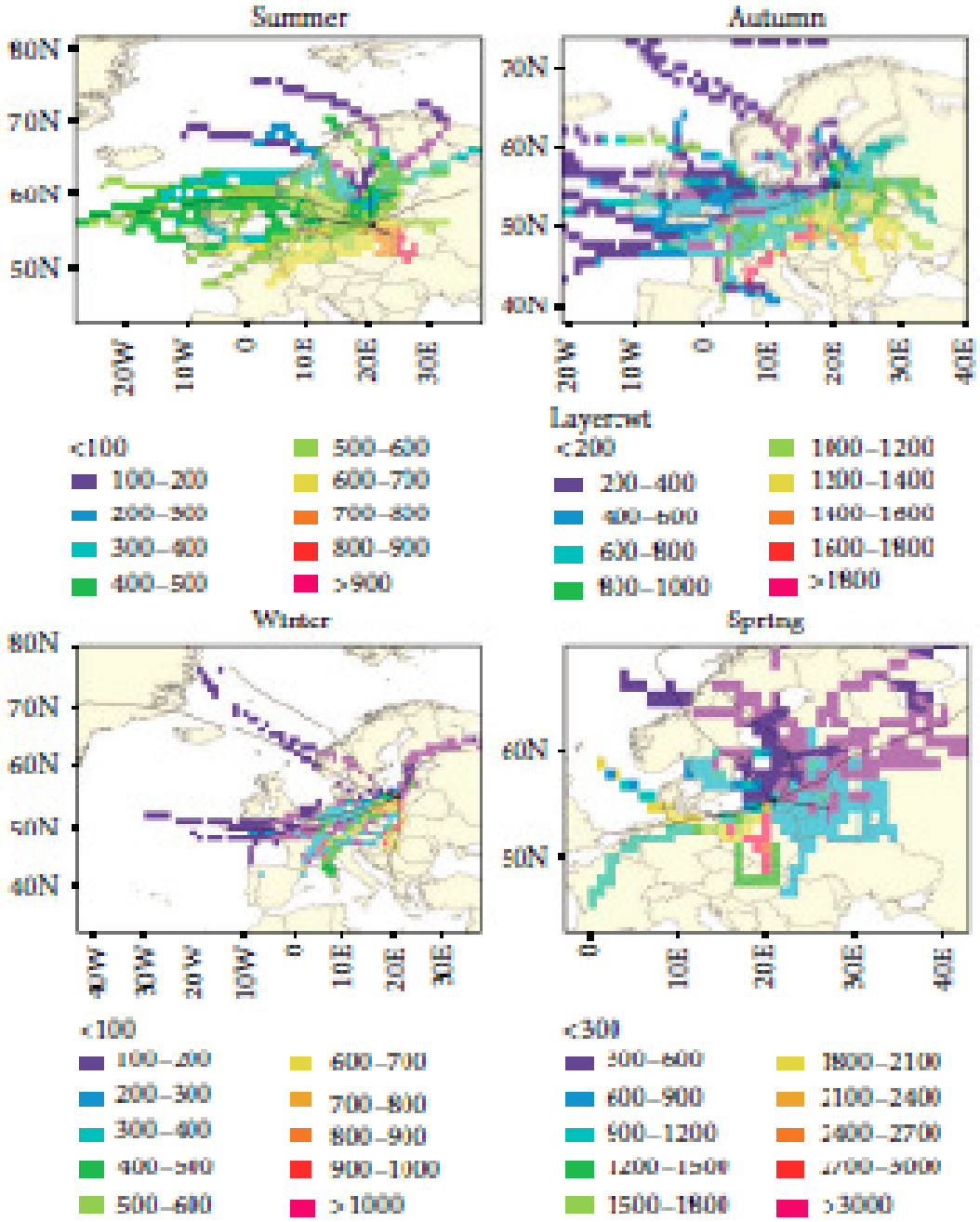

Fig. 25. CWT maps for seasonal variations of BC concentration (24-h mean). Air mass backward trajectories were computed for 72-h over Preila station at100 m AGL

4.2.3 Conclusions

1. In 2013 the background level of black carbon in the South Eastern Baltic Sea region was estimated to be 0.71 $\mu g \cdot m^{-3}$ (*SD* 0.50 $\mu g \cdot m^{-3}$).
2. For all seasons the lowest black carbon concentrations were found in the clusters, representing air masses from the N and NW and were in the range from 0.22 $\mu g \cdot m^{-3}$ to 0.45 $\mu g \cdot m^{-3}$.
3. The long range transport of air masses is the main contributor to the increase of the background level of black carbon mass concentration in the South-Eastern Baltic Sea region. In autumn it contributed up to 50%, in winter – up to 350% and in spring – up to 80% to the increase of estimated background level (0.71 $\mu g \cdot m^{-3}$).
4. In winter season the highest black carbon concentration was observed from all directions with the peak concentration of 3.10 $\mu g \cdot m^{-3}$ (*SD* 1.20 $\mu g \cdot m^{-3}$), which represented air masses arriving from the S and SW (Poland, Kaliningrad and Belarus) and affected by fossil fuel combustion and biomass burning sources.
5. The lowest black carbon concentration from all directions were observed in summer with seasonal concentration equal to 0.50 $\mu g \cdot m^{-3}$ (*SD* 0.36 $\mu g \cdot m^{-3}$). This indicates that there was no transport of pollution from biomass burning and fossil fuel combustion sources.

4.3 Characterisation of pollution events from vegetation burning in the South-Eastern Baltic Sea region

Biomass burning is important pollution source in the atmosphere. The forest fires, vegetation burning or domestic heating can increase the presence of particulate pollution on local scale and it can be transported by air masses into other regions, thus having a significant impact on pollution levels there (Beverland *et al.*, 2000; Abdalmogith and Harrison, 2005). In spring the air masses are occasionally polluted by vegetation fires in the South-Eastern Baltic Sea and nearby regions. Short-term measurement was conducted at Preila station from the 1st to the 31st of March, 2014. During the campaign ACSM and an aethalometer were deployed for continuous measurement of aerosol chemical constituents and black carbon. In order to estimate the potential pollution sources in this study, different receptor modelling techniques (CWT, PSCF and air mass trajectory cluster analysis) and statistical methods (PCA) were applied. PM_{10}, trace gas and meteorology data was obtained from the EPA station (City centre) situated in Klaipeda (40 km North from Preila).

4.3.1 Pollutant analysis and meteorological parameter variations during the vegetation burning in the marine background environment

In March 24-h limit values for PM_{10} (50.0 $\mu g \cdot m^{-3}$) were exceeded 9 out of 31 days (Fig. 26). The PM_{10} mass concentration varied from 10.3 to 114.6 $\mu g \cdot m^{-3}$. Higher concentrations were observed from the 7th to 10th of March and several separate days had higher daily peaks, particularly for the 30th of March daily average was 60.6 $\mu g \cdot m^{-3}$. During the biomass burning episode (10th of March), the daily average of PM_{10} mass concentration (114.6 $\mu g \cdot m^{-3}$) was three times higher than a monthly average (38.1 $\mu g \cdot m^{-3}$) in March.

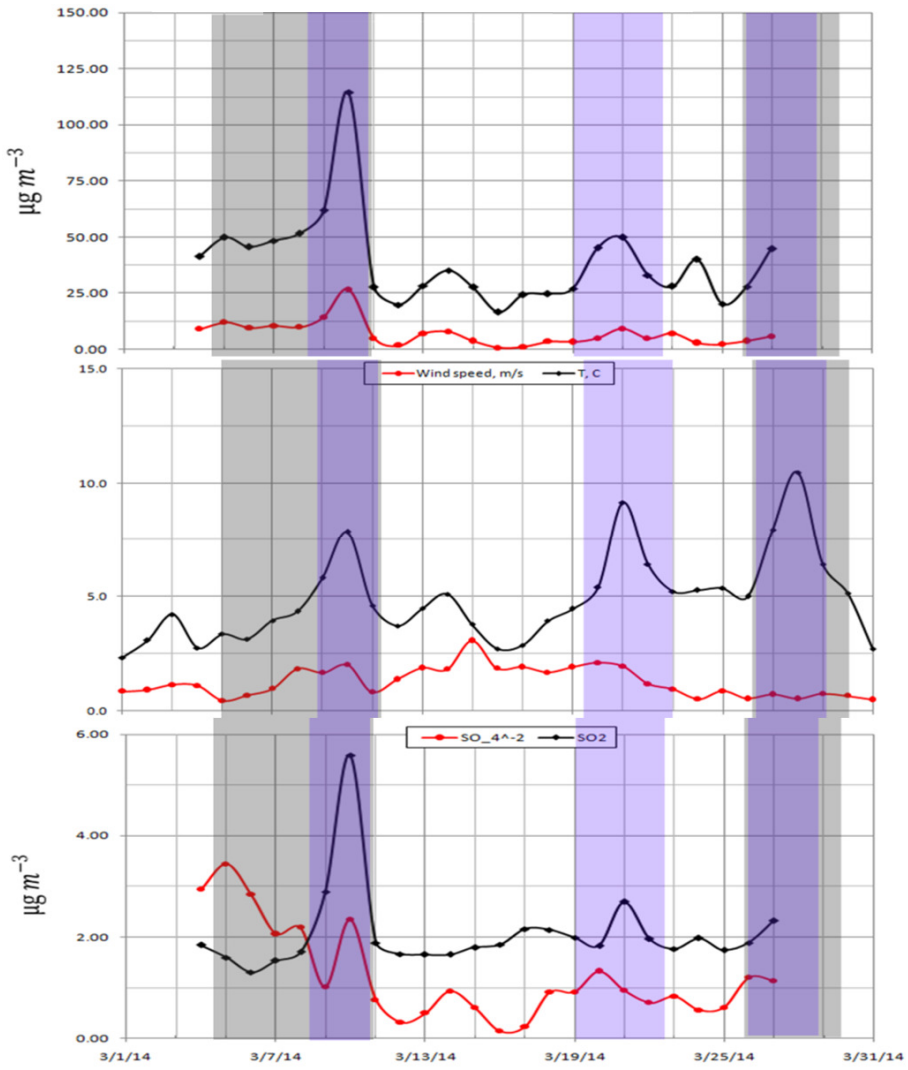

Fig. 26. A) Time series of PM_{10} mass concentration derived from EPA station in Klaipeda city centre and NR-$PM_{1.0}$ total component loading of ACSM measurements at Preila station during March 2014. B) Meteorological data (*WS* and *T*) for Klaipeda region. C) Time series of SO_2 trace gas mass concentration at EPA station in Klaipeda and NR-$PM_{1.0}$ SO_4^{2-} loading of ACSM measurements at Preila station.

Usually, the vegetation burning occurs during the good weather conditions. Meteorological data, obtained from the EPA station, which is located in the city centre of Klaipeda, can reveal the real weather conditions in this region at the time of the pollution events. There were two prolonged events of high pressure (from the 5th to 14th of March and from the 26th to 30th of

March). On average the atmospheric pressure difference was 13.1 hPa (1st episode) and 8.8 hPa higher (2nd episode) than standard pressure at sea level (1013.25 hPa). It was warmer in March than in the previous year, the monthly temperature average was 3.8°C. During these events, the average temperatures were 4.6°C and 7.0°C and the warmest days were observed on the 10th of March (7.9°C) and the 28th of March (10.5°C). During these events the wind was mild and didn't exceed 2.9 $m \cdot s^{-1}$.

Biomass burning is the second largest source of trace gases in the atmosphere (Bond *et al.*, 2004). The trace gases observed in the plumes originate from several sources: vegetation burning and release of volatile organic compounds (VOC's) within the plants. Emissions from wildfires contain enough amount of CO, NO_x, hydrocarbons and PAHs, to be present in the atmosphere for the participation in ozone, NO_x and GHG cycles (Friedli *et al.*, 2001). The NO_x and CO gases are good indicators of biomass burning, especially for fossil fuel combustion (Andreae and Merlet, 2001). The NO_x mass concentration varied from 7.6 to 60.9 $\mu g \cdot m^{-3}$ and CO from 180 to 480 $\mu g \cdot m^{-3}$ during March, there was no increase in concentration during the biomass burning events. It could be explained that EPA station is located in the urban environment, and NO_x and CO emissions are strongly influenced by local sources, i.e. transport and domestic heating. The sulphur dioxide (SO_2) mass concentration was obtained from the EPA database and SO_4^{2-} loadings – from ACSM.

In order to support the idea of air mass transport of pollutants from vegetation burning areas, carbon stable isotope analysis was performed. The measured $\delta^{13}C_{TC}$ values varied from −28.5‰ to -26.7‰. The lowest $\delta^{13}C_{TC}$ values (−28.5‰) were detected during the period with the highest pollution episode from 9th to 10th of March, 2014. Biomass fuel, which is used for domestic and industrial heating, typically consists of wood. Burning wood products generate aerosol particles with less negative $\delta^{13}C_{TC}$ values, i.e. -26.0 ± 0.1‰ for combustion source of wooden pellets (Garbaras *et al.*, 2015). In case of vegetation burning the $\delta^{13}C_{TC}$ values are more negative and strongly

depend on the grass type. Carbon in materials originated by photosynthesis is depleted of the heavier isotopes. Moreover, there are two types of plants with different biochemical pathways: the C_3 carbon fixation shows higher degree of fractionation and the is less ^{13}C depleted. The C_3 plants commonly growing in the parts of Eastern Europe are *Poa trivialis* and *Convolvulus*. The $\delta^{13}C_{TC}$ values for various grasses are: $-31.3 \pm 0.2‰$ for *Poa trivialis*, $-30.1 \pm 0.2‰$ for *Convolvulus* (Ulevicius *et al.*, 2010) and $-28.4 \pm 0.2‰$ for straw pellets (Garbaras *et al.*, 2015). In our previous study, during the similar pollution event from wildfires in Kaliningrad (Russia) isotopic values were more negative, i.e. $-30.9 \pm 0.2‰$ (Ulevicius *et al.*, 2010). It can be concluded that more negative $\delta^{13}C_{TC}$ values from polluted air mass transport were represented by vegetation burning.

4.3.2 Principal component analysis of atmospheric pollutants

PCA was applied for PM_{10}, BC, trace gas and meteorological data. Initial eigenvalues showed that the first three principal components were significant and explained 76.6% (PC_1 – 42.2%, PC_2 – 21.3% and PC_3 – 13.1%) of variance in data (Table 6). PM_{10}, BC, NO_2 and SO_2 had the most significant factor loadings for primary component (PC_1). Thus, this component could be associated with open vegetation burning source. PC_2 had strong meteorological (*WS* and *RH*) and CO factor loadings. Negative correlation of *WS* and *RH* with PM_{10} could be explained with the increase of the wind, pollutants were better diluted and mixed. CO gases indicated that the source originated from domestic heating or traffic emission incomplete fuel combustion. For PC_3 only *WD* had a strong factor loading. BC factor loadings (0.65 and 0.35) for PC_1 and PC_2 correlated with main pollutants such as PM_{10} (0.87 and 0.21). Moreover, BC correlated well with CO in PC_2 and PC_3. Both of these factors originate from incomplete combustion sources.

Table 6. PCA factor matrix. PM_{10}, trace gas and meteorological data were obtained from the EPA station (City centre) in Klaipėda and BC from Preila measurement station. Significant factor loadings (with absolute values > 0.6) are in bold.

Factors	PC_1	PC_2	PC_3
PM_{10}	**0.87**	0.21	–0.07
BC	**0.65**	0.39	0.18
SO_2	0.59	0.42	–0.26
NO_2	**0.80**	–0.29	–0.06
CO	0.28	**0.79**	0.14
WD	0.07	–0.05	**0.96**
WS	0.58	**–0.75**	0.03
RH	–0.24	**–0.72**	–0.01
Variance explained	42.2%	21.3%	13.1%

4.3.3 Cluster analysis of air mass trajectories and aerosol constituents

Clustering of air masses is representation of similar trajectories by movement and direction. The air masses from W and NW direction, represented in the 2nd, 4th and 5th clusters (Fig. 27), were longer and moved faster, while trajectories in the 1st, 3rd and 6th clusters were shorter and moved slower. Six clusters by their representative trajectories are shown in Fig. 27 as well as corresponding average BC concentration associated with each cluster. Based on the analysis of the whole trajectory data set, the most frequently arriving directions was SW (3rd cluster; 27%), W and NW (5th cluster; 23%), followed by NE (6th cluster; 20%), SE (1st cluster; 13%), W (2nd cluster; 10%) and SW (4th cluster; 7%). Biomass burning in Belarus and Ukraine was indicated due to high CWT values. The trajectories of the 3rd cluster were the shortest, therefore air masses spent more time over the same area (i.e. Kaliningrad and Poland). It indicated the accumulation of pollutants from the vegetation burning, which had

occurred at that time of the year. In this cluster, the highest BC concentration reached up to 12.00 µg·m^{-3} and average total non-refractory aerosol component loading was 7.20 µg·m^{-3}.

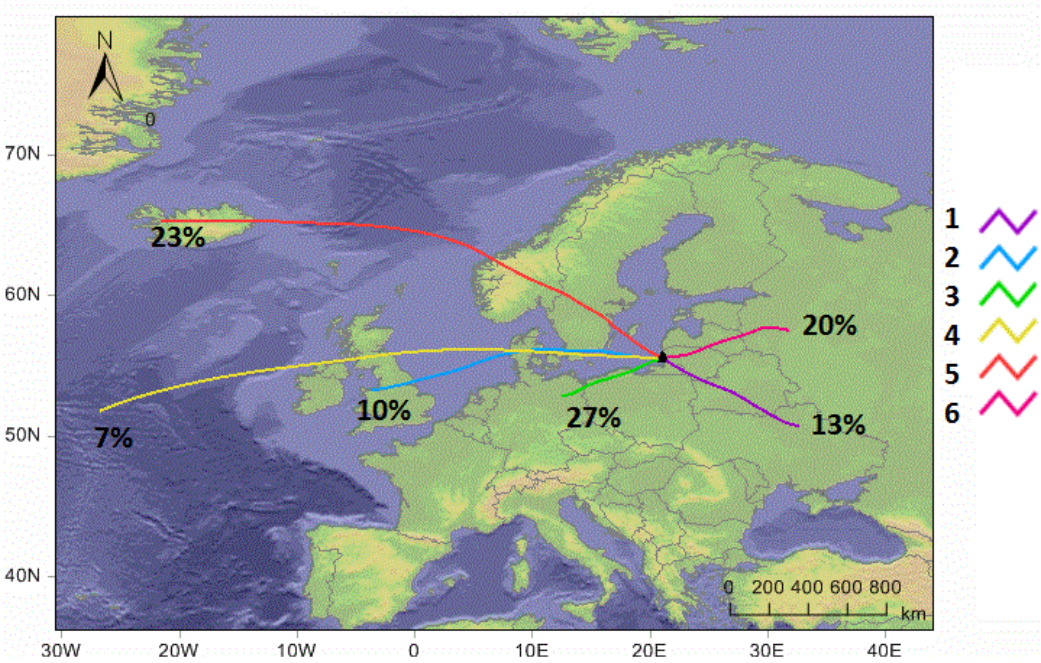

Fig. 27. Representation of air mass backward trajectories over Preila station grouped into six clusters during March 2014

Table 7. The clusters and the mean concentration of organic matters, nitrate, sulphate, ammonium, chloride and BC for each cluster

Clusters	Org., µg·m^{-3}	SO_4^{2-}, µg·m^{-3}	NO_3^-, µg·m^{-3}	NH_4^+, µg·m^{-3}	Cl^-, µg·m^{-3}	BC, µg·m^{-3}
1st	8.94	2.25	0.56	1.68	0.23	1.29
2nd	5.64	0.91	1.10	1.34	0.18	0.51
3rd	3.30	1.2	3.23	1.03	0.21	0.50
4th	6.81	2.21	1.42	1.28	0.06	0.25
5th	1.60	0.71	1.26	0.3	0.08	0.08
6th	4.62	1.12	1.54	1.35	0.23	0.60

The 4th and 5th clusters were represented by clean and fast moving air masses from the W and NW and resulted in BC concentrations equal or lower than estimated mean value of 0.75 $\mu g \cdot m^{-3}$ in Preila.

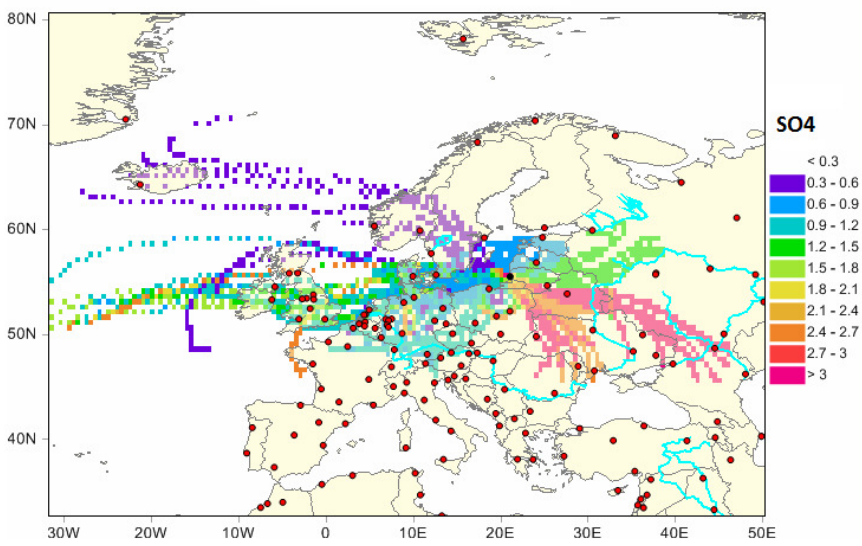

Fig. 28. CWT map for SO_4^{2-} ($\mu g \cdot m^{-3}$), major source areas are dark red-shaded ($\leq 90^{th}$ percentile of study CWTs); non-sources areas are light blue-shaded ($\leq 10^{th}$ percentile of study CWTs).

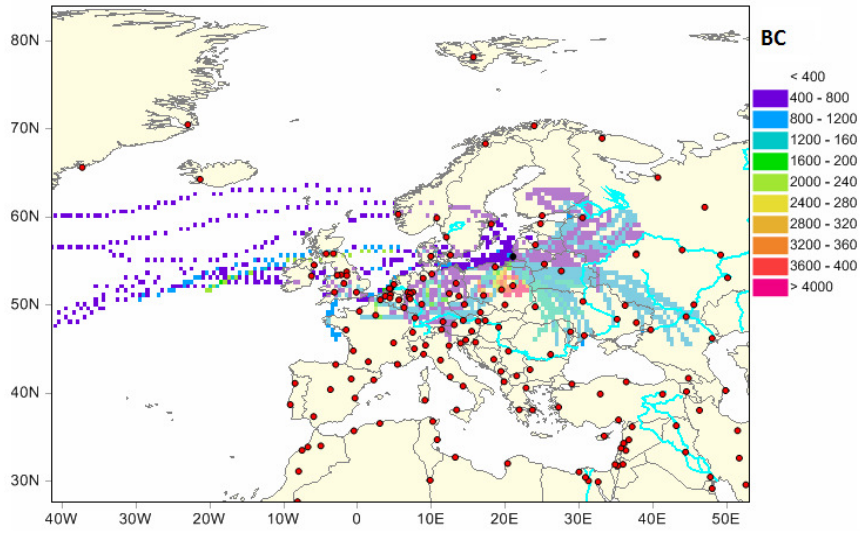

Fig. 29. CWT map for BC ($\mu g \cdot m^{-3}$), major source areas are dark red-shaded ($\leq 90^{th}$ percentile of study CWTs); non-sources areas are light blue-shaded ($\leq 10^{th}$ percentile of study CWTs).

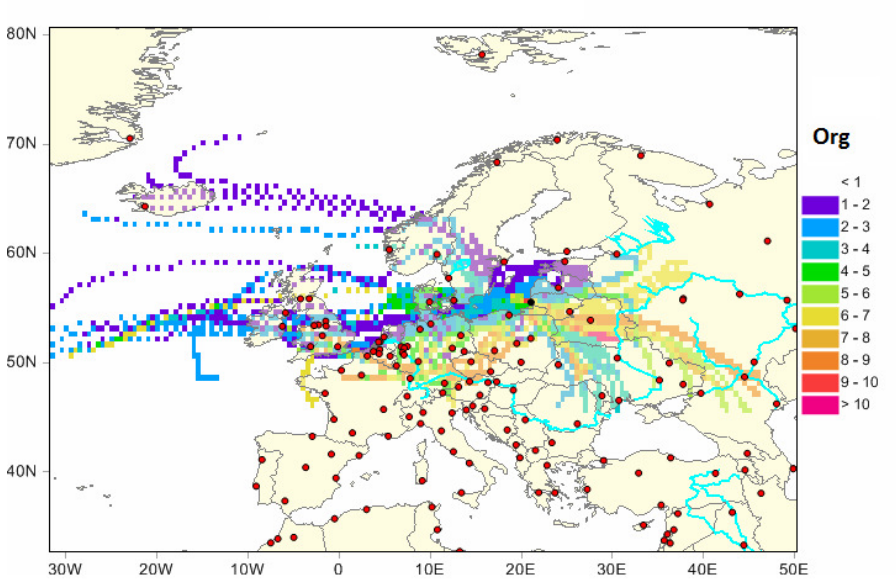

Fig. 30. CWT map for organic matter ($\mu g \cdot m^{-3}$), major source areas are dark red-shaded ($\leq 90^{th}$ percentile of study CWTs); non-sources areas are light blue-shaded ($\leq 10^{th}$ percentile of study CWTs).

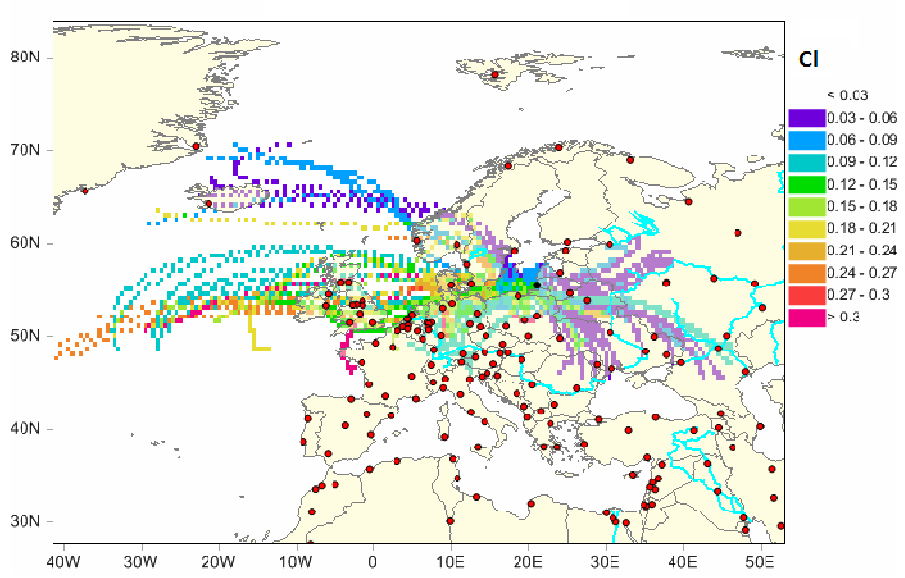

Fig. 31. CWT map for Cl^- ($\mu g \cdot m^{-3}$), major source areas are dark red-shaded ($\leq 90^{th}$ percentile of study CWTs); non-sources areas are light blue-shaded ($\leq 10^{th}$ percentile of study CWTs).

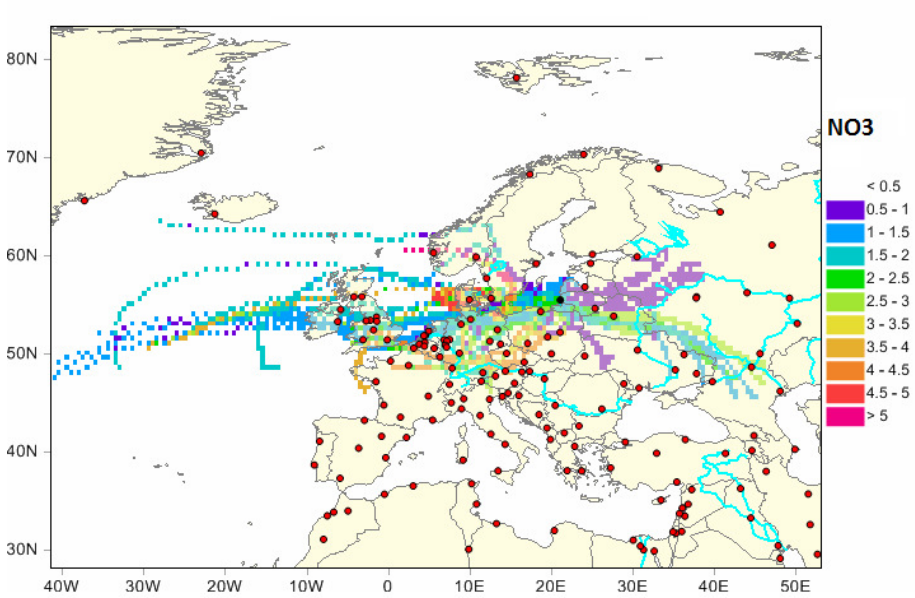

Fig. 32. CWT map for NO_3 ($\mu g \cdot m^{-3}$), major source areas are dark red-shaded ($\leq 90^{th}$ percentile of study CWTs); non-sources areas are light blue-shaded ($\leq 10^{th}$ percentile of study CWTs).

Most polluted 1st and 3rd clusters represent polluted transport pathway for organic components, nitrate, sulphate, ammonium, chloride and BC (Table 7, Figs. 28–32). The air masses associated with these clusters originated from the biomass burning areas, indicating that it is an important transport pathway that caused high concentrations at Preila station.

It should be noted that the trajectories in the 3rd cluster are the shortest among all the six clusters, indicating the accumulation of pollutants arrived from open vegetation burning areas. 1st cluster represents the second most polluted transport pathways with the high concentrations, but the observed air masses were related to the southeast pathways (Belarus and Ukraine). Along such pathways the high biomass burning emissions was located, which was indicated by high CWT values. The average BC concentrations for 4th and 5th clusters were lowest indicating that the pathway from west is relatively cleaner than that from continent.

The 1st cluster represented the SE air mass trajectory pathway with the highest mean concentrations for the whole measurement period (Table 7). Air

masses that reach Preila station from the west have already passed highly industrialized regions in Western Europe, namely Belgium, Netherlands, southern England and western Germany. This area has the highest population density in Europe. The BC and NO_3^- concentrations significantly increase when the air masses cross Poland. In Europe residential wood combustion is the largest anthropogenic source of OA (Kulmala *et al.*, 2011 and Visschedijk *et al.*, 2009).

4.3.4 New particle formation events

Observed NPF could be attributed to the grass burning and secondary biomass burning product transformation, i.e. gases released by fires together with primary particles (Pratt *et al.*, 2011) could undergo oxidation in the atmosphere to form lower volatility compounds, which condense to form SOA and contribute to the increase in PNC (Fig. 33) (Kroll and Seinfeld, 2008). At 13:00, there is significant NPF on the 9th and 10th of March followed by subsequent growth during the following three hours. The total particle number concentration increased up to $1.3 \cdot 10^4$ cm^{-3} (*SD* $0.6 \cdot 10^3$ cm^{-3}), which was extremely higher than the mean observations in this area ($2.7 \cdot 10^3$ cm^{-3}; *SD* $0.9 \cdot 10^3$ cm^{-3}) and is comparable only with spring concentration maxima ($1.3 \cdot 10^4$ cm^{-3}; *SD* $1.0 \cdot 10^3$ cm^{-3}). Meanwhile, the diurnal pattern of *WD* was observed mainly coming from the S–SW (190°–215°) with slightly higher speed in the daytime (2–3 m·s^{-1}) and decreasing at night.

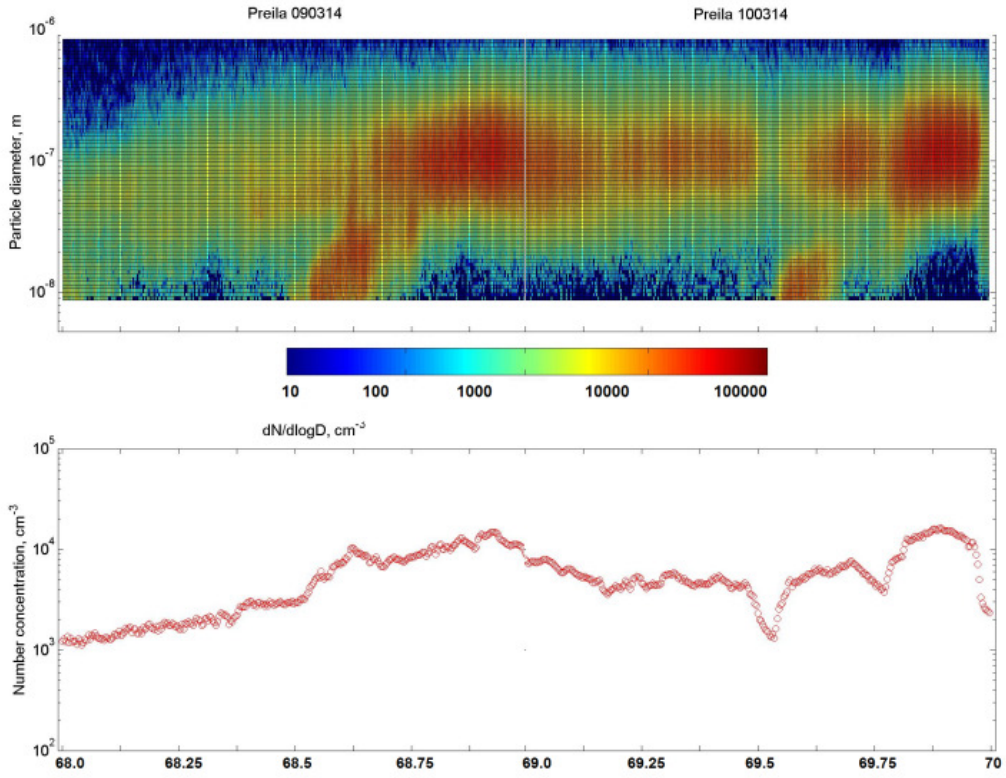

Fig. 33. NPF event in Preila site on the 9th March 2014: particle size distribution data as a surface plot. The measured aerosol PNSDs are fitted and parameterised by a multi-lognormal distribution ($dN/d\log D_p$ in notation of cm^{-3}).

T and *RH* were 10°C and 62%, respectively, on NPF event days, which are higher than that the values on non-event days (5°C and 77%). This result is consistent with the theory that lower RH is favourable to the enhancement of atmospheric nucleation (Hamed *et al.*, 2007). The mean wind speed on NPF event days was slightly higher (1.8 $m \cdot s^{-1}$) than that on non-event days (1.3 $m \cdot s^{-1}$), which is favourable to the dilution of the pollutants. The most striking difference between typical (Kulmala and Kerminen, 2008) observed NPF events is imprinted in the aerosol size distribution and number concentration when stable accumulation mode particle existed in the aged plume (Fig. 33).

Table 8. Characteristics of nucleation rates, ACSM data and associated meteorological parameters observed during nucleation (mean formation rate 0.6 $cm^{-3} \cdot s^{-1}$) during vegetation burning events

Parameters	**Mean**	**Median**	**SD**	**Min**	**Max**
PNC, cm^{-3}	5,960	5,110	3,820	1,120	16,230
Surface area, $\mu m^2 \cdot cm^{-3}$	344	308	271	15	1187
Volume, $\mu m^3 \cdot cm^{-3}$	15	14	11	0.4	51
p, hPa	1,025	1,024	10	1,020	1,028
T, °C	10.1	8.0	3.6	3.4	13.4
RH, %	62	61	18	45	92
WS, $m \cdot s^{-1}$	1.8	1.6	0.8	0.5	3.1
WD, °	209	208	34	135	286
Incoming radiation, $W \cdot m^{-2}$	290	256	146	190	371
Org., $\mu g \cdot m^{-3}$	22.9	19.8	19.5	0.5	78.6
SO_4^{2-}, $\mu g \cdot m^{-3}$	2.0	2.0	1.2	0.04	4.6
NO_3^-, $\mu g \cdot m^{-3}$	6.5	6.3	4.8	0.1	17.8
NH_4^+, $\mu g \cdot m^{-3}$	2.7	2.6	1.7	0.1	6.2
Cl^-, $\mu g \cdot m^{-3}$	1.1	0.5	1.3	0.0	5.4

The nucleated particles grew in size and reached the detection size limit of the instrument at 12:30 which overlapped with the distribution of particles from vegetation burning emissions. The secondary particles were mixed with the existed primary accumulation mode particles which is an indication that the source region for nucleation mode aerosol is further away from the measurement point. Larger particles could decrease the number of newly formed particles due to coagulation on their surface (Kulmala *et al.*, 2001).

4.3.5 Organic aerosol triangular method

For the characterisation of the aging of OA in the atmosphere during vegetation burning events, f_{44} and f_{43} components were extracted from the

ACSM measurements at Preila station for the period from 9th to 15th of March, 2014 (Fig. 34). One dot represent 30 min measurement for aerosol component loadings and the colour represents the date of measurements were conducted. On March 14th–15th air masses were not affected by regional vegetation burning events and the f_{43} vs. f_{44} values were found mostly in the upper area of triangular plot. Thus, the contribution was mainly due to factor LV-OOA. During the vegetation burning episode on March 9th–10th, the values were observed in the lower triangular area around one of its lines ($y = -6.0204\,x + 0.4154$) (Ng *et al.*, 2010). It indicates that oxidation state of OA components was stable during the episode and the main contribution of SV-OOA factor was estimated.

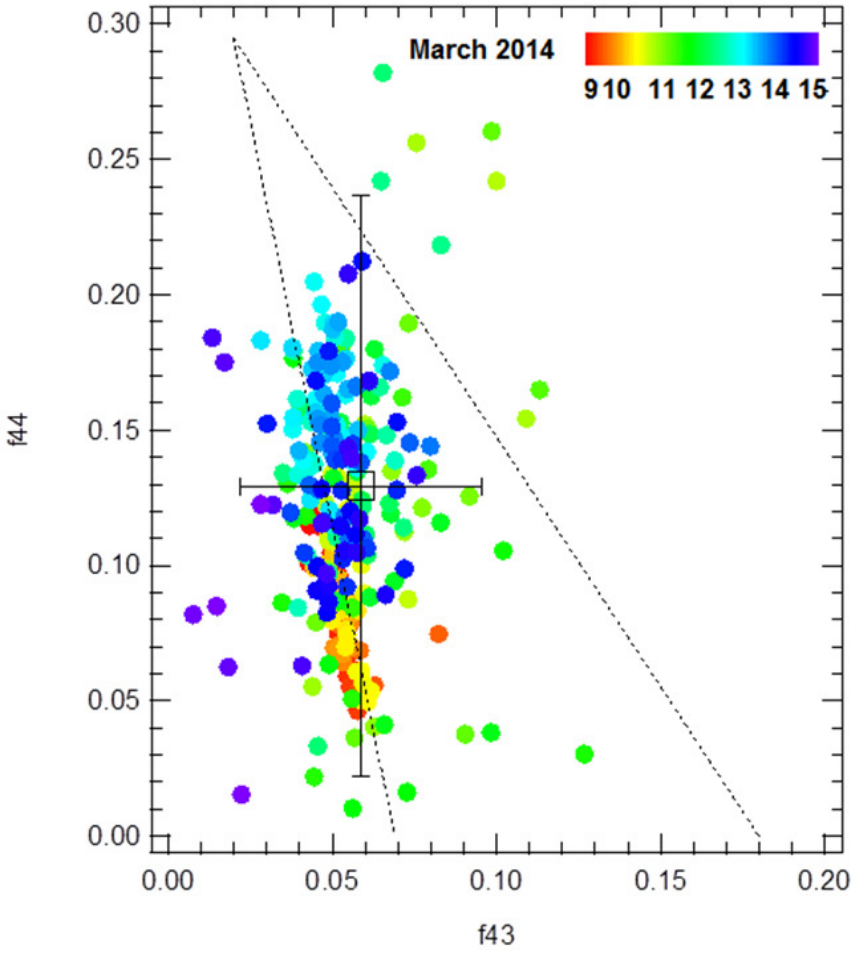

Fig. 34. The fractional signals f_{43} and f_{44} of vegetation burning and OOA during the study. Dotted line shows the limits of OOA

4.3.6 Conclusions

1. During the regional spring vegetation burning mass concentration of organic aerosol is increased up to 50% in the background of South-Eastern Baltic Sea region.
2. The most polluted air masses were originated from SW (Poland, Kaliningrad, Belarus) areas, where vegetation fires occurred, indicating that it is an important transport pathway of pollutants, causing the increase of background level values of NR-$PM_{1.0}$ component loadings concentration in the South-Eastern Baltic Sea region.
3. The $\delta^{13}C_{TC}$ value of –28.5% indicated the dominance of the aerosol derived from the vegetation burning as no significant carbon isotope fractionation occurs between the aerosol particles from biomass burning and the raw biomass material.

4.4 Aerosol particle number size distribution and carbon stable isotope ratio application for fossil fuel combustion and non-fossil emission source identification

In this study, measurements were conducted at the urban background station in Vilnius. The filter samples were collected with a 11-stage cascade impactor (MOUDI) for 72-h each. There were 5 filter sampling periods from the 12th to 29th of October, 2012. The combined SMPS and APS measurements were running from the 19th to the 29th of October, 2012. During the measurements, the SMPS was scanning the particles with mobility diameter (D_M) in the range of 7–299 nm and the APS – with D_A 0.5–20.0 μm.

4.4.1 Aerosol particle size distribution and carbon stable isotope ratio analysis

The conversion of aerosol particle number to mass concentration was applied as had been described in Chapter 3.2.4. As seen in Table 9, the aerosol mass concentrations measured with SMPS and APS for fine mode (D_A: 0.10–0.17 μm, < 0.3 μm and 0.5–1.0 μm) particles were 17.71 ± 0.50 μg·m^{-3}, 8.07 ± 0.50 μg·m^{-3} and 3.93 ± 0.50 μg·m^{-3} during the 19th–22nd, the 23rd–26th and the 26th–29th of October, 2012, respectively. The same trend was observed for the coarse fraction (D_A: 1.7–20.5 μm) for the corresponding periods: 8.20 ± 0.50 μg·m^{-3}, 3.94 ± 0.50 μg·m^{-3} and 1.91 ± 0.50 μg·m^{-3}, respectively. Two distinct periods associated with contrasting pollution patterns were examined in more detail. The first period was characterised by the highest particle mass concentration calculated from the SMPS-APS data (17.71 ± 0.50 μg·m^{-3}) during the 19th–22nd of October, 2012 and the lowest variability of $\delta^{13}C_{TC}$ range was from −25.2‰ to −28.0‰). The second period was characterised by the lowest mass concentration in the fine mode (3.93 ± 0.50 μg·m^{-3}) during the 26th–29th of October, 2012 and a similar variability of $\delta^{13}C_{TC}$ values from −24.3‰ to −28.0‰.

Table 9. Evaluation of aerosol mass concentration contribution to MOUDI cascades derived from particle size distribution data obtained from SMPS-APS tandem measurements

Measurement period		APS/SMPS					
		Inlet+Cas .X	Cas.VII+ VIII+IX	Cas.IV+ V+VI	Cas. II+III	Cas.I	Total conc.
		D_{50}: 9.7–17.5 µm (µg·m^{-3})	D_{50}: 1.7–6.0 µm (µg·m^{-3})	D_{50}: < 0.3 µm; 0.5–1.0 µm (µg·m^{-3})	D_{50}: 0.10–0.17 µm (µg·m^{-3})	D_{50}: 0.07 µm (µg·m^{-3})	0.02–0.30 µm; 0.5–20.5 µm (µg·m^{-3})
Start time	End time						
09/19/2013	09/22/2013	3.44	4.76	12.47	5.24	0.47	**26.38**
09/23/2013	09/26/2013	0.52	3.42	4.90	3.17	0.31	**12.32**
09/26/2013	09/29/2013	0.25	1.66	2.12	1.81	0.25	**6.09**

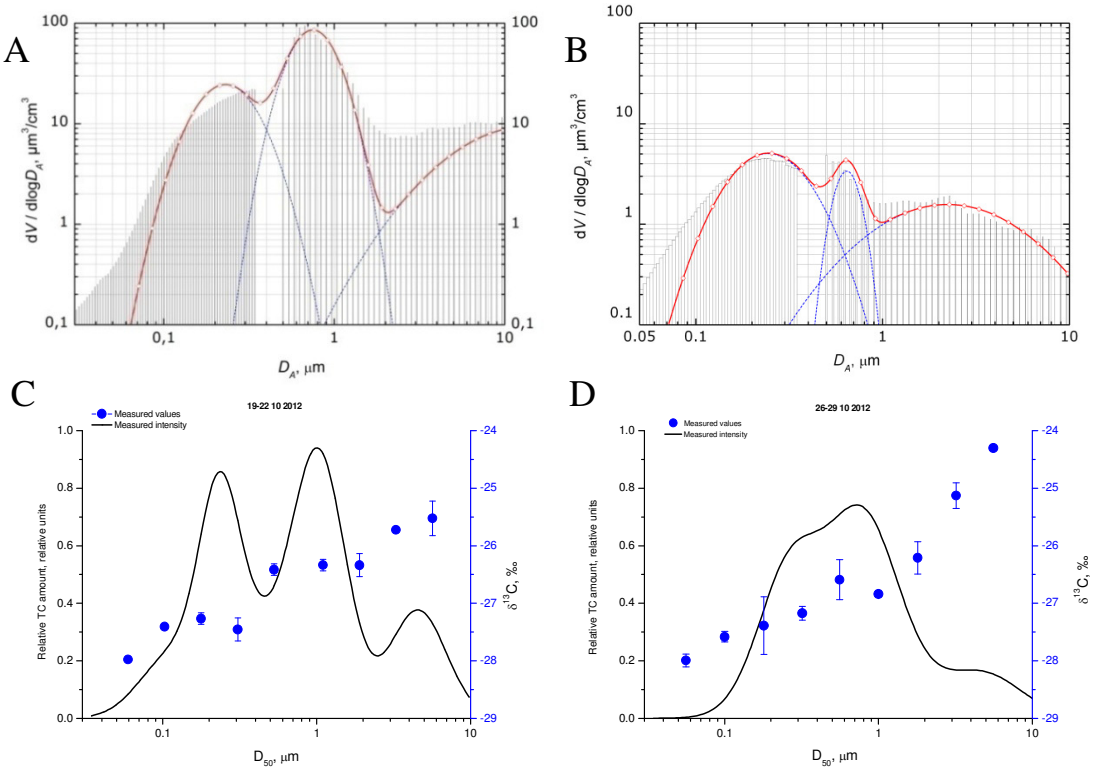

Fig. 35. Aerosol particle volume distribution dV/dlogD_A of a combined SMPS-APS data for the two periods: A) the 21st of October, 2012 and B) the 28th of October, 2012. Carbon isotope $\delta^{13}C_{TC}$ values in size segregated aerosol particles for the two contrasting periods: C) the 19th–22nd of October, 2012 and D) the 26th–29th of October, 2012 along with the measured relative intensity of carbon signal in size segregated particles.

Aerosol volumetric particle size distribution, measured by the SMPS-APS (Fig. 35 A, B) and the TC signal intensity size distribution (Fig. 35 C, D) revealed resemblance between the modes. The smallest TC particle mode had D_A = 0.23 μm. This mode is typically considered as the primary anthropogenic aerosol particles with average $\delta^{13}C_{TC}$ = −28.0‰ suggesting fossil fuel combustion. The peak of fine aerosol particles was observed at D_A = 0.70 μm. Both sources were contributing to the carbonaceous particle mass in this range. The isotopically heaviest (the most enriched in ^{13}C) carbonaceous particles were observed in the coarse particle mode D_A = 7.05 μm.

4.4.2 Air mass trajectory analysis and carbon stable isotope ratio variations

It was demonstrated that $\delta^{13}C_{TC}$ values of $PM_{2.5}$ depended on the sector air masses had been originated from (Garbaras *et al.*, 2008). The smallest variation of $\delta^{13}C_{TC}$ values by −28.0‰ was observed in the southern (continental) air masses (Fig. 36 A), corresponding to 5th sector and 4th sector (Ovadnevaite *et al.*, 2007). 5th sector was classified as polluted sector characterised by various types of pollution such as re-suspended road dust, petrol and diesel emission, oil and coal combustion, ferrous and non-ferrous smelters (Swietlicki, 1989). The average $\delta^{13}C_{TC}$ value was equal to −27.3 ± 0.6‰ for the fine particles and −25.8 ± 0.5‰ in the coarse particle mode during the period of the 19th–22nd of October, 2012.

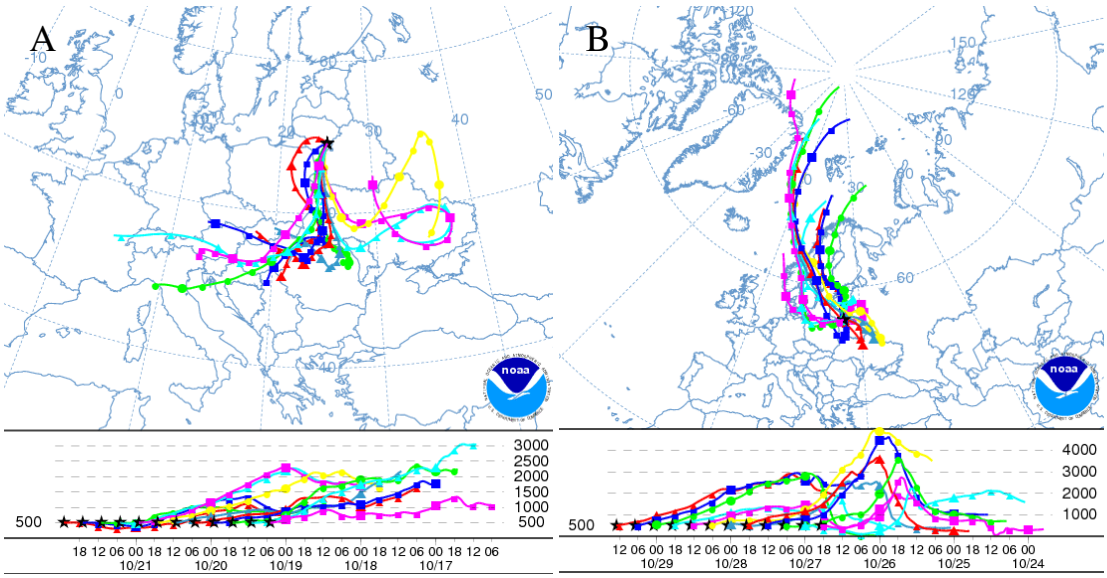

Fig. 36. The air mass backward trajectories were obtained by HYSPLIT-4 model (Draxler and Rolph, 2015) during the filter sampling periods: A) the 19th–22nd of October, 2012 air masses dominated from the south direction and B) the 26th–29th of October, 2012 air masses arrived from the N and NW direction.

Meanwhile, the average $\delta^{13}C_{TC}$ values observed mostly in the northern air masses (Fig. 36 B) during the period of the 26th and 29th of October, 2012 were equal to −27.3 ± 0.5‰ in the fine mode and −25.4 ± 1.0‰ in the coarse particle mode. Similar carbon stable isotope ratios during two contrasting periods suggested a mixing of a few sources with distinct stable carbon isotope values. One such source could be a major contributor of fine particles while the contribution of the second source was probably more variable.

The meteorological parameters (*WD*, *WS* and *p*, etc.) can reveal local pollution sources, which can affect aerosol particle size distribution and the variation of the stable isotope ratio. For instance, a change in the *WD* and *WS* resulted in the sharp decrease of $\delta^{13}C_{TC}$ values in $PM_{2.5}$ and PM_{10} from −24.0‰ to −29.0‰ (López-Veneroni, 2009). In our case, the *WD* from 0^{o} to 90^{o} was used for estimating local urban pollution of anthropogenic sources, i.e. fossil fuel combustion, biomass burning and road dust.

The largest variability in $\delta^{13}C_{TC}$ values (6.7‰) was associated with the air masses, spending the shortest time over the urban sector (13 of the sampling time). It suggested that the air masses, which avoided the urban sector, had possessed a different isotopic signature.

4.4.3 Bayesian isotope mixing model application for fossil fuel combustion and non-fossil fuel emission source identification

A two source mixing model was applied with size segregated aerosol particles, deposited on the filters. The source mixing equation was applied to verify the idea of mixing of two distinct sources Eq. (16). It is proposed that one source can be attributed mainly to the city pollution. It was revealed that the $\delta^{13}C_{TC}$ values of fossil fuel combustion in aerosol may vary in different European regions and for Lithuanian ethanol fuel (E85, consisting of 85% of ethanol and 15% of gasoline) was -28.6 ± 0.7‰, and for diesel -31.6 ± 0.1‰ (Mašalaitė *et al.*, 2012). Typically, the $\delta^{13}C_{TC}$ values for diesel and gasoline are fairly constant for the same measurement region, and it was observed during our measurements that aerosol particles in the fine particle mode ($D_P < 1.0$ μm) the average $\delta^{13}C_{TC}$ value was of −28.0‰. It was reasonable to consider $\delta^{13}C_{TC} = -28.0$‰ as the primary source for fossil fuel combustion.

The second source in this model is referred to non-fossil fuel, which can be influenced both by biomass burning and biogenic emissions. The $\delta^{13}C_{TC}$ values obtained from biomass burning might be scattered broadly and are strongly influenced by the fuel source: for instance, in Garbaras *et al.* (2015) studies wood pellets were -27.0 ± 0.2‰ and sunflower stalk pellets were -25.1 ± 0.2‰.

The fractional source contributions were calculated using Eq. (16). The first source was chosen as the fossil fuel source with $\delta^{13}C_1$ equal to −28.0‰. The second source was termed as the non-fossil fuel source and the $\delta^{13}C_{TC}$ values varied in the range of −24.0‰ to −26.0‰. In fact, the source values of both sources were varied, but only a few pairs of the values allowed

constraining to the measured isotope values. For example, if fractional contribution of either source in any size interval exceeded 100% (and the other source fractional contribution becoming negative) such values were declared unreasonable. In the end only the fossil fuel combustion source value of −28‰ was reasonable while the non-fossil fuel source value of either −25‰ or −25.5‰ produced reasonable fractional contributions. The fossil fuel combustion was the main contributor (from 100% to 60%) to the carbonaceous PM in the fine mode range ($D_P < 1.0$ µm). A transition region was identified in the particle range from 0.5 to 2.0 µm. The two sources were found to almost equally contributing to carbonaceous PM in this range. The non-fossil fuel source was dominant (from 60% to 100%) in the coarse fraction ($D_P > 2$ µm). Similar results were obtained for the two contrasting periods: the 19^{th}–22^{th} and the 26^{th}–29^{th} of October, 2012. Thus the use of the two source mixing equation let us to explain the distribution of $\delta^{13}C_{TC}$ values in size segregated carbonaceous particles.

4.4.4 Conclusions

1. The highest aerosol mass concentration ($17.71 \pm 0.50\ \mu g \cdot cm^{-3}$) in the fine particle mode ($V_{TOT} = 262 \pm 139\ cm^{-3}$, $D_A = 0.23 \pm 0.02\ \mu m$, $\sigma_g = 1.54 \pm 0.06$) was reached in the sampling of October 19th–22nd, 2012, while $\delta^{13}C_{TC}$ was in the range from −25.2‰ to −28.0‰. It was indicated as a polluted episode.
2. The lowest aerosol mass concentration ($3{,}93 \pm 0{,}50\ \mu g \cdot m^{-3}$) in the fine particle mode ($V_{TOT} = 98 \pm 76\ cm^{-3}$, $D_A = 0.22 \pm 0.02\ \mu m$, $\sigma_g = 1.62 \pm 0.02$) was reached in the sampling of October 26th–29th, 2012, while $\delta^{13}C_{TC}$ was in the range from −24.3‰ to−28.0‰. It was indicated as a clean episode.
3. The fossil fuel combustion source was modelled with constrained $\delta^{13}C_{TC} = -28.0$‰ values and contributed to the fine particle mode ($V_{TOT} = 180 \pm 138\ cm^{-3}$, $D_A = 0.23 \pm 0.02\ \mu m$, $\sigma_g = 1.58 \pm 0.16$) from 60% to 100%. The secondary source was attributed to the non-fossil fuel source emission and modelled with constrained $\delta^{13}C_{TC} = -25.3 \pm 0.3$‰ values and contributed from 60% to 100% in the coarse particle mode ($V_{TOT} = 176 \pm 185\ cm^{-3}$, $D_A = 7.05 \pm 3.56\ \mu m$, $\sigma_g = 1.98 \pm 0.30$).
4. Application of the Bayesian isotope mixing model explained the $\delta^{13}C_{TC}$ variation in the size segregated carbonaceous aerosol particles.

Main conclusions

1. The long-range transport of air masses increased the background level values of particle number concentration in Vilnius city. In autumn the air masses arriving from W and SE increased by 40% and 120% of the estimated background level ($5.0 \cdot 10^3$ cm^{-3}), respectively. In winter the air masses arriving from SW and NW resulted in 20% and 55% increase of the estimated background level ($1.0 \cdot 10^4$ cm^{-3}), respectively. In spring the air masses arriving from SW and NW increased 65% and 130% of the estimated background level ($5.0 \cdot 10^3$ cm^{-3}), respectively.
2. The long-range transport of air masses is the main contributor to the increase of the background level of black carbon mass concentration in the South-Eastern Baltic Sea region. In autumn the air masses arriving from S and SE contributed up to 50% to the increase of the estimated background level (0.71 μg·m^{-3}). In winter season the air masses arriving from NE, SW and S resulted in 50%, 220% and 350% increase of the background level, respectively. In spring season the air masses affected by vegetation fires contributed 80% of increase of the background level.
3. During the regional spring vegetation burning mass concentration of organic aerosol was increased up to 50% in the background environment of South-Eastern Baltic Sea region.
4. The fossil fuel combustion source was modelled with constrained $\delta^{13}C_{TC} = -28.0‰$ values and contributed to the fine particle mode ($V_{TOT} = 180 \pm 138$ cm^{-3}, $D_A = 0.23 \pm 0.02$ μm, $\sigma_g = 1.58 \pm 0.16$) from 60% to 100%. The secondary source was attributed to the non-fossil source with constrained $\delta^{13}C_{TC} = -25.3 \pm 0.3‰$ values and contributed to the coarse particle mode ($V_{TOT} = 176 \pm 185$ cm^{-3}, $D_A = 7.05 \pm 3.56$ μm, $\sigma_g = 1.98 \pm 0.30$) from 60% to 100%.

SUMMARY

Fine and ultrafine particles play important role in the climate systems, however the largest uncertainties of the anthropogenic radiative forcing (RF) occurs due to the underestimation of aerosol contribution. Thus, it is important to assess the spatial variability and pollution sources of atmospheric aerosol constituents.

In this work the receptor modelling—potential source contribution function (PSCF), chemical weighted trajectory (CWT) analysis and air mass trajectory cluster analysis—of aerosol particle number concentration (PNC) and black carbon (BC) sources was applied. The effects of air mass transport of atmospheric pollutants from regional biomass burning and vegetation fires in the South-Eastern Baltic Sea region were estimated. The aerosol component loadings were investigated by aerosol chemical speciation monitor (ACSM) and aethalometer, particle number concentration and size distribution were depicted by condensational particle counter (CPC), scanning mobility particle sizer (SMPS) and aerodynamic particle sizer (APS), stable isotope mass spectrometry was conducted on collected filters.

Results from receptor modelling indicated that the long-range transport (LRT) of air masses had increased the PNC background level values ($1.0 \cdot 10^4$ cm^{-3}) up to 55% during the winter period in Vilnius city. In autumn and spring the estimated background level values ($5.0 \cdot 10^3$ cm^{-3}) were increased up to 130%. The background BC level in the South-Eastern Baltic Sea region was estimated to be 0.71 μg·m^{-3}. Receptor modelling of BC concentration showed that during the whole study period the lowest concentrations had been observed in the clusters from N and NW and had varied in the range from 0.22 μg·m^{-3} to 0.45 μg·m^{-3}. The increase of BC concentration was affected in winter by biomass burning up to 350% and in spring – by vegetation fires up to 80%.

It was proved that the combined aerosol particle sizing technique and carbon stable isotope ratio ($\delta^{13}C_{TC}$) analysis were suitable for fossil fuel

combustion and non-fossil emission source estimation. From the Bayesian isotope mixing model the fossil fuel source main contribution was indentified in the fine particle mode from 60% to 100% with $\delta^{13}C_{TC} = -28.0‰$ and the non-fossil source main contribution – in the coarse particle mode from 60% to 100% with $\delta^{13}C_{TC} = -25.3‰$.

ACKNOWLEDGMENTS

The work was supported by the Lithuanian State Science and Studies Foundation under project No. ESF-2O11-O4.

I'd like to sincerely thank my supervisor dr. V. Ulevičius for the support and guidance on this hard scientific path.

I'd like to thank dr. S. Byčenkienė for consulting on the PhD thesis, support and bringing me into the world of receptor modelling.

I'm grateful to my colleagues dr. K. Plauškaitė-Šukienė, dr. D. Jasinevičienė, dr. D. Valiulis, dr. G. Mordas, dr.I. Garbarienė, dr. J. Šakalys, , dr. N. Prokopčiuk, , A. Andriejauskas, dr. J. Andriejauskienė, J. Didžbalis, J. Pauraitė and K. Senuta for working together in encouraging environment, for achieving the goals, for immense support and for helping me to succeed.

I'd like to thank colleagues dr. A. Garbaras, dr. A. Mašalaitė and prof. V. Remeikis from Mass spectrometry laboratory at Center for physical sciences and technology for productive collaboration and for performing stable isotope ratio (^{13}C:^{12}C) analysis.

I'd like to thank my family for encouraging me to continue on this scientific endeavour.

And thanks to other supporters, who wished me all the best on this work.

REFERENCES

Aalto, P., Hämeri, K., Paatero, P., Kulmala, M., Bellander, T., Berglind, N., *et al.*: Aerosol particle number concentration measurements in five European cities using TSI-3022 condensation particle counter over a three-year period during health effects of air pollution on susceptible subpopulations., J. Air Waste Manag. Assoc., 55(8), 1064–1076, 2005.

Abdalmogith, S. S. and Harrison, R. M.: The use of trajectory cluster analysis to examine the long-range transport of secondary inorganic aerosol in the UK, Atmos. Environ., 39(35), 6686–6695, 2005.

Allan, R. P.: Simulation of the Earth's radiation budget by the European Centre for Medium-Range Weather Forecasts 40-year reanalysis (ERA40), J. Geophys. Res., 109(D18), D18107, 2004.

Andreae, M. O. and Merlet, P.: Emission of trace gases and aerosols from biomass burning, Global Biogeochem. Cycles, 15(4), 955–966, 2001.

Anttila, P., Makkonen, U., Hellén, H., Kyllönen, K., Leppänen, S., Saari, H., *et al.*: Impact of the open biomass fires in spring and summer of 2006 on the chemical composition of background air in south-eastern Finland, Atmos. Environ., 42(26), 6472–6486, 2008.

APS TSI model 3321 instruction manual, 2004, http://www.wmo-gaw-wcc-aerosol-physics.org/files/APS_3321.pdf , (2015-04-17).

Ara Begum, B., Kim, E., Jeong, C.-H., Lee, D.-W. and Hopke, P. K.: Evaluation of the potential source contribution function using the 2002 Quebec forest fire episode, Atmos. Environ., 39(20), 3719–3724, 2005.

Ashbaugh, L. L., Malm, W. C. and Sadeh, W. Z.: A residence time probability analysis of sulfur concentrations at grand Canyon National Park, Atmos. Environ., 19(8), 1263–1270, 1985.

Asmi, A., Collaud Coen, M., Ogren, J. A., Andrews, E., Sheridan, P., Jefferson, A., *et al.*: Aerosol decadal trends – Part 2: In-situ aerosol particle number concentrations at GAW and ACTRIS stations, Atmos. Chem. Phys. Discuss., 12(8), 20849–20899, 2012.

Barkstrom, B., Harrison, E., Smith, G., Green, R., Kibler, J., Cess, R., *et al.*: Earth Radiation Budget Experiment (ERBE) Archival and April 1985 Results, Bull. Am. Meteorol. Soc., 70(10), 1254–1262, 1989.

Baron, P. A. and Willeke, K.: Aerosol measurement: principles, techniques and applications. 2001, n.d.

Beddows, D. C. S., Dall'Osto, M. and Harrison, R. M.: Cluster Analysis of Rural, Urban, and Curbside Atmospheric Particle Size Data, Environ. Sci. Technol., 43(13), 4694–4700, 2009.

Belis, C. A., Larsen, B. R., Amato, F., El Haddad, I., Favez, O., Harrison, R. M., *et al.*: Air Pollution Source Apportionment, 2014.

Beverland, I. J., Tunes, T., Sozanska, M., Elton, R. A., Agius, R. M. and Heal, M. R.: Effect of long-range transport on local PM 10 concentrations in the UK, Int. J. Environ. Health Res., 10(3), 229–238, 2000.

Bond, T. C., Doherty, S. J., Fahey, D. W., Forster, P. M., Berntsen, T., DeAngelo, B. J., et al: Bounding the role of black carbon in the climate system: A scientific assessment, J. Geophys. Res. Atmos., 118(11), 5380–5552, 2013.

Bond, T. C.: A technology-based global inventory of black and organic carbon emissions from combustion, J. Geophys. Res., 109(D14), 2004.

Boucher, O. and Lohmann, U.: The sulfate-CCN-cloud albedo effect., Tellus B, 47(3), 281–300, 1995.

Bougiatioti, A., Stavroulas, I., Kostenidou, E., Zarmpas, P., Theodosi, C., Kouvarakis, G., *et al.*: Processing of biomass-burning aerosol in the eastern Mediterranean during summertime, Atmos. Chem. Phys., 14(9), 4793–4807, 2014.

Boutton, T. W.: Stable carbon isotope ratios of natural materials: I. Sample preparation and mass spectrometric analysis, Carbon Isot. Tech., 155–171, 1991.

Brand, W. A.: High precision isotope ratio monitoring techniques in mass spectrometry, J. mass Spectrom., 31(3), 225–235, 1996.

Brook, R. D., Rajagopalan, S., Pope, C. A., Brook, J. R., Bhatnagar, A., Diez-Roux, A. V., *et al.*: Particulate Matter Air Pollution and Cardiovascular Disease: An Update to the Scientific Statement From the American Heart Association, Circulation, 121(21), 2331–2378, 2010.

Burkart, J., Steiner, G., Reischl, G. and Hitzenberger, R.: Long-term study of cloud condensation nuclei (CCN) activation of the atmospheric aerosol in Vienna, Atmos. Environ., 45(32), 5751–5759, 2011.

Butler, J.H. and Montzka, S.A., The NOAA annual greenhouse gas index (AGGI), http://www.esrl.noaa.gov/gmd/aggi/aggi.html , (2015-01-17).

Byčenkienė, S., Ulevicius, V. and Kecorius, S.: Characteristics of black carbon aerosol mass concentration over the East Baltic region from two-year measurements, J. Environ. Monit., 13(4), 1027, 2011.

Canagaratna, M. R., Jayne, J. T., Jimenez, J. L., Allan, J. D., Alfarra, M. R., Zhang, Q., *et al.*: Chemical and microphysical characterization of ambient aerosols with the aerodyne aerosol mass spectrometer, Mass Spectrom. Rev., 26(2), 185–222, 2007.

Capes, G., Johnson, B., McFiggans, G., Williams, P. I., Haywood, J. and Coe, H.: Aging of biomass burning aerosols over West Africa: Aircraft measurements of chemical composition, microphysical properties, and emission ratios, J. Geophys. Res., 113, D00C15, 2008.

Carslaw, K. S., Lee, L. A., Reddington, C. L., Pringle, K. J., Rap, A., Forster, *et al.*: Large contribution of natural aerosols to uncertainty in indirect forcing, Nature, 503(7474), 67–71, 2013.

Chamaillard, K., Kleefeld, C., Jennings, S. G., Ceburnis, D. and O'Dowd, C. D.: Light scattering properties of sea-salt aerosol particles inferred from modeling studies and ground-based measurements, J. Quant. Spectrosc. Radiat. Transf., 101(3), 498–511, 2006.

Cheng, I., Zhang, L., Blanchard, P., Dalziel, J. and Tordon, R.: Concentration-weighted trajectory approach to identifying potential sources of speciated atmospheric mercury at an urban coastal site in Nova Scotia, Canada, Atmos. Chem. Phys., 13(12), 6031–6048, 2013.

Cheung, H. C., Morawska, L. and Ristovski, Z. D.: Observation of new particle formation in subtropical urban environment, Atmos. Chem. Phys., 11(8), 3823–3833, 2011.

Chow, J. C., Watson, J. G., Chen, L.-W. A., Arnott, W. P., Moosmüller, H. and Fung, K.: Equivalence of Elemental Carbon by Thermal/Optical Reflectance and Transmittance with Different Temperature Protocols, Environ. Sci. Technol., 38(16), 4414–4422, 2004.

Chung, C. E., Ramanathan, V. and Decremer, D.: Observationally constrained estimates of carbonaceous aerosol radiative forcing, Proc. Natl. Acad. Sci., 109(29), 11624–11629, 2012.

Clarke, A. D., Shinozuka, Y., Kapustin, V. N., Howell, S., Huebert, B., Doherty, S., *et al.*: Size distributions and mixtures of dust and black carbon aerosol in Asian outflow: Physiochemistry and optical properties, J. Geophys. Res., 109(D15), D15S09, 2004.

Cyrys, J., Pitz, M., Heinrich, J., Wichmann, H.-E. and Peters, A.: Spatial and temporal variation of particle number concentration in Augsburg, Germany, Sci. Total Environ., 401(1-3), 168–175, 2008.

Dall'Osto, M., Monahan, C., Greaney, R., Beddows, D. C. S., Harrison, R. M., Ceburnis, D., *et al.*: A statistical analysis of North East Atlantic (submicron) aerosol size distributions, Atmos. Chem. Phys., 11(24), 12567–12578, 2011.

Danielsen, E. F. and Bleck, R.: Research in four-dimensional diagnosis of cyclonic storm cloud systems., 1967.

De Foy, B. and Schauer, J. J.: Origin of high particle number concentrations reaching the St. Louis, Midwest Supersite, J. Environ. Sci., 2015.

DeCarlo, P. F., Slowik, J. G., Worsnop, D. R., Davidovits, P. and Jimenez, J. L.: Particle Morphology and Density Characterization by Combined Mobility and Aerodynamic Diameter Measurements. Part 1: Theory, Aerosol Sci. Technol., 38(12), 1185–1205, 2004.

Dorling, S. R., Davies, T. D. and Pierce, C. E.: Cluster analysis: A technique for estimating the synoptic meteorological controls on air and

precipitation chemistry—Method and applications, Atmos. Environ. Part A. Gen. Top., 26(14), 2575–2581, 1992.

Draxler, R. R. and Rolph, G. D.: HYSPLIT (HYbrid Single-Particle Lagrangian Integrated Trajectory) Model access via NOAA ARL READY, http://ready.arl.noaa.gov/HYSPLIT.php , (2015-01-17).

Du, S. and Rodenburg, L. A.: Source identification of atmospheric PCBs in Philadelphia/Camden using positive matrix factorization followed by the potential source contribution function, Atmos. Environ., 41(38), 8596–8608, 2007.

Dubey, P. and Dhaniyala, S.: Analysis of Scanning DMA Transfer Functions, Aerosol Sci. Technol., 42(7), 544–555, 2008.

Dusek, U., Meusinger, C., Oyama, B., Ramon, W., de Wilde, P. A., Holzinger, R., *et al.*: A thermal desorption system for measuring δ13C ratios on organic aerosol, J. Aerosol Sci., 66, 72–82, 2013.

Forster, P. M. F. and Taylor, K. E.: Climate Forcings and Climate Sensitivities Diagnosed from Coupled Climate Model Integrations, J. Clim., 19(23), 6181–6194, 2006.

Forster, P., Ramaswamy, V., Artaxo, P., Berntsen, T., Betts, R., Fahey, D. W., *et al.*: Changes in atmospheric constituents and in radiative forcing. Chapter 2, in Climate Change 2007. The Physical Science Basis., 2007.

Friedli, H. R., Atlas, E., Stroud, V. R., Giovanni, L., Campos, T. and Radke, L. F.: Volatile organic trace gases emitted from North American wildfires, Global Biogeochem. Cycles, 15(2), 435–452, 2001.

Fuchs, N. A.: On the stationary charge distribution on aerosol particles in a bipolar ionic atmosphere, Geofis. Pura e Appl., 56(1), 185–193, 1963.

Gao, J., Wang, J., Cheng, S.-H., Xue, L.-K., Yan, H.-Z., Hou, L.-J., *et al.*: Number concentration and size distributions of submicron particles in Jinan urban area: Characteristics in summer and winter, J. Environ. Sci., 19(12), 1466–1473, 2007.

Garbaras, A., Masalaite, A., Garbariene, I., Ceburnis, D., Krugly, E., Remeikis, *et al.*: Stable carbon fractionation in size-segregated aerosol particles

produced by controlled biomass burning, J. Aerosol Sci., 79, 86–96, 2015.

Garbaras, A.: Tracing of atmospheric aerosol sources using stable carbon isotopes, Lith. J. Phys., 48(3), 259–264, 2008.

Gildemeister, A. E., Hopke, P. K. and Kim, E.: Sources of fine urban particulate matter in Detroit, MI, Chemosphere, 69(7), 1064–1074, 2007.

Goldstein, A. H. and Galbally, I. E.: Known and unexplored organic constituents in the earth's atmosphere, Environ. Sci. Technol., 41(5), 1514–1521, 2007.

Gomišček, B., Hauck, H., Stopper, S. and Preining, O.: Spatial and temporal variations of PM1, PM2.5, PM10 and particle number concentration during the AUPHEP—project, Atmos. Environ., 38(24), 3917–3934, 2004.

Hadley, O. L. and Kirchstetter, T. W.: Black-carbon reduction of snow albedo, Nat. Clim. Chang., 2(6), 437–440, 2012.

Hallquist, M., Wenger, J. C., Baltensperger, U., Rudich, Y., Simpson, D., Claeys, M., *et al.*: The formation, properties and impact of secondary organic aerosol: current and emerging issues, Atmos. Chem. Phys., 9(14), 5155–5236, 2009.

Hamed, A., Joutsensaari, J., Mikkonen, S., Sogacheva, L., Dal Maso, M., Kulmala, M., *et al.*: Nucleation and growth of new particles in Po Valley, Italy, Atmos. Chem. Phys., 7(2), 355–376, 2007.

Han, Y.-J., Holsen, T. M. and Hopke, P. K.: Estimation of source locations of total gaseous mercury measured in New York State using trajectory-based models, Atmos. Environ., 41(28), 6033–6047, 2007.

Hand, J. L. and Kreidenweis, S. M.: A New Method for Retrieving Particle Refractive Index and Effective Density from Aerosol Size Distribution Data, Aerosol Sci. Technol., 36(10), 1012–1026, 2002.

Hansen, A. D. A. and Schnell, R. C.: The aethalometer, Magee Sci. Company, Berkeley, California, USA, 1–209, 2005.

Harris, S. J. and Maricq, M. M.: Signature size distributions for diesel and gasoline engine exhaust particulate matter, J. Aerosol Sci., 32(6), 749–764, 2001.

Harrison, R. M., Dall'Osto, M., Beddows, D. C. S., Thorpe, A. J., Bloss, W. J., Allan, J. D., *et al.*: Atmospheric chemistry and physics in the atmosphere of a developed megacity (London): an overview of the REPARTEE experiment and its conclusions, Atmos. Chem. Phys. Discuss., 11(11), 30145–30271, 2011.

Harrison, R. M., Smith, D. J. T. and Luhana, L.: Source Apportionment of Atmospheric Polycyclic Aromatic Hydrocarbons Collected from an Urban Location in Birmingham, U.K., Environ. Sci. Technol., 30(3), 825–832, 1996.

Henry, R. C., Chang, Y.-S. and Spiegelman, C. H.: Locating nearby sources of air pollution by nonparametric regression of atmospheric concentrations on wind direction, Atmos. Environ., 36(13), 2237–2244, 2002.

Hinds, W. C.: Aerosol technology: properties, behavior, and measurement of airborne particles, John Wiley & Sons., 2012.

Hoh, E. and Hites, R. A.: Sources of Toxaphene and Other Organochlorine Pesticides in North America As Determined by Air Measurements and Potential Source Contribution Function Analyses, Environ. Sci. Technol., 38(15), 4187–4194, 2004.

Holben, B. N., Eck, T. F., Slutsker, I., Tanré, D., Buis, J. P., Setzer, A., *et al.*: AERONET—A Federated Instrument Network and Data Archive for Aerosol Characterization, Remote Sens. Environ., 66(1), 1–16, 1998.

Holmes, N. S.: A review of particle formation events and growth in the atmosphere in the various environments and discussion of mechanistic implications, Atmos. Environ., 41(10), 2183–2201, 2007.

Hopke, P. K.: Recent developments in receptor modeling, J. Chemom., 17(5), 255–265, 2003.

Hoppel, W. A.: Surface source function for sea-salt aerosol and aerosol dry deposition to the ocean surface, J. Geophys. Res., 107(D19), 4382, 2002.

Hsu, Y.-K., Holsen, T. M. and Hopke, P. K.: Comparison of hybrid receptor models to locate PCB sources in Chicago, Atmos. Environ., 37(4), 545–562, 2003.

Hu, S., Fruin, S., Kozawa, K., Mara, S., Winer, A. M. and Paulson, S. E.: Aircraft Emission Impacts in a Neighborhood Adjacent to a General Aviation Airport in Southern California, Environ. Sci. Technol., 43(21), 8039–8045, 2009.

Huang, R.-J., Zhang, Y., Bozzetti, C., Ho, K.-F., Cao, J.-J., Han, Y., *et al.*: High secondary aerosol contribution to particulate pollution during haze events in China, Nature, 2014.

Hussein, T., Puustinen, A., Aalto, P. P., Mäkelä, J. M., Hämeri, K. and Kulmala, M.: Urban aerosol number size distributions, Atmos. Chem. Phys., 4(2), 391–411, 2004.

Hyvärinen, A.-P., Kolmonen, P., Kerminen, V.-M., Virkkula, A., Leskinen, A., Komppula, M., *et al.*: Aerosol black carbon at five background measurement sites over Finland, a gateway to the Arctic, Atmos. Environ., 45(24), 4042–4050, 2011.

Jennings, S. G., McGovern, F. M. and Cooke, W. F.: Carbon mass concentration measurements at mace head, on the west coast of Ireland, Atmos. Environ. Part A. Gen. Top., 27(8), 1229–1239, 1993.

Jeon, S. J., Meuzelaar, H. L. C., Sheya, S. A. N., Lighty, J. S., Jarman, W. M., Kasteler, C., *et al.*: Exploratory Studies of PM 10 Receptor and Source Profiling by GC/MS and Principal Component Analysis of Temporally and Spatially Resolved Ambient Samples, J. Air Waste Manage. Assoc., 51(5), 766–784, 2001.

Jolliffe, I.: Principal Component Analysis, in Encycl. Stat. Behav. Sci., John Wiley & Sons, Ltd, Chichester, UK., 2005.

Kabashnikov, V. P., Chaikovsky, A. P., Kucsera, T. L. and Metelskaya, N. S.: Estimated accuracy of three common trajectory statistical methods, Atmos. Environ., 45(31), 5425–5430, 2011.

Kanakidou, M., Seinfeld, J. H., Pandis, S. N., Barnes, I., Dentener, F. J., Facchini, M. C., *et al.*: Organic aerosol and global climate modelling: a review, Atmos. Chem. Phys., 5(4), 1053–1123, 2005.

Karvosenoja, N., Tainio, M., Kupiainen, K., Tuomisto, J. T., Kukkonen, J. and Johansson, M.: Evaluation of the emissions and uncertainties of PM2. 5 originated from vehicular traffic and domestic wood combustion in Finland, Boreal Environ. Res., 13(5), 465–474, 2008.

Ke, L., Ding, X., Tanner, R. L., Schauer, J. J. and Zheng, M.: Source contributions to carbonaceous aerosols in the Tennessee Valley Region, Atmos. Environ., 41(39), 8898–8923, 2007.

Ketzel, M., Wåhlin, P., Kristensson, A., Swietlicki, E., Berkowicz, R., Nielsen, O. J., *et al.*: Particle size distribution and particle mass measurements at urban, near-city and rural level in the Copenhagen area and Southern Sweden, Atmos. Chem. Phys., 4(1), 281–292, 2004.

Khlystov, A., Stanier, C. and Pandis, S. N.: An Algorithm for Combining Electrical Mobility and Aerodynamic Size Distributions Data when Measuring Ambient Aerosol Special Issue of Aerosol Science and Technology on Findings from the Fine Particulate Matter Supersites Program, Aerosol Sci. Technol., 38(sup1), 229–238, 2004.

Kim, S. H., Woo, K. S., Liu, B. Y. H. and Zachariah, M. R.: Method of measuring charge distribution of nanosized aerosols, J. Colloid Interface Sci., 282(1), 46–57, 2005.

Kirchstetter, T. W. and Novakov, T.: Controlled generation of black carbon particles from a diffusion flame and applications in evaluating black carbon measurement methods, Atmos. Environ., 41(9), 1874–1888, 2007.

Kittelson, D. B. and Watts, W.: Nanoparticle Emissions from engines, in Proc. Third Joint ESFNSF Symposium on" Nanoparticles: Applications in

Material Science and Environmental Science and Engineering, Dublin, Ireland, pp. p19–21., 2000.

Kittelson, D., Johnson, J., Watts, W., Wei, Q., Drayton, M., Paulsen, D., *et al.*: Diesel Aerosol Sampling in the Atmosphere., 2000.

Koch, D., Schulz, M., Kinne, S., McNaughton, C., Spackman, J. R., Balkanski, *et al.*: Evaluation of black carbon estimations in global aerosol models, Atmos. Chem. Phys., 9(22), 9001–9026, 2009.

Kroll, J. H. and Seinfeld, J. H.: Chemistry of secondary organic aerosol: Formation and evolution of low-volatility organics in the atmosphere, Atmos. Environ., 42(16), 3593–3624, 2008.

Kulmala, M. and Kerminen, V.-M.: On the formation and growth of atmospheric nanoparticles, Atmos. Res., 90(2-4), 132–150, 2008.

Kulmala, M., Asmi, A., Lappalainen, H. K., Baltensperger, U., Brenguier, J.-L., Facchini, M. C., *et al.*: General overview: European Integrated project on Aerosol Cloud Climate and Air Quality interactions (EUCAARI) – integrating aerosol research from nano to global scales, Atmos. Chem. Phys., 11(24), 13061–13143, 2011.

Kulmala, M., Maso, M. D., Makela, J. M., Pirjola, L., Vakeva, M., Aalto, P., *et al.*: On the formation, growth and composition of nucleation mode particles, Tellus B, 53(4), 479–490, 2001.

Kulmala, M., Petäjä, T., Mönkkönen, P., Koponen, I. K., Dal Maso, M., Aalto, P. P., *et al.*: On the growth of nucleation mode particles: source rates of condensable vapor in polluted and clean environments, Atmos. Chem. Phys., 5(2), 409–416, 2005.

Kulmala, M., Riipinen, I., Sipila, M., Manninen, H. E., Petaja, T., Junninen, H., *et al.*: Toward Direct Measurement of Atmospheric Nucleation, Science (80-.)., 318(5847), 89–92, 2007.

Kulmala, M., Vehkamäki, H., Petäjä, T., Dal Maso, M., Lauri, A., Kerminen, V.-M., *et al.*: Formation and growth rates of ultrafine atmospheric particles: a review of observations, J. Aerosol Sci., 35(2), 143–176, 2004.

Kumar, A., Sarin, M. M. and Srinivas, B.: Aerosol iron solubility over Bay of Bengal: Role of anthropogenic sources and chemical processing, Mar. Chem., 121(1-4), 167–175, 2010.

Lanz, V. A., Alfarra, M. R., Baltensperger, U., Buchmann, B., Hueglin, C. and Prévôt, A. S. H.: Source apportionment of submicron organic aerosols at an urban site by factor analytical modelling of aerosol mass spectra, Atmos. Chem. Phys., 7(6), 1503–1522, 2007.

Lavanchy, V. M. H., Gäggeler, H. W., Nyeki, S. and Baltensperger, U.: Elemental carbon (EC) and black carbon (BC) measurements with a thermal method and an aethalometer at the high-alpine research station Jungfraujoch, Atmos. Environ., 33(17), 2759–2769, 1999.

Lenschow, P., Abraham, H. J., Kutzner, K., Lutz, M., Pruß, J. D. and Reichenbächer, W.: Some ideas about the sources of PM10, Atmos. Environ., 35, 23–33, 2001.

Lewis, C. W., Klouda, G. A. and Ellenson, W. D.: Radiocarbon measurement of the biogenic contribution to summertime PM-2.5 ambient aerosol in Nashville, TN, Atmos. Environ., 38(35), 6053–6061, 2004.

Lohmann, U. and Ferrachat, S.: Impact of parametric uncertainties on the present-day climate and on the anthropogenic aerosol effect, Atmos. Chem. Phys., 10(23), 11373–11383, 2010.

Lohmann, U., Rotstayn, L., Storelvmo, T., Jones, A., Menon, S., Quaas, J., *et al.*: Total aerosol effect: radiative forcing or radiative flux perturbation?, Atmos. Chem. Phys., 10(7), 3235–3246, 2010.

López-Veneroni, D.: The stable carbon isotope composition of PM2.5 and PM10 in Mexico City Metropolitan Area air, Atmos. Environ., 43(29), 4491–4502, 2009.

Lucey, D., Hadjiiski, L., Hopke, P. K., Scudlark, J. R. and Church, T.: Identification of sources of pollutants in precipitation measured at the mid-Atlantic US coast using potential source contribution function (PSCF), Atmos. Environ., 35(23), 3979–3986, 2001.

Mann, G. W., Carslaw, K. S., Reddington, C. L., Pringle, K. J., Schulz, M., Asmi, A., *et al.*: Intercomparison and evaluation of global aerosol microphysical properties among AeroCom models of a range of complexity, Atmos. Chem. Phys., 14(9), 4679–4713, 2014.

Maricq, M. M., Chase, R. E., Podsiadlik, D. H., Siegl, W. O. and Kaiser, E. W.: The Effect of Dimethoxy Methane Additive on Diesel Vehicle Particulate Emissions., 1998.

Marković, D. M., Marković, D. A., Jovanović, A., Lazić, L. and Mijić, Z.: Determination of O3, NO2, SO2, CO and PM10 measured in Belgrade urban area, Environ. Monit. Assess., 145(1-3), 349–359, 2008.

Mašalaitė, A., Garbaras, A. and Remeikis, V.: Stable isotopes in environmental investigations, Lith. J. Phys., 52(3), 261–268, 2012.

Mauderly, J. L. and Chow, J. C.: Health Effects of Organic Aerosols, Inhal. Toxicol., 20(3), 257–288, 2008.

Meinshausen, M., Smith, S. J., Calvin, K., Daniel, J. S., Kainuma, M. L. T., Lamarque, J.-F., *et al.*: The RCP greenhouse gas concentrations and their extensions from 1765 to 2300, Clim. Change, 109(1-2), 213–241, 2011.

Meyer, N. K.: Particulate, black carbon and organic emissions from small-scale residential wood combustion appliances in Switzerland, Biomass and Bioenergy, 36, 31–42, 2012.

Molnár, A., Mészáros, E., Hansson, H. C., Karlsson, H., Gelencsér, A., Kiss, G., *et al.*: The inportance of organic and elemental carbon in the fine atmospheric aerosol particles, Atmos. Environ., 33(17), 2745–2750, 1999.

Mooibroek, D., Schaap, M., Weijers, E. P. and Hoogerbrugge, R.: Source apportionment and spatial variability of PM2.5 using measurements at five sites in the Netherlands, Atmos. Environ., 45(25), 4180–4191, 2011.

Morawska, L., Bofinger, N. D., Kocis, L. and Nwankwoala, A.: Submicrometer and Supermicrometer Particles from Diesel Vehicle Emissions, Environ. Sci. Technol., 32(14), 2033–2042, 1998.

Morawska, L., Ristovski, Z., Jayaratne, E. R., Keogh, D. U. and Ling, X.: Ambient nano and ultrafine particles from motor vehicle emissions: Characteristics, ambient processing and implications on human exposure, Atmos. Environ., 42(35), 8113–8138, 2008.

Mordas, G., Manninen, H. E., Petäjä, T., Aalto, P. P., Hämeri, K. and Kulmala, M.: On Operation of the Ultra-Fine Water-Based CPC TSI 3786 and Comparison with Other TSI Models (TSI 3776, TSI 3772, TSI 3025, TSI 3010, TSI 3007), Aerosol Sci. Technol., 42(2), 152–158, 2008.

Moroni, B., Castellini, S., Crocchianti, S., Piazzalunga, A., Fermo, P., Scardazza, F., *et al.*: Ground-based measurements of long-range transported aerosol at the rural regional background site of Monte Martano (Central Italy), Atmos. Res., 155, 26–36, 2015.

Müller, D.: Raman lidar observations of aged Siberian and Canadian forest fire smoke in the free troposphere over Germany in 2003: Microphysical particle characterization, J. Geophys. Res., 110(D17), D17201, 2005.

Narukawa, M., Kawamura, K., Li, S.-M. and Bottenheim, J. W.: Stable carbon isotopic ratios and ionic composition of the high-Arctic aerosols: An increase in δ 13 C values from winter to spring, J. Geophys. Res., 113(D2), D02312, 2008.

Ng, N. L., Canagaratna, M. R., Jimenez, J. L., Chhabra, P. S., Seinfeld, J. H. and Worsnop, D. R.: Changes in organic aerosol composition with aging inferred from aerosol mass spectra, Atmos. Chem. Phys., 11(13), 6465–6474, 2011b.

Ng, N. L., Herndon, S. C., Trimborn, A., Canagaratna, M. R., Croteau, P. L., Onasch, T. B., Sueper, D., *et al.*: An Aerosol Chemical Speciation Monitor (ACSM) for Routine Monitoring of the Composition and Mass Concentrations of Ambient Aerosol, Aerosol Sci. Technol., 45(7), 780–794, 2011a.

Ning, Z., Chan, K. L., Wong, K. C., Westerdahl, D., Močnik, G., Zhou, J. H., *et al.*: Black carbon mass size distributions of diesel exhaust and urban aerosols measured using differential mobility analyzer in tandem with Aethalometer, Atmos. Environ., 80, 31–40, 2013.

O'Dowd, C. D.: Coastal new particle formation: Environmental conditions and aerosol physicochemical characteristics during nucleation bursts, J. Geophys. Res., 107(D19), 8107, 2002.

Ovadnevaite, J., Kvietkus, K. and Marsalka, A.: 2002 summer fires in Lithuania: Impact on the Vilnius city air quality and the inhabitants health, Sci. Total Environ., 356(1-3), 11–21, 2006.

Ovadnevaite, J., Kvietkus, K. and Šakalys, J.: Evaluation of the impact of long-range transport and aerosol concentration temporal variations at the Eastern coast of the Baltic Sea, Environ. Monit. Assess., 132, 365–375, 2007.

Park, K., Park, J. Y., Kwak, J.-H. H., Cho, G. N. and Kim, J.-S. S.: Seasonal and diurnal variations of ultrafine particle concentration in urban Gwangju, Korea: Observation of ultrafine particle events, Atmos. Environ., 42(4), 788–799, 2008.

Parnell, A. C., Phillips, D. L., Bearhop, S., Semmens, B. X., Ward, E. J., Moore, J. W., *et al.*: Bayesian stable isotope mixing models, Environmetrics, n/a–n/a, 2013.

Paschalidou, A. K., Kassomenos, P. and Karanikola, P.: Disaggregating the contribution of local dispersion and long-range transport to the high PM10 values measured in a Mediterranean urban environment, Sci. Total Environ., 527-528, 119–125, 2015.

Pekey, H., Karakaş, D. and Bakogˇlu, M.: Source apportionment of trace metals in surface waters of a polluted stream using multivariate statistical analyses, Mar. Pollut. Bull., 49(9-10), 809–818, 2004.

Pekney, N. J., Davidson, C. I., Zhou, L. and Hopke, P. K.: Application of PSCF and CPF to PMF-Modeled Sources of PM 2.5 in Pittsburgh, Aerosol Sci. Technol., 40(10), 952–961, 2006.

Pérez, N., Pey, J., Cusack, M., Reche, C., Querol, X., Alastuey, A., *et al.*: Variability of Particle Number, Black Carbon, and PM 10 , PM 2.5 , and PM 1 Levels and Speciation: Influence of Road Traffic Emissions on Urban Air Quality, Aerosol Sci. Technol., 44(7), 487–499, 2010.

Peters, T. M. and Leith, D.: Concentration measurement and counting efficiency of the aerodynamic particle sizer 3321, J. Aerosol Sci., 34(5), 627–634, 2003.

Peters, T. M., Ott, D. and O'Shaughnessy, P. T.: Comparison of the Grimm 1.108 and 1.109 Portable Aerosol Spectrometer to the TSI 3321 Aerodynamic Particle Sizer for Dry Particles, Ann. Occup. Hyg., 50(8), 843–850, 2006.

Petterssen, S.: Weather Analysis and Forecasting, in Weather Analysis and Forecasting, p. 221–223, McGraw-Hill, New York., 1940.

Petzold, A., Ogren, J. A., Fiebig, M., Laj, P., Li, S.-M., Baltensperger, U., *et al.*: Recommendations for reporting "black carbon" measurements, Atmos. Chem. Phys., 13(16), 8365–8379, 2013.

Pey, J., Querol, X., Alastuey, A., Rodríguez, S., Putaud, J. P. and Van Dingenen, R.: Source apportionment of urban fine and ultra-fine particle number concentration in a Western Mediterranean city, Atmos. Environ., 43(29), 4407–4415, 2009.

Pey, J., Rodríguez, S., Querol, X., Alastuey, A., Moreno, T., Putaud, J. P. and Van Dingenen, R.: Variations of urban aerosols in the western Mediterranean, Atmos. Environ., 42(40), 9052–9062, 2008.

Phillips, D. L. and Gregg, J. W.: Source partitioning using stable isotopes: coping with too many sources, Oecologia, 136(2), 261–269, 2003.

Phillips, D. L. and Gregg, J. W.: Uncertainty in source partitioning using stable isotopes, Oecologia, 127(2), 171–179, 2001.

Plauškaitė, K., Ulevicius, V., Špirkauskaitė, N., Byčenkienė, S., Zieliński, T., Petelski, T., *et al.*: Observations of new particle formation events in the south-eastern Baltic Sea, OCEANOLOGIA, 52(1), 53–75, 2010.

Pollack, J. B. and Cuzzi, J. N.: Scattering by Nonspherical Particles of Size Comparable to a Wavelength: A New Semi-Empirical Theory and Its Application to Tropospheric Aerosols, J. Atmos. Sci., 37(4), 868–881, 1980.

Pope III, C. A.: Lung Cancer, Cardiopulmonary Mortality, and Long-term Exposure to Fine Particulate Air Pollution, JAMA, 287(9), 1132, 2002.

Pöschl, U.: Aerosol particle analysis: challenges and progress, Anal. Bioanal. Chem., 375(1), 30–32, 2003.

Pratt, K. A., Murphy, S. M., Subramanian, R., DeMott, P. J., Kok, G. L., Campos, T., *et al.*: Flight-based chemical characterization of biomass burning aerosols within two prescribed burn smoke plumes, Atmos. Chem. Phys., 11(24), 12549–12565, 2011.

Radzi Bin Abas, M., Rahman, N. A., Omar, N. Y. M. ., Maah, M. J., Abu Samah, A., Oros, D. R., *et al.*: Organic composition of aerosol particulate matter during a haze episode in Kuala Lumpur, Malaysia, Atmos. Environ., 38(25), 4223–4241, 2004.

Reche, C., Querol, X., Alastuey, A., Viana, M., Pey, J., Moreno, T., *et al.*: New considerations for PM, Black Carbon and particle number concentration for air quality monitoring across different European cities, Atmos. Chem. Phys., 11(13), 6207–6227, 2011.

Rizzo, M. and Scheff, P.: Fine particulate source apportionment using data from the USEPA speciation trends network in Chicago, Illinois: Comparison of two source apportionment models, Atmos. Environ., 41(29), 6276–6288, 2007.

Rodríguez, S., Van Dingenen, R., Putaud, J.-P., Dell'Acqua, A., Pey, J., Querol, X., *et al.*: A study on the relationship between mass concentrations, chemistry and number size distribution of urban fine aerosols in Milan, Barcelona and London, Atmos. Chem. Phys., 7(9), 2217–2232, 2007.

Rodríguez, S., Van Dingenen, R., Putaud, J.-P., Martins-Dos Santos, S. and Roselli, D.: Nucleation and growth of new particles in the rural

atmosphere of Northern Italy—relationship to air quality monitoring, Atmos. Environ., 39(36), 6734–6746, 2005.

Russell, L. M., Bahadur, R. and Ziemann, P. J.: Identifying organic aerosol sources by comparing functional group composition in chamber and atmospheric particles, Proc. Natl. Acad. Sci., 108(9), 3516–3521, 2011.

Ruuskanen, J., Tuch, T., Ten Brink, H., Peters, A., Khlystov, A., Mirme, A., *et al.*: Concentrations of ultrafine, fine and PM2.5 particles in three European cities, Atmos. Environ., 35(21), 3729–3738, 2001.

Saarikoski, S., Sillanpää, M., Sofiev, M., Timonen, H., Saarnio, K., Teinilä, K., *et al.*: Chemical composition of aerosols during a major biomass burning episode over northern Europe in spring 2006: Experimental and modelling assessments, Atmos. Environ., 41(17), 3577–3589, 2007.

Saarnio, K., Teinilä, K., Aurela, M., Timonen, H. and Hillamo, R.: High-performance anion-exchange chromatography–mass spectrometry method for determination of levoglucosan, mannosan, and galactosan in atmospheric fine particulate matter, Anal. Bioanal. Chem., 398(5), 2253–2264, 2010.

Šakalys, J., Valiulis, D., Meinorė, E., Dudoitis, V., Kvietkus, K. and Ulevičius, V.: Density assessment method of chemical components in urban submicron aerosol particles, Lith. J. Phys., 55(2), 2015.

Salma, I., Borsòs, T., Weidinger, T., Aalto, P., Hussein, T., Dal Maso, M., *et al.*: Production, growth and properties of ultrafine atmospheric aerosol particles in an urban environment, Atmos. Chem. Phys., 11(3), 1339–1353, 2011.

Salvador, S. and Chan, P.: Determining the number of clusters/segments in hierarchical clustering/segmentation algorithms, in 16th IEEE International Conference on Tools with Artificial Intelligence, pp. 576–584, IEEE Comput. Soc., n.d.

San José, R., Stohl, A., Karatzas, K., Bohler, T., James, P. and Pérez, J. L.: A modelling study of an extraordinary night time ozone episode over Madrid domain, Environ. Model. Softw., 20(5), 587–593, 2005.

Schwartz, S. E. and Lewis, E. R.: Interactive comment on “Are black carbon and soot the same?” by PR Buseck *et al.*: Disagreement on proposed nomenclature, Atmos. Chem. Phys. Discuss, 12, C9099–C9109, 2012.

Seinfeld, J. H. and Pandis, S. N.: Atmospheric chemistry and physics: from air pollution to climate change, John Wiley & Sons., 2012.

Semmens, B. X., Ward, E. J., Moore, J. W. and Darimont, C. T.: Quantifying Inter- and Intra-Population Niche Variability Using Hierarchical Bayesian Stable Isotope Mixing Models, edited by W. M. Getz, PLoS One, 4(7), e6187, 2009.

Shen, S., Jaques, P. A., Zhu, Y., Geller, M. D. and Sioutas, C.: Evaluation of the SMPS–APS system as a continuous monitor for measuring PM2.5, PM10 and coarse (PM2.5?10) concentrations, Atmos. Environ., 36(24), 3939–3950, 2002.

Simmonds, P., Manning, A., Derwent, R., Ciais, P., Ramonet, M., Kazan, V., *et al.*: A burning question. Can recent growth rate anomalies in the greenhouse gases be attributed to large-scale biomass burning events?, Atmos. Environ., 39(14), 2513–2517, 2005.

Sioutas, C., Delfino, R. J. and Singh, M.: Exposure Assessment for Atmospheric Ultrafine Particles (UFPs) and Implications in Epidemiologic Research, Environ. Health Perspect., 113(8), 947–955, 2005.

Sioutas, C.: Evaluation of the Measurement Performance of the Scanning Mobility Particle Sizer and Aerodynamic Particle Sizer, Aerosol Sci. Technol., 30(1), 84–92, 1999.

Sirois, A. and Bottenheim, J. W.: Use of backward trajectories to interpret the 5-year record of PAN and O 3 ambient air concentrations at Kejimkujik National Park, Nova Scotia, J. Geophys. Res., 100(D2), 2867, 1995.

Source[1]: Aerosol size distribution, http://www.ems.psu.edu/~lno/Meteo437/Aermode3.jpg, (2015-05-20).

Source[2]: Anhropogenic radiative forcing, http://www.climatechange2013.org/images/report/WG1AR5_ALL_FINAL.pdf, (2015-05-20).

Source[3]: ACSM schematic representation, http://www.dwd.de/EN/research/observing_atmosphere/composition_atmosphere/aerosol/cont_nav/acsm.html, (2015-05-20).

Source[4]: Lithuanian air monitoring data, http://stoteles.gamta.lt/, (2015-06-15).

Source[5]: The Lithuanian Road Administration under the Ministry of Transport and Communications of the Republic of Lithuania traffic intensity information, http://www.lakd.lt/lt.php/lietuvos_keliai/eismo_intensyvumas/17877, (2015-06-01).

Spracklen, D. V., Carslaw, K. S., Kulmala, M., Kerminen, V.-M., Sihto, S.-L., Riipinen, I., *et al.*: Contribution of particle formation to global cloud condensation nuclei concentrations, Geophys. Res. Lett., 35(6), L06808, 2008.

Srinivas, B., Kumar, A., Sarin, M. M. and Sudheer, A. K.: Impact of continental outflow on chemistry of atmospheric aerosols over tropical Bay of Bengal, Atmos. Chem. Phys. Discuss., 11(7), 20667–20711, 2011.

Steinfeld, J. I.: Atmospheric Chemistry and Physics: From Air Pollution to Climate Change, Environ. Sci. Policy Sustain. Dev., 40(7), 26–26, 1998.

Stocker, T., Dahe, Q. and Plattner, G. K. E.: Working Group I Contribution to the IPCC Fifth Assessment Report Climate Change 2013, The Physical Science Basis, Final Draft underlying Sci. Assess. IPCC,(Stockholm), 2013.

Streets, D. G. and Waldhoff, S. T.: Present and future emissions of air pollutants in China:, Atmos. Environ., 34(3), 363–374, 2000.

Swietlicki, E.: European source region identification og long range transported ambient aerosol based on PIXE analysis and related techniques, 1989.

Szidat, S., Jenk, T. M., Synal, H.-A. A., Kalberer, M., Wacker, L., Hajdas, I., *et al.*: Contributions of fossil fuel, biomass-burning, and biogenic emissions to carbonaceous aerosols in Zurich as traced by 14 C, J. Geophys. Res., 111(D7), D07206, 2006.

Thomas, S. and Morawska, L.: Size-selected particles in an urban atmosphere of Brisbane, Australia, Atmos. Environ., 36(26), 4277–4288, 2002.

Tuch, T. M., Herbarth, O., Franck, U., Peters, A., Wehner, B., Wiedensohler, A., *et al.*: Weak correlation of ultrafine aerosol particle concentrations <800 nm between two sites within one city, J. Expo. Sci. Environ. Epidemiol., 16(6), 486–490, 2006.

Ulevicius, V., Byčenkienė, S., Remeikis, V., Garbaras, A., Kecorius, S., Andriejauskienė, J., *et al.*: Characterization of pollution events in the East Baltic region affected by regional biomass fire emissions, Atmos. Res., 98(2-4), 190–200, 2010.

Viana, M., Kuhlbusch, T. a J., Querol, X., Alastuey, A., Harrison, R. M., Hopke, P. K., *et al.*: Source apportionment of particulate matter in Europe: A review of methods and results, J. Aerosol Sci., 39(10), 827–849, 2008.

Virkkula, A., Mäkelä, T., Hillamo, R., Yli-Tuomi, T., Hirsikko, A., Hämeri, K., *et al.*: A Simple Procedure for Correcting Loading Effects of Aethalometer Data, J. Air Waste Manage. Assoc., 57(10), 1214–1222, 2007.

Visschedijk, A. J. H., van der Gon, H., Dröge, A. C., der Brugh, H. and Kooter, I. M.: A European high resolution and size-differentiated emission inventory for elemental and organic carbon for the year 2005, TNO report., 2009.

Volkamer, R., Jimenez, J. L., San Martini, F., Dzepina, K., Zhang, Q., Salcedo, D., *et al.*: Secondary organic aerosol formation from anthropogenic air pollution: Rapid and higher than expected, Geophys. Res. Lett., 33(17), L17811, 2006.

Wang, Y. Q., Zhang, X. Y. and Arimoto, R.: The contribution from distant dust sources to the atmospheric particulate matter loadings at XiAn, China during spring., Sci. Total Environ., 368(2-3), 875–83, 2006.

Wardoyo, A. Y.: Biomass burning : particle emissions, characteristics, and airborne measurements, Queensland University of Technology, 2007. http://eprints.qut.edu.au/16492/ , (2015-01-17).

Watson, J. G., Chow, J. C. and Chen, L.-W. A.: Summary of organic and elemental carbon/black carbon analysis methods and intercomparisons, Aerosol Air Qual. Res, 5(1), 65–102, 2005.

Watson, J. G., Zhu, T., Chow, J. C., Engelbrecht, J., Fujita, E. M. and Wilson, W. E.: Receptor modeling application framework for particle source apportionment, Chemosphere, 49(9), 1093–1136, 2002.

Wehner, B., Uhrner, U., von Löwis, S., Zallinger, M. and Wiedensohler, A.: Aerosol number size distributions within the exhaust plume of a diesel and a gasoline passenger car under on-road conditions and determination of emission factors, Atmos. Environ., 43(6), 1235–1245, 2009.

Weingartner, E., Saathoff, H., Schnaiter, M., Streit, N., Bitnar, B. and Baltensperger, U.: Absorption of light by soot particles: determination of the absorption coefficient by means of aethalometers, J. Aerosol Sci., 34(10), 1445–1463, 2003.

Wexler, A. S. and Johnston, M. V.: What Have We Learned from Highly Time-Resolved Measurements during EPA's Supersites Program and Related Studies?, J. Air Waste Manage. Assoc., 58(2), 303–319, 2008.

Widory, D., Roy, S., Le Moullec, Y., Goupil, G., Cocherie, A. and Guerrot, C.: The origin of atmospheric particles in Paris: a view through carbon and lead isotopes, Atmos. Environ., 38(7), 953–961, 2004.

Wiedensohler, A., Birmili, W., Nowak, A., Sonntag, A., Weinhold, K., Merkel, *et al.*: Mobility particle size spectrometers: harmonization of technical standards and data structure to facilitate high quality long-term observations of atmospheric particle number size distributions, Atmos. Meas. Tech., 5(3), 657–685, 2012.

Zawadzka, O., Markowicz, K. M., Pietruczuk, A., Zielinski, T. and Jaroslawski, J.: Impact of urban pollution emitted in Warsaw on aerosol properties, Atmos. Environ., 69, 15–28, 2013.

Zeng, Y. and Hopke, P. K.: A study of the sources of acid precipitation in Ontario, Canada, Atmos. Environ., 23(7), 1499–1509, 1989.

Zhang, L.: A size-segregated particle dry deposition scheme for an atmospheric aerosol module, Atmos. Environ., 35(3), 549–560, 2001.

Zhang, Q., Jimenez, J. L., Canagaratna, M. R., Allan, J. D., Coe, H., Ulbrich, I., *et al.*: Ubiquity and dominance of oxygenated species in organic aerosols in anthropogenically-influenced Northern Hemisphere midlatitudes, Geophys. Res. Lett., 34(13), n/a–n/a, 2007.

Zhang, Q., Worsnop, D. R., Canagaratna, M. R. and Jimenez, J. L.: Hydrocarbon-like and oxygenated organic aerosols in Pittsburgh: insights into sources and processes of organic aerosols, Atmos. Chem. Phys., 5(12), 3289–3311, 2005.

Zhang, X. Y., Wang, Y. Q., Zhang, X. C., Guo, W. and Gong, S. L.: Carbonaceous aerosol composition over various regions of China during 2006, J. Geophys. Res., 113(D14), D14111, 2008.

Zhu, L., Huang, X., Shi, H., Cai, X. and Song, Y.: Transport pathways and potential sources of PM10 in Beijing, Atmos. Environ., 45(3), 594–604, 2011.